Atmosphere–Vegetation Feedback in the Climate System of the Last Glacial

Atmosphären-Vegetations-Wechselwirkung im Klimasystem des letzten Glazials

Diplomarbeit im Fach Meteorologie

von Alexandra Jahn

angefertigt am Potsdam Institut für Klimafolgenforschung

vorgelegt dem Fachbereich für Geowissenschaften der Freien Universität Berlin

im August 2004

Gutachter: Prof. Dr. Cubasch
Prof. Dr. Claussen

Abstract

Using the climate system model CLIMBER-2.3, the role of the atmosphere-vegetation feedback during the last glacial (MIS 3 – MIS 2) has been investigated.

It could be shown in equilibrium experiments of the last glacial maximum (21,000 years before present) that by using a prescribed present day vegetation distribution a different equilibrium solution for the Atlantic ocean circulation was found than when the interactive dynamic vegetation module of CLIMBER-2.3 was used. The use of an interactive vegetation, thereby, led to North Atlantic Deep Water (NADW) formation south of Iceland and a weaker thermohaline circulation than for the use of a present day vegetation, which caused a stronger thermohaline circulation than even today, with NADW formation taking place in the Nordic Seas (50-70° N). This difference in ocean circulation caused a cooling of up to 7 °C over the North Atlantic when the interactive vegetation was used. This is only indirectly a result of the interactive vegetation, the real reason being the strong non-linear behavior of the thermohaline circulation (Ganopolski and Rahmstorf 2001) that makes it possible for a small change to trigger the transition to a different circulation mode when it delivers the change necessary to cross the threshold of the ocean circulation. I demonstrated that the change in ocean circulation could not only be triggered by the use of the interactive vegetation, but also by an additional decrease of CO_2 concentration by 10 ppm, which is the difference between the CO_2 concentration of 200 ppm used in PMIP (2001) and the reconstructed CO_2 concentration of 190 ppm (Petit et al. 1999).

Furthermore, I showed that in the high northern latitudes the taiga-tundra feedback, amplified by the sea-ice-albedo feedback, caused temperature changes about as large as the cooling that was caused there by the lowering of CO_2 from its preindustrial to its LGM level.

In transient experiments over part of the last glacial period (60,000–20,000 years before present) it could be shown that the cooling caused by the atmosphere-vegetation feedback had the same magnitude as the warming caused by it during the Mid-Holocene in a study of Ganopolski et al. (1998a). Furthermore, it has been found that, probably due to the more southward sea-ice extend, the synergy between the taiga-tundra feedback and the sea-ice-albedo feedback is smaller during the last glacial than during the Mid-Holocene.

Therefore, I concluded that the use of the dynamic vegetation module in CLIMBER-2.3 improves the simulations as it causes an additional cooling over the northern latitudes that at the same time triggers the change in ocean circulation, so that overall the simulation agrees better with reconstructions.

Zusammenfassung

Mit dem Klimasystemmodell CLIMBER-2.3 wurde die Rolle der Atmosphären-Vegetations-Wechselwirkung während des letzten Glazials (MIS 3–MIS 2) untersucht.
In Gleichgewichtsexperimenten für das Letzte Glaziale Maximum (21.000 Jahre vor heute) konnte gezeigt werden, dass die Ozeanzirkulation im Atlantik zwei verschiedene Gleichgewichtszustände erreichte, wenn einmal das interaktive Vegetations-Modell verwendet wurde und das andere mal eine Vegetationsverteilung vorgeschrieben wurde, die der vorindustriellen entspricht. Dabei führte die Verwendung des interaktiven, dynamischen Vegetations-Modells zu einer Bildung von Nordatlantischem Tiefenwasser südlich von Island und einer thermohalinen Zirkulation, die schwächer war, als wenn die vorgeschriebene, vorindustrielle Vegetationsverteilung benutzt wurde. Diese führte zu einer stärkeren thermohalinen Zirkulation als heute und außerdem fand auch die Bildung des Nordatlantischen Tiefenwassers im Nordmeer (50–70° N) statt. Die Abschwächung und Verlagerung der thermohalinen Zirkulation nach Süden verursachte eine zusätzliche Abkühlung über dem Nord Atlantik von bis zu 7 °C . Dieser Temperaturunterschied ist jedoch nur indirekt eine Folge der interaktiven Vegetation, da die Ozeanzirkulation ein stark nicht-lineares System ist (Ganopolski and Rahmstorf 2001), so dass eine kleine zusätzliche Änderung des Klimas dazu führen kann, dass die Ozeanzirkulation in einen anderen Zustand "umspringt", wenn durch die zusätzliche Änderung ein Schwellenwert überschritten wird. Dies konnte für das LGM nicht nur durch die Verwendung der interaktiven Vegetation erreicht werden, sondern auch durch eine zusätzliche Absenkung des CO_2 Gehalts der Atmosphäre um 10 ppm, was genau den Unterschied ausmacht zwischen dem CO_2 Gehalt der in den PMIP (2001) Simulationen benutzt wurde (200 ppm) und der CO_2 Konzentration von 190 ppm aus Rekonstruktionen (Petit et al. 1999).
Des Weiteren konnte ich zeigen, dass der Taiga-Tundra Effekt, verstärkt durch den Meereis-Albedo Effekt, über den hohen nördlichen Breiten zu einer Abkühlung führte, die ungefähr gleich groß war wie die Abkühlung dort durch die Absenkung des CO_2 Gehaltes von dem vorindustriellen auf den LGM Wert.
Durch die transienten Experimente für einen Teil des letzten Glazials (60.000–20.000 Jahre vor heute) wurde demonstriert, dass die Abkühlung durch die Atmosphären-Vegetations-Wechselwirkung vom Betrag her in etwa gleich groß war wie die Erwärmung, die durch eben diese Wechselwirkung während des mittleren Holozän von Ganopolski et al. (1998a) gefunden wurde. Gleichzeitig war der Synergieterm zwischen der Atmosphären-Vegetations-Wechselwirkung und der Atmosphären-Ozean-Wechselwirkung während der betrachteten Periode des Glazials kleiner als im mittleren Holozän, wahrscheinlich weil die Rückkopplung durch den Meereis-Albedo Effekt kleiner war, da sich die Meereisbedeckung im Glazial viel weiter südlich erstreckte als im Holozän.
Insgesamt habe ich gezeigt, dass die Benutzung des dynamischen Vegetationsmodells in CLIMBER-2.3 die Simulationsergebnisse verbesserte, da die interaktive Vegetation nicht nur die Umstellung der Ozeanzirkulation auslöste, sondern auch eine zusätziche Abkühlung über den hohen nördlichen Breiten bewirkte, so dass insgesamt eine bessere Übereinstimmung mit Rekonstruktionen erreicht wurde.

Contents

Introduction

The increased media coverage on hurricanes, tornados and devastating thunderstorms and floods all over the world and in addition the personal experience of the exceptionally warm summer in Europe in 2003 caused the term "climate change" or "climate catastrophe", as the media likes to put it, to be something everybody suddenly talks about.

And indeed, the climate is changing. It has always changed, as we, for example, know from climate reconstructions from ice cores that now reach back 800,000 years (EPICA community members 2004). The long term climate change from ice ages to interglacials is, thereby, caused mainly by insolation changes (Milankovitch 1930), while the climate change the public refers to is the recent anthropogenic climate change that caused a warming of globally 0.4–0.8 °C (IPCC 2001) in the past century due to greenhousegas emissions. Whether the anthropogenic climate change is indeed related to the above described events is still highly debated as the number of storms and floods has always changed over the years so that it is probably too early to definitely be able to state that there is a trend that is correlated with the anthropogenic warming (IPCC 2001). There is, however, no question that the anthropogenic warming will cause changes in the future decades and centuries that will have drastic regional impacts so that predictions of when and where which changes might occur are in high demand.

In order to estimate how the anthropogenic climate change will influence the climate in the future decades and centuries and to develop strategies to stop or dampen the effect, a thorough understanding of the climate dynamics is necessary so that we can construct even more sophisticated and integrated climate system models to investigate possible future climate changes. As the simulations for the future cannot be validated by data, the models have to be tested for past climates. This is the best way to determine their performance for a climate different from the present one. The successful simulation of different past climate states increases the confidence in the simulations for the future and also improves our knowledge about how the climate system works. This knowledge can then be used to further improve the models.

The traditional definition of climate, which is the definition that most people outside of climatology still refer to, was based on the mean atmospheric conditions: climate is averaged weather. The ocean and the biosphere are, thereby, seen only as static boundary conditions. This old definition has been replaced by a more integrated def-

inition, as, for example, found in Peixoto and Oort (1992) where climate is define as "the mean physical state of the climate system". This broader conception of climate includes not only the atmosphere but also recognizes that the ocean, the cryosphere and the biosphere are important parts of the climate system that are necessary to achieve a thorough understanding of the climate dynamics.

The realization that the biosphere also significantly influences the climate is, thereby, the most recent development, as coupled atmosphere-ocean GCMs[1] were seen as state-of-the-art climate models for quite some time. However, an increasing amount of studies (e.g. Levis and Foley 1999; Crowley and Baum 1997; Kubatzki and Claussen 1998; Wyputta and McAveney 2001) has shown that vegetation plays an important role in the climate system and that its consideration is fundamental to the understanding of climate changes, especially on the sub-continental scale (IPCC 2001). One example for its importance is the so-called Biome Paradox that stands for the phenomena that the winters during the Mid-Holocene were warmer than today in spite of decreased insolation. This warming could only be explained by including vegetation dynamics in addition to atmosphere and ocean dynamics, as it is the effect of the synergism between the taiga-tundra-feedback and the sea-ice-albedo feedback (Ganopolski et al. 1998a).

Studies of past climates have shown that, due to the different stability of circulation patterns and the fact that thresholds in the climate system are probably not static but change with the background climate (Ganopolski and Rahmstorf 2001), the climate system reacts differently to the same forcings at different climate states. This most likely also applies to the influence of the vegetation atmosphere feedback, so that it is necessary to investigate the role of this feedback during different climate states in order to fully understand its role and possible impact on the climate in general.

As it has been shown that the vegetation feedback and its synergism have had such an important influence during the Mid-Holocene (e.g. Biome Paradox), it is the motivation of this work to also explore the role of this feedback and its synergism for the last glacial period, which is known to have been very different from the current interglacial period. The difference between these two climate states can already be seen in the relative stability of the climate in the Holocene in contrast to the frequent and rapid climate changes (Dansgaard/Oeschger and Heinrich Events) during the glacial. Hence, it is very interesting to explore how the vegetation feedback and its synergism interact with the glacial climate and how it compares to the Holocene. The goal of this work is, therefore, to investigate the role of vegetation and the role of the atmosphere-vegetation feedback and its synergies during the last glacial period. In order to be able to solve this task, two tools are used: CLIMBER-2.3, a climate model of intermediate complexity, and the factor separation technique developed by Stein and Alpert (1993). CLIMBER-2.3 is used to perform equilibrium and transient experiments with different model setups for the LGM and part of the last glacial period from 60,000–20,000 years before present (60–20 ky BP). The factor separation method of Stein and Alpert (1993) is used to analyze the model results and to separate and quantify the influence of the atmosphere-

[1] GCM stands for General Circulation Models

vegetation feedback and its synergies.

The investigation of the atmosphere-vegetation feedback during the last glacial will be performed in two different ways:

- In equilibrium experiments for the LGM the influence of internal and external forcings compared to the effect of the interactive vegetation (as a feedback) are compared in order to determine the importance of the atmosphere-vegetation feedback. In addition, the relative importance of the other used forcings for the LGM will also be investigated and compared to existing studies for the LGM (chapter 5).

- Transient simulations for part of the last glacial period (60–20 ky BP) are performed to investigate the influence of the atmosphere-ocean and atmosphere-vegetation feedback and their synergy in the glacial climate of this period. Different reference states will be used and the results will be compared to results from the Mid-Holocene (chapter 6).

The two parts of this work are linked in the sense that in both studies the influence of the atmosphere-vegetation feedback during a glacial climate state is the main focus. Furthermore, the results from the transient experiment for the LGM will be compared with the results from the equilibrium experiments for the LGM, as far as this is possible due to the different factors that are analyzed in the two studies.

The climate at the LGM has been studied extensively, for example in the Paleoclimate Model Intercomparison Project (PMIP 2000). The studies that have been performed in this project were undertaken mainly with atmosphere-only models or coupled atmosphere-ocean models, using CLIMAP (1981) data as boundary conditions. This means that the vegetation was also prescribed in most of these studies, either to reconstructions or to the present day vegetation. The studies, in which vegetation reconstructions were used, have already shown that a realistic vegetation was able to cause changes large enough to reconcile data with model results in some places (Crowley and Baum 1997). Other studies have used atmosphere-vegetation models to explore the role of vegetation during the LGM (e.g. Kubatzki and Claussen 1998), but there the feedbacks with the ocean were missing. Only recently, coupled atmosphere-ocean-vegetation models have been used to investigate the climate at the LGM (e.g. Ganopolski 2003). This means that there are a number of studies that have already investigated the influence of a prescribed or interactive vegetation on the simulation of the climate at the LGM. Not so much work has been done so far on the consistent separation of the influence of the vegetation from the influence of forcings at the LGM, which then makes it possible to compare their effects in a consistent way. Therefore, this work will not so much focus on the comparison of model results with data, but will rather compare the effects of different forcings and feedbacks on the simulated climate at the LGM. For the last glacial period in general there have not been many transient studies with coupled atmosphere-ocean-vegetation models yet, so that it will be espe-

cially interesting to see, if the vegetation influence differs between 60,000 and 20,000 years BP. The explicit questions I want to answer in this work are the following:

- What is the role of the atmosphere-vegetation feedback and its synergies at the LGM compared to the effect of other factors?
- Where are the "hot-spots" of the atmosphere-vegetation feedback and are they the same as in the Holocene?
- What is the role of the atmosphere-vegetation feedback and its synergy with the atmosphere-ocean feedback compared to the atmosphere-ocean feedback during the glacial?
- Is the atmosphere-vegetation feedback more important at some time of the glacial (between 60–20 ky BP) than at others?
- How does the effect and importance of the atmosphere-vegetation feedback and its synergies compare to its effects in the Mid-Holocene, as found in earlier studies with CLIMBER?

Structure of the Thesis

The work starts in chapter 1 with a summary of the most important features of the glacial climate, including the description of the mechanism of Heinrich and Dansgaard/Oeschger events and the stability of the glacial ocean circulation, based on the theory proposed by Ganopolski and Rahmstorf (2001), which is later on used to explain and interpret the results. As the main focus of this work is on the role of feedbacks, chapter 2 gives an overview over the mechanisms of the most important feedbacks that I refer to in this work and to introduces the Stein and Alpert (1993) Factor Separation Technique. Chapter 3 provides a description of the climate model used in this work as well as a short comparison of the different climate model classes. The setup of all experiments is shown in chapter 4, while chapter 5 and chapter 6 contain the results and interpretation of the simulations. Since the motivation for this work was the previous investigation of the influence of the vegetation and its feedbacks with the climate system during the Holocene, an important part of this work is the comparison of the results from the glacial climate with results from the Holocene (at the end of chapter 6). A summary of the main results and the conclusions that can be drawn from them are presented in chapter 7, as well as an outlook that shows questions that have emerged from the work performed and possible future tasks that could help to complete the picture and improve the understanding of the climate system and especially the role that vegetation dynamics play in it.

Chapter 1

Glacial Climate

1.1 The Last Glacial Period

The last glacial period lasted from about 110 ky BP to 14 ky BP. Based on the analysis of the oxygen-isotope ratio of microfossil shells in marine sediment cores, the glacial-interglacial periods are referred to as marine isotope stages (MIS), starting with the current interglacial that is named MIS 1. The last glacial period is, therefore, also referred to as MIS 4 – MIS 2. The peak of the last glacial, called the Last Glacial Maximum (LGM), is today defined[1] as the climate at 21±2 ky BP (Mix et al. 2002). The PMIP (2000) studies showed a range of modeled global annual temperatures for the LGM, with a cooling of 6–2° C, compared to today.

At the LGM, the inland ice sheets reached their maximum extent and covered about 28.5 million square kilometers of land that is at present ice free, with the Laurentide ice sheet that covered North America being the largest ice sheet. The increase in inland ice was a slow process that took several ten thousand years and that was coupled with a decrease in sea-level that reached a level of 115 m below present day at the LGM (Peltier 1994). This sea level drop caused a closing of the Bering Strait and the exposure of additional land areas. The closing of the Bering Strait had the consequence that less heat was transported into the Arctic Ocean from the North Atlantic, and so it cooled much more than would be expected just as a result of the colder air temperatures. Together with the larger meltwater runoff into the Arctic Ocean, the conditions for sea-ice expansion were good (Dawson 1992), so that at the LGM sea-ice cover extended southwards to 60° N in summer and 40° N in winter (Crowley and North 1990; Dawson 1992) while at present it only reaches south to about 78° N in winter. The increase in sea-ice in turn caused a southward shift of the Atlantic storm tracks to the new margin of the sea-ice area, changing the precipitation pattern over the Atlantic and

[1] Until about 15 years ago, the time around 18 ky BP was referred to as LGM, based on the results of the radiocarbon method, so that sometimes the LGM is still dated as 18 ^{14}C ky BP instead of 21 calendar ky BP.

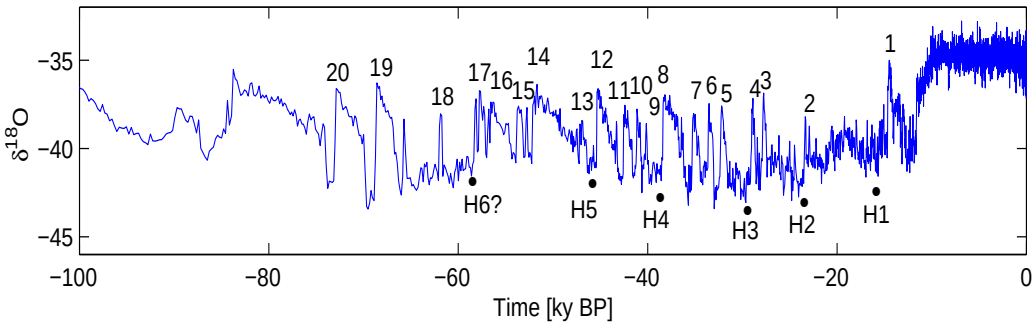

Figure 1.1: Record of δ^{18}O [in ‰] from the GISP2 core (Grootes and Stuiver 1997; Grootes et al. 1993; Stuiver et al. 1995) for the last glacial up to today as a proxy of atmospheric temperatures over Greenland. D/O events are numbered above the curve while HE are marked below the curve by black dots and numbers.

over Europe during the glacial compared to today. In North America, the Laurentide ice sheet caused a shift of precipitation to the south as well.

The inland ice sheets caused a global albedo of about 0.22 at the LGM with much higher values directly over the ice sheets so that the cooling was especially strong there while it was not so strong in the tropics. This led to a stronger pole-equator temperature gradient that caused globally increased windspeeds. This could be inferred from the higher dust concentrations in ice cores for the glacial period when compared to today, that also show that the glacial climate was in general dryer than at present.

Climate reconstructions from ice cores and other climate archives (see Voelker et al. 2002 for an overview of data) also show that the last glacial period was perturbed by rapid temperature changes with a large amplitude (Fig. 1.1), the so-called Dansgaard/Oeschger events (D/O events) (Dansgaard et al. 1982, 1993) and Heinrich events (HE) (Heinrich 1998).

D/O events

Even though D/O and Heinrich events have received much interest in recent years, neither the physical mechanism of them nor their effects on the climate system are yet fully understood (Claussen et al. 2003). What is known is that D/O events are characterized by a rapid warming of 5–10 °C within a few decades in Greenland and the North Atlantic, followed by a warm plateau phase with a slow cooling over several centuries that is terminated by an abrupt temperature drop back to stadial conditions (Fig. 1.1). The waiting time between two events is often around 1500 years, but sometimes it also increases to 3000 years or even 4500 years (Alley et al. 2001). Paleoclimate reconstructions show (e.g. Voelker et al. 2002) that D/O events are not just seen in the North Atlantic, even though there their influence is largest, but that they are seen in many climate records world wide, with records on the Southern Hemisphere (SH) showing a

cooling when the Northern Hemisphere (NH) is warming, a phenomenon that is called the bipolar see-saw effect (Stocker 1998).

In order to explain D/O events, several suggestions have been made, with most of them involving the thermohaline circulation of the Atlantic. Most of these suggestions claim that some perturbation of the hydrological cycle at high northern latitude influences the Atlantic thermohaline circulation so that it is either weakened (e.g. Broecker et al. 1990; Birchfield et al. 1994; Winton and Sarachik 1993), shifted southwards (Rahmstorf 1994, 1995; Ganopolski and Rahmstorf 2001) or completely shut down (Broecker et al. 1985) during the cold phase of D/O events. The cause of the perturbation differs from one suggestion to another, reaching from an external freshwater forcing to internal oscillations. In other suggestions, the tropics as seen as the main driver of D/O events, via changes in the Indian and Asian monsoon (Leuschner and Sirocco 2000; Kudrass et al. 2001) or changes in the El Niño-Southern Oscillation system (Clements and Cane 1999; Cane and Clements 1999).

Claussen et al. (2003) have investigated the question of the location of the trigger of D/O events with CLIMBER-2 by exploring the global-scale response of the glacial climate to perturbations of the hydrological cycle in the tropics versus the high latitudes. They found out that perturbations of the tropical Sea Surface Temperature (SST) are unlikely to be the trigger for D/O events via the mechanism of oceanic heat transport and atmospheric transport of heat and moisture because the resulting changes in the North Atlantic are too small to cause D/O events with global signatures as seen in the data.

Ganopolski and Rahmstorf (2001) showed with CLIMBER-2 that a shift of the North Atlantic Deep Water formation site (NADW) can explain many observed features of D/O events like their spatial pattern, the bipolar sea-sea effect (Stocker 1998) and also the described three-phase evolution of D/O events in time. The exact mechanism they propose is that the rapid warming of the D/O events is a result of a rapid northward shift of the thermohaline circulation due to a jump of the NADW formation site towards the north, into a so-called "warm" (or interstadial) glacial mode of the circulation. The warm plateau phase of the D/O event is caused by the slow weakening of the circulation because this "warm" mode is not stable during glacial times (Ganopolski and Rahmstorf 2001). When a threshold is passed, the circulation flips back to the stable "cold" (or stadial) glacial mode, with the NADW formation site further in the south that causes the cooling back to stadial conditions as seen in the Greenland ice cores . To start the D/O events in the model, a small trigger is necessary in order to cause the flip to the "warm" glacial ocean mode. As soon as the D/O event is triggered, it then follows its own internal dynamics and does not need an additional forcing (Ganopolski and Rahmstorf 2001). The exact nature of the trigger of D/O events is, thereby, still unknown and actively debated, with some solar cycle being the prime suspect (Bond et al. 2001; Van Geel et al. 1999; Braun et al. 2004). To trigger the D/O events in their model Ganopolski and Rahmstorf (2002) have prescribed a freshwater forcing (of unknown origin) in the North Atlantic that consists of a small periodic forcing (with the period of 1500 years) and white noise, so that via stochastic resonance (Rahmstorf and Alley 2002) D/O events were triggered that agree well with climate reconstructions.

The switch to the "warm" glacial mode occurs when the freshwater forcing in the Nordic Seas decreases far enough to cross the threshold of the glacial ocean circulation (Ganopolski an Rahmstorf 2001). The same kind of forcing used by Ganopolski and Rahmstorf (2002) was also used for the experiments over the glacial period in this work to trigger D/O and Heinrich events.

Heinrich Events

Heinrich events are spaced at irregular intervals of some 10,000 years (Fig. 1.1). They are characterized by distinct layers of coarse grain material in the sediment of the North Atlantic which has been identified as ice rafted debris, carried out into the ocean by massive iceberg discharges. The spatial distribution of the ice rafted debris suggests that the main source of the icebergs discharge was the Laurentide ice sheet (Bond et al. 1992; Chappel 2002). Sediment data shows that during HE the NADW formation was greatly reduced or even shut down, due to the large freshwater perturbation in the North Atlantic caused by the icebergs (Broecker et al. 1992). The effect of HE on climate is a cooling of the subtropical Atlantic and a warming of the Southern Hemisphere while Greenland does not experience a pronounced cooling. This is consistent with the above explained theory by Ganopolski and Rahmstorf (2001) that explains D/O events as the results of a latitudinal shift in NADW formation, as HE occur when the system is already in a stadial mode so that NADW formation is taking place south of Greenland before a HE starts. A further weakening or even a collapse of the circulation does, therefore, not influence Greenland temperatures very much while they do lead to a considerable cooling in the subtropical Atlantic and a warming of the Southern Ocean (Ganopolski and Rahmstorf 2001). In most Antarctic sites HE are associated with a warming that is much stronger than during other stadials, as a result of an even stronger see-saw effect due to the collapse of the circulation (Blunier et al. 1998; Crowley 1992; Stocker 1998). The "off" mode of the circulation during HE is not a stable state in the glacial, so that as soon as the freshwater forcing stops, the circulation starts up again, causing a warming back to interstadial conditions. These interstadials that follow HE are in most cases particular warm and it is also seen in the data that successive D/O events tend to become progressively colder until the next HE starts (referred to as Bond cycle).

1.2 Stability of the Glacial Ocean Circulation

It already became apparent in the explanation of D/O and Heinrich events in the previous paragraph that the ocean plays a very important role in the climate system of the glacial. Therefore, I will give a short overview of the theory by Ganopolski and Rahmstorf (2001) about glacial ocean stability, as this will be an important aspect in the interpretation of my results later on.

Various modeling studies showed that the Atlantic thermohaline circulation is sensitive to freshwater input in the North Atlantic and that it is a non-linear system with thresholds for transitions between qualitatively different ocean circulation modes (e.g. Weaver and Sarachik 1991; Ganopolski and Rahmstorf 2001). Ganopolski and Rahmstorf (2001) have shown that the stability pattern of glacial climates differs from today's. They found that a freshwater input in the tropics did not yield a clear bifurcation point where the circulation collapses as seen for the present day ocean, but that the glacial ocean shows a smoother, less non-linear response in form of a gradual shift to the south combined with a shallower circulation. For freshwater input in the Nordic Seas (50-70° N), however, the glacial climate was much closer to the bifurcation point already so that even a small negative anomaly (a small decrease in freshwater flux) caused the circulation to jump from the "cold" glacial mode to the "warm" glacial mode (see Fig. 1 in Ganopolski and Rahmstorf 2001 for the stability diagram for present day and glacial climate). Following the theory of Ganopolski and Rahmstorf (2001), the "warm" glacial mode is, thereby, not a stable state in the glacial, in contrast to the present day where the "warm" interglacial mode is one of the two stable modes of the ocean. The other stable mode of the present day ocean would be an "off" mode with a collapsed circulation, but this "off" mode is also not stable in the glacial. During the glacial, the only stable ocean mode is the "cold" conveyor mode with NADW formation south of Iceland, so that D/O and Heinrich events are only transient phenomena because they are both caused by unstable ocean modes that have to return to a stable state (Ganopolski and Rahmstorf 2001). That D/O events are longer and occur more frequently during the earlier, warmer part of the last glacial period and become increasingly shorter and spaced longer appart towards the LGM is explained by Ganopolski and Rahmstorf (2001) as a result of the changing stability of the "cold" mode during the glacial, which, due to colder temperature, becomes more stable towards the LGM. Since it gets harder to trigger flips to the "warm" mode when the "cold" mode is more stable, this explains why during the warmer part of the glacial the D/O events occur almost every 1500 years, while they are spaced longer apart in full glacial conditions between 30–20 ky BP. They also found that the duration of the D/O events is only weakly dependent on the forcing which triggers the event, but that a warmer background climate leads to longer events due to a more stable "warm" mode and, therefore, a longer decay time in a warmer glacial climate (Ganopolski and Rahmstorf 2002).

1.3 Orbital Forcing

The seasonal and latitudinal distribution of energy received from the sun is modulated by oscillations of the earth's orbital parameters, especially from the precession of the equinoxes (19,000 and 23,000 years cycle), changes in the eccentricity of the earths orbit (400,000 and 101,000 years cycle) and the obliquity (41,000 years). The eccentricity of the earths orbit is, thereby, the only parameter that changes the globally and annually averaged solar radiation received by the earth, while the precession of the equinoxes

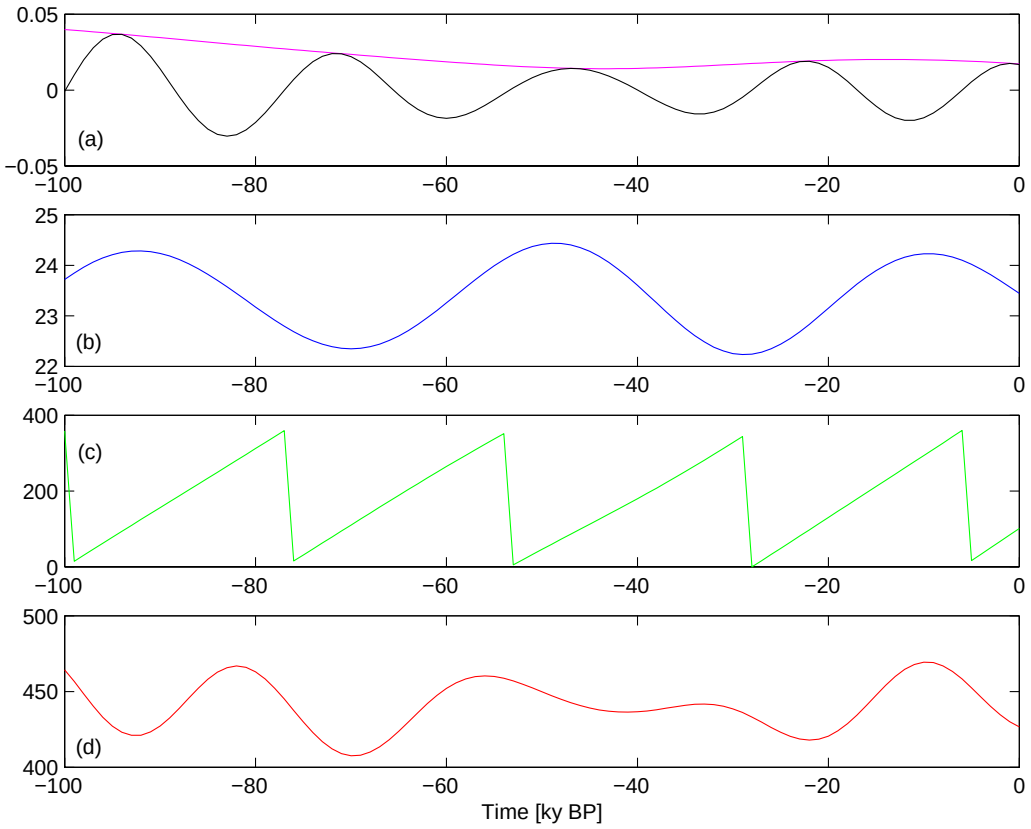

Figure 1.2: Insolation changes during the last glacial (Berger and Loutre 1991). In (a) the eccentricity (magenta) and the climatic precession (black) are shown. (b) shows the obliquity [in °] (blue) and (c) the longitude of the perihel [in °] (green) and in (d) the insolation in 65N for July in W/m^2 (red).

and the obliquity change the seasonal and latitudinal variation of the insolation.

The theory of orbital forced glacial-interglacial cycles was first proposed by Milankovitch in 1930, but was abandoned again when first conflicts with estimates from data about the timing of the ice ages occurred. When longer and better climate records became available, it was recognized through spectral analysis that indeed the dominant variation in the ice ages was a 100,000 years cycle (Broecker and van Donk 1970) and that also a 41,000 and 23,000 years cycle was present in the data (Hays et al. 1976). The insolation theory of Milankowitch was, therefore, revived in order to explain at least part of the glacial-interglacial cycles, but it continues to be disputed even today (see Muller and MacDonald (2000) for an overview and history of the astronomical causes of ice ages).

During the 40,000 year long period investigated in this work, the orbital parameters and consequently the insolation changed (Fig. 1.2). At the LGM, the orbital parameters were very similar to today, with the obliquity being 22.95° at the LGM and 23.45° today.

The position of the equinoxes was found at January 15 in the LGM and at January 3 today. The considerable larger inland ice sheets in the LGM compared to today, in spite of the almost equal orbital parameters at the LGM and today, are a result of the dependance of the ice sheets on the total insolation changes of the previous tens of thousands of years (Webb et al. 1993).

1.4 Climate Reconstructions

Past climates have been reconstructed from various records like ice cores, deep sea sediment cores, lake sediment cores, corals, tree rings and fossils using various climate proxies. The methods used to extract information about the climate (e.g. information about temperature, precipitation rates, atmospheric composition, vegetation distribution) from these records and to date them are described in great detail in many climate textbooks (e.g. Muller and MacDonald 2000; Peixoto and Oort 1992) that I want to refer to for further information.

Climate reconstructions are used to compare model results with them in order to test the performance of the models. For this comparison and also to force models with past climate boundary conditions, global climate reconstruction for past climates were needed instead of just local reconstructions. In 1971, CLIMAP (Climate Long-Range Investigation, Mapping and Prediction) was started in order to collect reconstructions from various sites from all over the globe and combine them to a map of the LGM climate state. The variables from CLIMAP were then used in modelling studies like PMIP (2000) (Paleoclimate Model Intercomparison Project) as boundary conditions for different models or as a tool for evaluating the model results. The CLIMAP data set is still used today, even though some parts are controversial due to better estimates today. This is especially true for the LGM tropical SSTs that are probably too high in CLIMAP and for the inland ice sheets that are, according to more recent estimates, also too high in CLIMAP (Peltier 1994).

Chapter 2

Feedbacks in the Climate System

2.1 Natural Feedbacks

The components of the climate system (atmosphere, hydrosphere, cryosphere, pedosphere and the biosphere) are connected via the fluxes of energy, substances and momentum. Their interactions are called feedbacks and they are non-linear processes that can have a pronounced impact on the sensitivity of the climate system to the external forcing, leading either to abrupt changes or to multiple equilibrium states. Feedbacks are divided into positive and negative feedbacks corresponding to their effect of either amplifying or dampening an initial external signal.
It is important to note that also feedbacks interact with each other and that these so-called synergies amplify or attenuate the final response of the system to an initial signal. Here, I first want to give an overview over the feedbacks that will turn out to be important for my work, before I start explaining their interactions (see also Claussen (2004) for a more detailed description of feedbacks).

2.1.1 Feedback Loops

On the following pages, feedback loops are described and visualized in figures. In these figures, the "+" sign always stands for a direct correlation (e.g. when temperature decreases, tree fraction also decreases) while the "−" sign stands for an anticorrelation (e.g. albedo increases but temperature decreases).

Water Vapor and Cloud Feedbacks

The water vapor feedback is a positive feedback because an increase in atmospheric water vapor, which is the strongest greenhouse gas, leads to a temperature increase due to the trapped radiation in the atmosphere that would otherwise escape. This warming increases the evaporation of water and also the water vapor saturation level

(Clausius-Clapeyron-Equation), leading to a further increase of water vapor in the atmosphere (Fig. 2.1).
If water vapor condensates and forms clouds, it can have a cooling or a warming effect. The global effect of clouds is not yet fully understood, but it is believed that cumulus clouds cause a net cooling because they reflect the incoming shortwave radiation at their bright tops while cirrus clouds, due to their absorption of outgoing longwave radiation, warm the atmosphere.

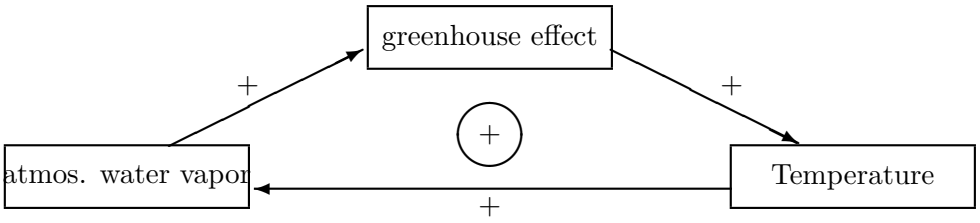

Figure 2.1: Water Vapor Feedback.

Snow/Ice-Albedo Feedback

There is a relation between the area covered by snow/ice (or the time an area is covered by snow/ice) and the temperature that is of the following nature: If the temperature drops, the snow/ice area extends or the time of snow/ice cover is extended. Because of the high albedo of snow/ice, this increases the surface albedo of the earth, leading to less absorption of incoming radiation and, therefore, an even more pronounced cooling. In addition, an extended time or area of snow/ice cover allows less heat flux from the ground/ocean to the atmosphere, which also leads to a further cooling of the atmosphere. In the opposite direction, a warming decreases the snow/ice area or the time of an snow/ice cover and over the now increased heat flux from the ground/ocean and the deceased albedo the initial warming is intensified. Hence, the snow/ice-albedo

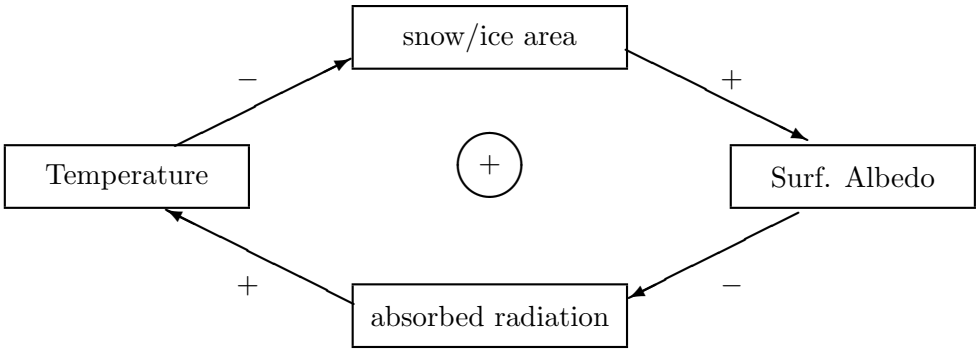

Figure 2.2: Snow/Ice-Albedo Feedback

feedback has the form of a positive feedback loop, amplifying an initial signal. The feedback loop is also shown in Figure 2.2. It is often referred to as the sea-ice-albedo effect.

Thermohaline Feedback

In the region of Atlantic deep water formation, a negative feedback exists that is caused by the thermohaline circulation: An increased SST causes a lower density of the surface water, leading to a decreased thermohaline overturning followed by less oceanic northward heat transport, thus reducing the SST and damping the initial signal (see also Figure 2.3.

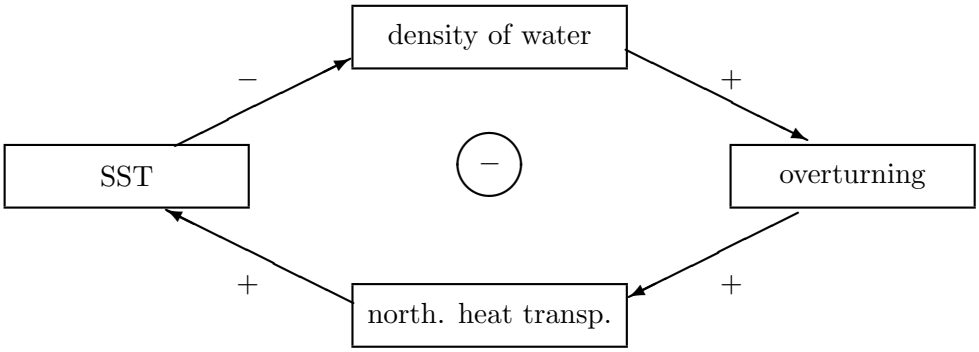

Figure 2.3: Thermohaline Feedback

Vegetation-Albedo Feedback

The albedo difference between grass and trees is only small so that a pure vegetation-albedo feedback is not able to cause big temperature changes. Nevertheless, especially when desert is replaced by vegetation, the lower albedo of trees compared to grass and grass compared to desert leads to an albedo induced warming, if trees replace grass or grass replaces desert, making the vegetation-albedo feedback a small but sometimes important positive feedback (see also Figure 2.4).

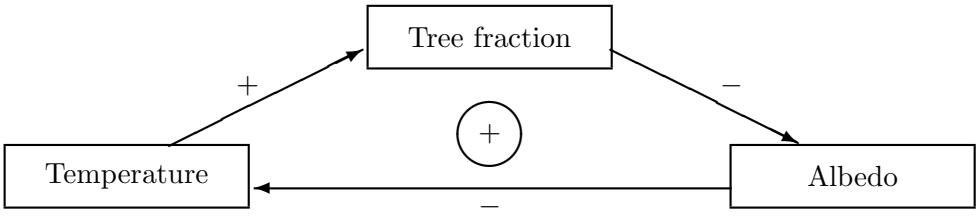

Figure 2.4: Vegetation-Albedo Feedback

Vegetation-Snow-Albedo Feedback

As soon as vegetation is snow-covered the albedo difference between trees and grass increases. This is due to the snow-masking effect of trees which greatly reduces the albedo of snow-covered forests compared to the albedo of snow-covered low vegetation like grass. Deforestation is then causing an increase of albedo that leads to a cooling due to less absorbed incoming radiation, which in turn triggers a further retreat of trees. Hence, the vegetation-snow-albedo effect is a positive feedback (as shown in Figure 2.5). It is important to note that the vegetation-snow-albedo effect is most significant in the snow thawing season in spring and early summer because there its effect either increases the duration of the snow-cover (for deforestation = cooling) or shortens it (for afforestation = warming). This feedback is often referred to as the taiga-tundra feedback.

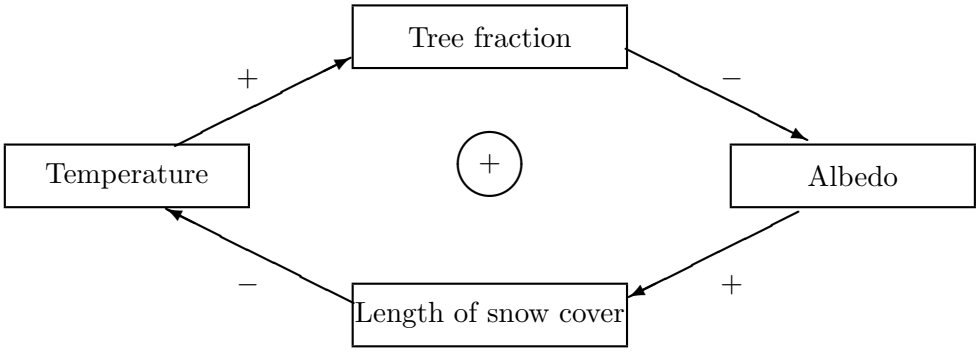

Figure 2.5: Vegetation-Snow-Albedo Feedback

Hydrological Feedback

Hydrological feedbacks are effective mainly in the growing seasons. They can work in both directions, with the direction depending on the time of day, the season and the region looked at (see also Claussen 2004). On annual average in high northern latitudes a negative hydrological feedback dominates: An initial reduction in temperature leads to a decrease in tree fraction. Since trees have a higher productivity, this causes a decrease in productivity and transpiration and thus a reduction of evaporative cooling (less latent heat flux) which warms the near surface atmosphere. This in turn causes an increase of trees, damping the initial signal. Therefore, this hydrological feedback is negative. It gets complicated, if one considers that a reduction of transpiration could reduce local rainfall and, therefore, hamper the regrowth of vegetation, which would then represent a positive feedback. Also, the near surface warming caused by a reduction in transpiration can be amplified further by a reduction in cloudiness and thus an increase in insolation, giving a negative feedback. The hydrological feedback loop, with its side-loops is shown in Figure 2.6.

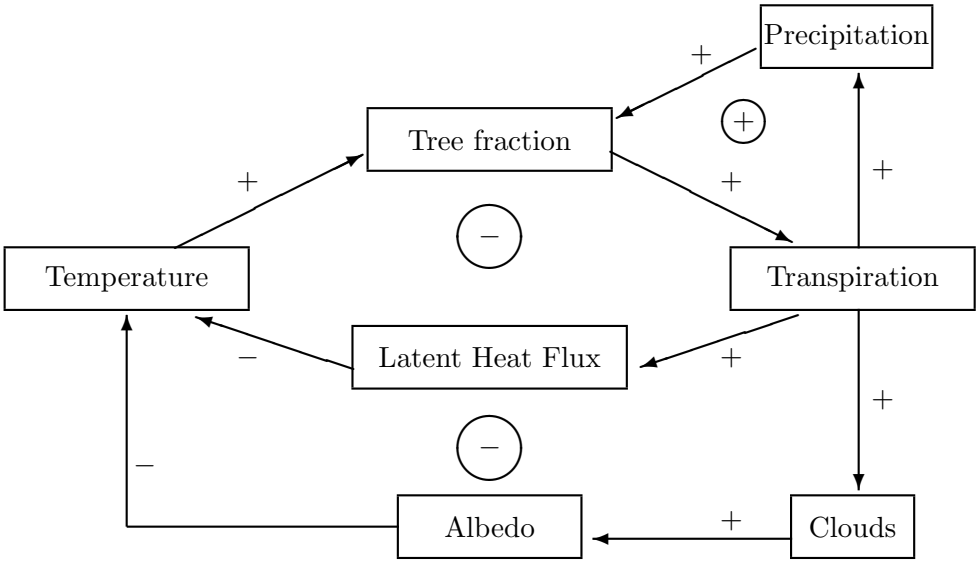

Figure 2.6: Hydrological Feedback, with side-loops

Biogeochemical Feedbacks

Beside biogeophysical[1] vegetation-atmosphere feedbacks there are also biogeochemical feedbacks which are caused by changes in biomass. One possible biogeochemical feedback is the CO_2 effect which is a negative feedback because an initial increase in biomass leads to a stronger CO_2 uptake by the vegetation so that atmospheric CO_2 concentrations drop, causing the greenhouse effect to become smaller and thus leading to a global surface cooling which reduces biomass (Fig. 2.7).

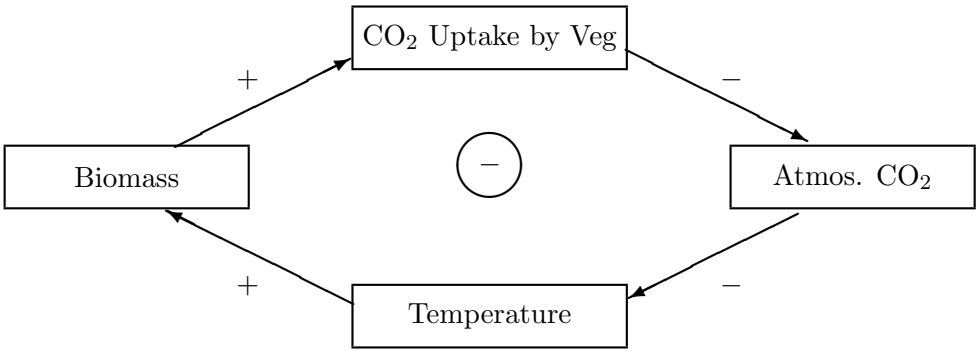

Figure 2.7: Biogeophysical CO_2 Feedback

[1]Biogeophysical feedbacks are caused by changes in surface structure due to vegetation influence. This means that the vegetation-albedo feedback as well as the vegetation-snow-albedo and the hydrological feedback belong to this class (Claussen et al. 2001).

2.1.2 Interaction and Importance of Feedbacks

Seasonal Dominance of Feedbacks

Which effect dominates when vegetation changes occur, depends on the timescale, season and place considered (see also Claussen et al. 2001; Brovkin et al. 2003). In high northern latitudes with seasonal snow cover, the annual contribution of the hydrological effect is much smaller than that of the radiative vegetation-snow feedback. The seasonal response differs from the annual response because the relative importance of the hydrological and radiative feedbacks factors changes over the year. In winter, changes in albedo due to vegetation changes do not have a pronounced effect due to the fact that the small amount of incoming radiation and the hydrological feedback is not active at all. This makes the negative oceanic thermohaline feedback the strongest feedback during winter. During the snow thawing season, when there is still snow on the ground, the radiative effects of vegetation and sea-ice are dominant, while the hydrological effect is not significant. In summer, the radiative effect is small due to the small albedo difference between trees and grass, while the hydrological effect is at its peak and dominates the overall effect until the end of the growing season in fall. In regions that are permanently snow free like the tropics, the changes of surface albedo are only due to the vegetation-albedo effect and are, therefore, very small. Due to the long growing season, the hydrological effect is quite important in the tropics, so that, overall, the hydrological feedback is dominant there.

Sensitivity of the Climate System to Changes in Forest Cover

Brovkin et al. (2003) have investigated the sensitivity of the climate system to changes in forest cover and found that the sensitivity is smaller for a warm climate than it is for a cold climate. This leads to a smaller temperature change due to deforestation with increasing temperature. The explanation they offer is that the warmer the climate, the earlier the snow melts and, therefore, the change in albedo due to the absence of forest is less important. In addition, a warmer climate with earlier snow melt also leads to a longer growing season, so that the negative hydrological effect is more important, thus reducing the already small radiative cooling even further. Another result of Brovkin et al. (2003) is that the climate sensitivity is higher for low values of tree fraction than for high values of tree fraction. This is the case because the higher the tree fraction, the higher is the snow masking effect, which leads to an overall lower albedo than for a smaller tree fraction. The lower albedo causes an earlier snow melt due to increased absorption of radiation. The earlier snow melt in turn weakens the positive radiative feedback and strengthens the negative hydrological feedback because of the increased duration of the growing season. In addition, due to the increased biomass, the hydrological effect is much stronger for a higher tree fraction than it is for a smaller one. All this leads to an overall smaller climate sensitivity for a higher tree fraction (Brovkin et al. 2003).

Importance of Feedbacks

Interactions of feedbacks, called synergism, are really important because they can often explain the behavior of the climate system that we cannot understand, if we only look at the feedbacks separately. One appropriate method to separate feedbacks from their synergies is explained in the next section (2.2) of this chapter.

An example for the importance of synergies is the so-called "Biome-Paradox" during the Holocene that can only be explained with the synergism between a biogeophysical and an atmosphere-ocean feedback (Ganopolski et al. 1998a).
The most important synergism in high northern latitudes is the interaction of the vegetation-snow-albedo effect and sea-ice-albedo effect. This synergy is a result of a vegetation induced cooling the high latitudes, which is most pronounced in spring and winter, thus allowing sea-ice to extent further. This in turn leads to a further cooling due to the sea-ice-albedo effect, which inhibits vegetation growth. As a result of this interaction, these two positive feedbacks greatly amplify the overall response of the climate system especially in the Northern Hemisphere.

2.2 Stein and Alpert Factor Separation Technique

The factor separation method has been developed by Stein and Alpert (1993) to isolate the pure contributions of different processes in a climate change signal as well as the influence and importance of their synergistic effects (Berger 2001).
Unfortunately, the synergy effects are ignored in many studies and the difference between an experiment where one factor is switched on and one in which it is turned off, is interpreted as the contribution caused by the factor alone. It has been shown in the past (e.g. in Ganopolski et al. 1998a; Mailhot and Chouinard 1988), that the synergistic effect is sometimes larger and maybe even of the opposite sign than the pure contribution alone, therefore, making the simple difference map between the runs highly misleading. The synergy terms are the result of the highly non-linear processes in the climate system (Berger 2001) and the technique developed by Stein and Alpert is a simple and consistent method to calculate the contribution of factors and synergistic terms to a signal.

Factor Separation for Two Factors

Applied to two processes, four experiments are needed in order to separate the factors. The first simulation is the reference simulation S_0 where none of the two factors is active. The second experiment is the fully coupled experiment S_{12} which includes both factors. In the two other simulations one component at a time will be coupled to the reference run while the other stays inactive, called experiments S_1 and S_2. From the Taylor expansion of any function of two variables the factor separation technique gives:

$$S_{12} = \hat{f}_0 + \hat{f}_1 + \hat{f}_2 + \hat{f}_{12} \tag{2.1}$$

with $\hat{f}_1$, $\hat{f}_2$, $\hat{f}_{12}$ and $\hat{f}_0$ representing the individual pure contribution of the first factor, the second factor, their synergy and the contribution that is independent of both factors. Following the theory of Stein and Alpert (1993), they are calculated using the following relationships:

$$\begin{aligned} \hat{f}_0 &= S_0 && (2.2)\\ \hat{f}_1 &= S_1 - S_0 && (2.3)\\ \hat{f}_2 &= S_2 - S_0 && (2.4)\\ \hat{f}_{12} &= S_{12} - S_1 - S_2 + S_0 && (2.5) \end{aligned}$$

It can be seen in equation (2.1) that the difference between the reference simulation S_{12} and the fully coupled simulation $S_0 = \hat{f}_0$ consists of the sum of $\hat{f}_1$, $\hat{f}_2$ and $\hat{f}_{12}$ and, therefore, all four simulations are necessary in order to fully separate the factors.

Factor Separation for n-Factors

In principle, the factor separation technique can be extended to as many factors as desired. When choosing the number of factors to be analyzed, however, one should consider that the number of simulations necessary increases with 2^n (Stein and Alpert 1993). For n-Factors the full simulation looks like the following:

$$S_{123\ldots n} = \hat{f}_0 + \sum_{i=1}^{n} \hat{f}_i + \sum_{i,j=1,2}^{n-1,n} \hat{f}_{ij} + \sum_{i,j,k=1,2,3}^{n-2,n-1,n} \hat{f}_{ijk} + \ldots + \hat{f}_{123\ldots n} \qquad (2.6)$$

In equation (2.6) $\hat{f}_i$ is the pure contribution of the factor i, $\hat{f}_{ij}$ is the contribution of the pure synergy between factor i and j ($i \neq j$), $\hat{f}_{ijk}$ the effect only caused by the synergy between the three factors i, j, k ($i \neq j \neq k$) and $\hat{f}_{123\ldots n}$ the synergy effect between all n factors that are considered. If one factor $i, j, k, \ldots, n$ is switched off, all synergy terms including it become zero and are not noted. This means that depending on how many factors one looks at, the applied equation (2.6) becomes:

$$\begin{aligned} S_0 &= \hat{f}_0 && && && (2.7)\\ S_i &= \hat{f}_0 + \hat{f}_i && i &= 1,\ldots,n && && (2.8)\\ S_{ij} &= \hat{f}_0 + \hat{f}_i + \hat{f}_j + \hat{f}_{ij} && i,j &= 1,\ldots,n && i \neq j && (2.9)\\ S_{ijk} &= \hat{f}_0 + \hat{f}_i + \hat{f}_j + \hat{f}_k + \hat{f}_{ij} + \hat{f}_{ik} + \hat{f}_{jk} + \hat{f}_{ijk} && i,j,k &= 1,\ldots,n && i \neq j \neq k && (2.10)\\ &\vdots\\ S_{123\ldots n} &= \hat{f}_0 + \sum_{i=1}^{n} \hat{f}_i + \sum_{i,j=1,2}^{n-1,n} \hat{f}_{ij} + \sum_{i,j,k=1,2,3}^{n-2,n-1,n} \hat{f}_{ijk} + \ldots + \hat{f}_{123\ldots n} && && && (2.11) \end{aligned}$$

Equations (2.7–2.11) contain

$$\binom{n}{0}, \binom{n}{1}, \binom{n}{2}, \ldots \binom{n}{n}$$

equations, respectively. This gives 2^n equations for 2^n unknowns $\hat{f}_0$, $\hat{f}_1$, $\hat{f}_2$, $\ldots$, $\hat{f}_n$, $\hat{f}_{12}$, $\ldots$, $\hat{f}_{123\ldots n}$. The equations are solved by recursive elimination of $\hat{f}_i$ from equation (2.8), then $\hat{f}_{ij}$ from equation (2.9) and so forth. Following Stein and Alpert (1993), the general solution for $\hat{f}_{i_1,i_2,\ldots,i_r}$ (with $0 \leq r \leq n$) then becomes:

$$\hat{f}_{i_1,i_2,\ldots,i_r} = \sum_{m=0}^{r} (-1)^{r-m} \left(\sum_{j_1,j_2,\ldots,j_m = i_1,i_2,\ldots,i_m}^{i_{r-m+1},i_{r-m+2},\ldots,i_r} S_{j_1,j_2,\ldots,j_m} \right) \tag{2.12}$$

The sum $\left(\sum_{j_1,j_2,\ldots,j_m = i_1,i_2,\ldots,i_m}^{i_{r-m+1},i_{r-m+2},\ldots,i_r} S_{j_1,j_2,\ldots,j_m} \right)$ is the sum over all combinations (without repetition) of r elements out of the class m and has, therefore, $\binom{r}{m}$ summands[2] which gives 2^r terms.
Applied to three factors, (2.12) gives (also compare to (2.2–2.5):

$$\hat{f}_0 = S_0 \tag{2.13}$$
$$\hat{f}_1 = S_1 - S_0 \tag{2.14}$$
$$\hat{f}_2 = S_2 - S_0 \tag{2.15}$$
$$\hat{f}_3 = S_3 - S_0 \tag{2.16}$$
$$\hat{f}_{12} = S_{12} - (S_1 + S_2) + S_0 \tag{2.17}$$
$$\hat{f}_{13} = S_{13} - (S_1 + S_3) + S_0 \tag{2.18}$$
$$\hat{f}_{23} = S_{23} - (S_2 + S_3) + S_0 \tag{2.19}$$
$$\hat{f}_{123} = S_{123} - (S_{12} + S_{13} + S_{23}) + (S_1 + S_2 + S_3) - S_0 \tag{2.20}$$

A similar way to calculate the pure contributions and synergistic effects is the extended factor separation technique (Kubatzki 2000; Kubatzki et al. 2000) and the extended classical feedback analysis (Claussen 2001). The extended classical feedback analysis originates from the classical feedback analysis that is used in electrical engineering and was first applied to climate dynamics by Peixoto and Oort (1992). In its original form it does not account for synergy effects, which is the reason why Claussen (2001) extended it.

Limitations of the Factor Separation Technique

In the attempt to separate the pure contributions from the non-linear synergy effects, the result is dependent on the factors chosen. Effects or contributions called "pure" anywhere in this thesis are only pure in respect to the other factors chosen. The calculated pure effects and synergistic terms also include the effects and synergies of

[2] This is true following the combination theory. Since it is also true that $\binom{n}{k} = \frac{n!}{k!(n-k)!}$ and $\sum_{k=0}^{n} \binom{n}{k} = 2^n$ this is the mathematical explanation why 2^n simulations are needed for the separation of n factors.

processes that are not explicitly looked at. The result also depends on the reference state, as the factors are deviations from that state. This means that what the factor separation technique accomplishes is to isolate an effect from all other factors also looked at, but it does not isolate it from all processes present in the model (Stein and Alpert 1993; Berger 2001). It also does not give its overall importance but its effect relative to the reference state it is compared to. Different reference states, therefore, yield different results. In respect to my work this means that synergy effects especially with the water vapor and the ocean are not separated because they are not factors looked at here. Another aspect is that no feedbacks with the cryosphere can appear as inland ice cover is prescribed and cannot change.

Taking into account all processes in the model would not be possible because of the fast increasing number of simulations necessary (2^n). In a first attempt to look at a high number of interesting factors, the number of simulations can be greatly reduced, if one restricts the calculation of factors to their pure effects and the synergy effects of each two factors. After this first look it becomes clear which factors and synergy terms are important and might, therefore, be worth a second look, so that only for them a full factor separation would then be performed.

Comparison with Taylor Expansion

The Factor Separation Technique by Stein and Alpert can also be interpreted as a Taylor Expansion[3] of a function of many variables (Dutrieux and Berger 1997). The sum of all terms with the partial derivatives of a single variable x_i in the Taylor Expansion can be identified with the pure contribution of the factor i in the factor separation method. The appropriately grouped terms of the mixed partial derivatives (with two, three, four, ... variables) in the Taylor expansion can then be set equal to the synergy terms of two, three, four, ... variables in the method of Stein and Alpert. Since the partial derivatives of higher order in the Taylor Expansion are seen as a symptom of the non-linearity of the system, the synergy terms can also be interpreted in this way (see Dutrieux and Berger (1997) for a more detailed description and the full comparison between Taylor Expansion and the Stein and Alpert Factor Separation Technique).

[3] A Function $F(x_1, x_2, \ldots, x_n)$ of n variables can be developed into a Taylor expansion around the point $\vec{x_0} = (x_{10}, \ldots, x_{n0})$:

$$F(x_1, x_2, \ldots, x_n) = \sum_{m=0}^{\infty} \frac{1}{m!} \left(\Delta x_1 \frac{\partial}{\partial x_1} + \ldots + \Delta x_n \frac{\partial}{\partial x_n} \right)^m F(x_{10}, \ldots, x_{n0})$$

The $\Delta x_i = x_i - x_{i0}$ $(i = 1, \ldots, n)$ in the equation are the deviation from the reference point.

Chapter 3

Model Description

3.1 The Spectrum of Climate System Models

In order to understand atmospheric processes better and to test hypotheses about how the climate system works, numerical climate models of different complexity have been developed.

Conceptual models which describe a limited number of processes and variables and normally have a reduced dimension (box or one to two dimensional models) belong to the first class of climate models. They are very useful to test hypotheses and to understand the physical mechanisms in climate because their results are more transparent than the results of General Circulation Models (GCMs). They are also much faster and cheaper to run, which makes it possible to do extensive sensitivity studies to test a mechanism or a feedback. Because of the high number of parameters that are fixed by the modeler and are not calculated independently and also because of the fact that they lack many important processes that we find in the real system, their applicability is limited.

Comprehensive models like atmosphere and ocean GCMs form the most complex class of models. They describe a large set of processes and feedbacks and are derived from the first principals of hydrodynamics. They are geographically explicit models with a high resolution on the order of 100 km. Due to the many processes they simulate in large detail and their high geographical resolution, they are computational very demanding and, therefore, slow and expensive to run. This makes it necessary for many GCMs to use flux adjustments[1] in order to obtain a realistic present state, which again imposes strong limitations on their usefulness for simulating climate states different from the present one. Until computer power makes it possible to run them over long times and without flux adjustments, they can only be used for relatively short simulations and time slice experiments and not for long-term climate change studies over tens or hundreds of thousands of years.

[1] Artificially prescribed fluxes of heat and fresh water between ocean and atmosphere that are required in order to arrive at a realistic and stable present day climate in many GCMs.

To fill this obvious gap between conceptual and comprehensive models, Earth System Models of Intermediate Complexity (EMICs) have been constructed. These models often have a low spatial resolution, but describe most processes and feedbacks that are also included in comprehensive models, only in a more reduced and simplified form. Therefore, they have a fast turnaround time, which makes them very useful for long-term simulations of climate dynamics and for paleoclimate studies.

To visualize this wide spectrum of climate models described above and to show the place of each model class in this spectrum, Claussen et al. (2002) proposed a new model spectrum in the form of Figure 3.1, instead of the already existent climate modeling pyramid (Fig. 3.2) from Henderson-Sellers and McGuffie (1987, 1998). This new classification became necessary because older ones did not take into account the importance of interacting subsystems, but mainly focused on the complexity of the description of processes. In the model spectrum proposed by Claussen et al. (2002), models are classified by the components of a three dimensional vector:

1. integration, which stands for the number of interacting components of the climate system that are explicitly described in the model
2. number of processes which are explicitly simulated in the model. Because this number is hard to estimate, one uses the cumulative dimensions of the atmosphere and ocean modules of the model to assign this component.
3. detail of description, which means the detail of geographical description of the modules of the model because that is important for the level to which physical processes can be explicitly described.

By using this spectrum approach, each model can be placed in the model spectrum and it becomes obvious to which class it belongs and where its strength lies in climate modeling tasks. One has to bear in mind that even in one class of climate models there can be big differences between models, as different aspects of a model are important for different problems, so that a vast number of different models has been developed.

3.2 CLIMBER-2.3

3.2.1 Structure and Resolution of CLIMBER-2

CLIMBER-2.3 is coarse resolution climate system model of intermediate complexity developed at the Potsdam Institute for Climate Impact Research (Petoukhov et al. 2000). The model consists of modules describing atmosphere, ocean, sea-ice, inland ice, land surface as well as terrestrial and marine biota processes, linked through momentum, energy, water and carbon fluxes (Fig. 3.3). It it important to note that CLIMBER-2 works

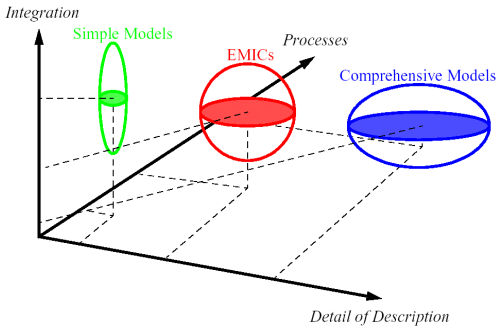

Figure 3.1: Spectrum of Climate Models from Claussen et al. 2000

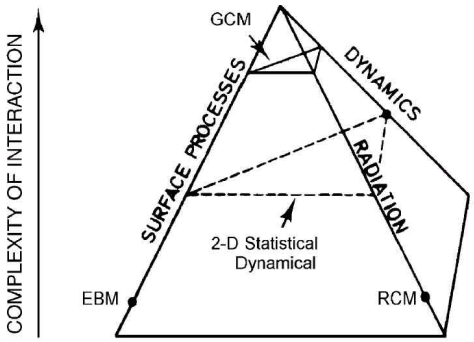

Figure 3.2: Model Pyramid from Henderson-Sellers and McGuffie (1987) (original Figure of Henderson-Sellers and McGuffie (1987) modified by Claussen et al. 2002)

without any flux adjustments between the atmospheric and oceanic modules. Because of its fast turnaround time, CLIMBER-2 is especially useful for long term simulations of global climate dynamics. CLIMBER-2.3 is the current version of CLIMBER-2 and differs from the previous versions CLIMBER-2.1/2.2 mainly by its higher resolution of the ocean grid and some changes in the physical parametrization. CLIMBER-2.3 has a coarse horizontal resolution that only resolves continents and subcontinents and the three ocean basins (Fig. 3.4). It employs two different horizontal resolutions for ocean and atmosphere. The atmosphere module has a 10 degree latitudinal and a 360/7 (approximately 51.4 degree) longitudinal resolution, which gives $18 * 7 = 126$ grid cells. This resolution is also used for the vegetation and land surface modules. The ocean latitudinal resolution is 2.5 degrees, while zonally the ocean is divided into three ocean sectors, corresponding to the Pacific-, the Atlantic- and the Indian Ocean.

The model uses six different surface types: open water, sea-ice, desert, grass, trees and glaciers. The fractions of land and ocean in one cell are prescribed in this work, but they could also change over time. The prescription of the land-ocean mask can be changed for paleoclimate simulations in order to account for a considerably different land-ocean distribution at past times compared to today. The land-ocean mask was designed in a way to minimize grid cells that include land as well as ocean, while at the same time trying to conserve the realistic size of the ocean in each latitude band and for each ocean as well as globally. Because of the low spatial resolution only very schematic land orography and ocean bathometry could be prescribed (Fig. 3.4).
Different surface types can coexist in one grid cell and their fractions are calculated in different modules of CLIMBER-2. Oceanic grid boxes can be covered in part by sea-ice, which is computed in percent of the ocean percentage of the grid box, while land grid

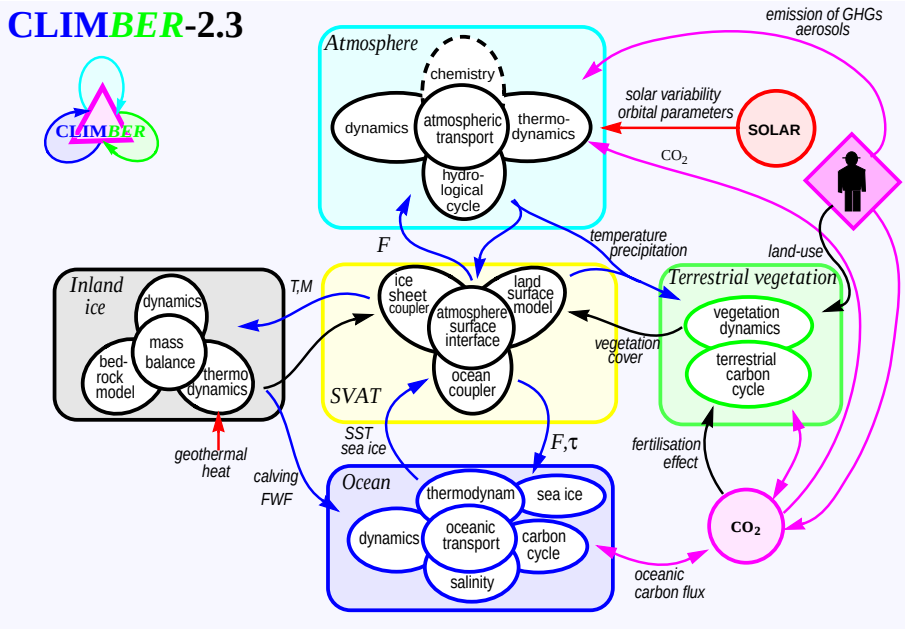

Figure 3.3: Components of CLIMBER-2.3 (from Claussen et al. 2000). Only the atmospheric module, the terrestrial vegetation module (with the terrestrial carbon cycle) and the ocean module were used in this work. The ocean carbon cycle (including marine biota) and the inland ice module were not used.

boxes can be covered by glaciers. Glacier fraction in the version of CLIMBER-2 used in this work was prescribed, but there is a possibility of using the inland ice module SICOPOLIS (Greve, 2000) for simulating inland ice coverage. The land surface that is glacier free is covered by fractions of trees, grass and desert. These fractions can be computed in the dynamic global vegetation module VECODE or be prescribed from empirical data or previous model results. The ocean dynamics can be calculated using the ocean module MUZON, but ocean characteristics like SST and sea-ice cover can also be prescribed from previous model results or data. It is also possible to run the ocean in a "slab" ocean mode, where heat fluxes are fixed and only the upper mixed ocean layer can adapt to atmospheric changes so that SST and sea-ice change accordingly. Finally the atmosphere-surface interface (ASI) calculates the fluxes of surface energy and water as well as surface temperature and soil moisture for the different surface types.

Anthropogenic influence can be incorporated over the CO_2 concentration but also by prescribing a vegetation distribution that accounts for deforestation or other land use changes. In this respect, it is important to note that the climate sensitivity to a doubling of CO_2 is 2.6 °C in the current version of CLIMBER-2 (CLIMBER-2.3), which is a low

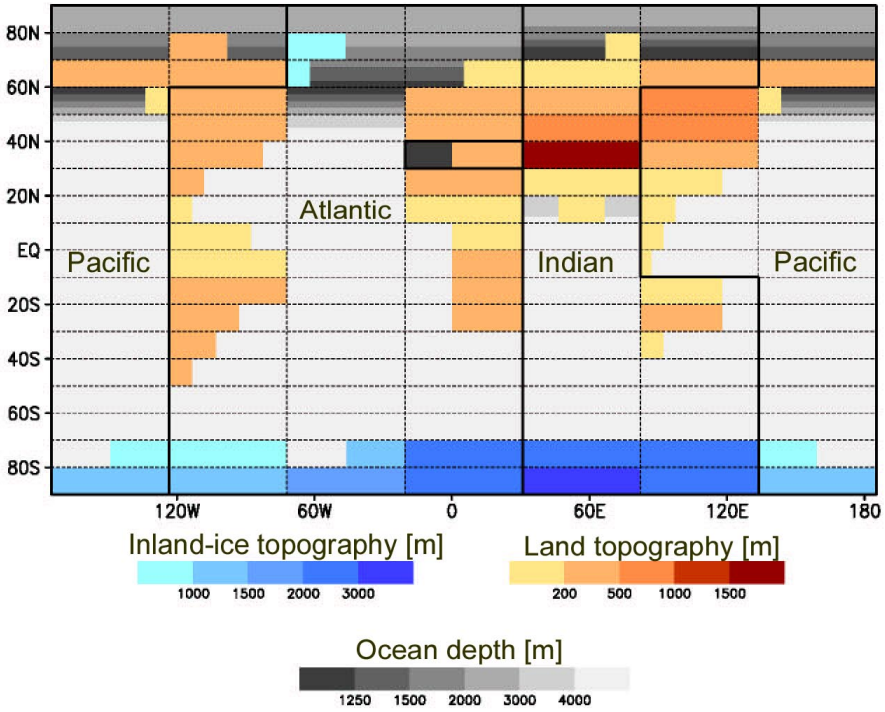

Figure 3.4: Resolution and present day orography of CLIMBER-2 (from Fast 2002).The dashed lines separate the atmospheric grid boxes in the model while the thick solid lines separate the three ocean basins (Atlantic, Pacific and Indian Ocean). The Mediterranean Sea belongs thereby to the Indian Ocean, even though it is separated from it by land masses in the model.

to moderate sensitivity compared to other models (Weaver et al. 1998).

3.2.2 Modules of CLIMBER-2.3 Used

Atmospheric Module (POTSDAM-2)

The atmospheric module of CLIMBER-2.3 is a 2.5 dimensional statistical-dynamical model called POTSDAM, which stands for Potsdam Statistical-Dynamical Atmosphere Model (Petoukhov et al. 2000). Because is uses the statistical-dynamical approach described in detail in Salzman (1978), the long-term evolution of the basic features of the atmosphere are expressed in terms of large-scale, long-term fields of the atmospheric variables wind velocity, temperature and humidity with a spatial scale of about 1000–3000 km and a seasonal temporal scale. Synoptic-scale eddies and waves are not

explicitly described but are represented in the model by their average statistical characteristics. The basic time step of the model is one day, so that the daily cycle of the atmospheric variables is not simulated.

It is called a 2.5-dimensional model because the model equations are first reduced to a set of 2-dimensional, vertically averaged prognostic equations for temperature and water vapor in the atmosphere. Based on the assumption that on the spatial and temporal scale used for this model the atmosphere has a universal vertical structure of temperature and humidity fields (shown in figure 3.5), a 3-dimensional atmosphere is then reconstructed in a second step. The number of vertical levels used are chosen

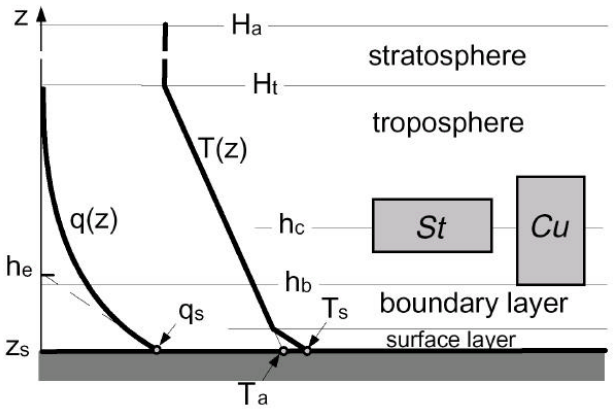

Figure 3.5: Parametrization of the vertical structure in CLIMBER: The temperature profile is assumed to be linear in the troposphere and to be constant with height in the stratosphere. Within the planetary boundary layer the near surface temperature is calculated using the boundary layer theory of Hansen et al. (1983) (Figure taken from Petoukhov et al. 2000).

so that they provide proper numerical accuracy. For wind velocity, energy and water transport 10 vertical levels are used.
Two types of clouds are considered in the model, large scale stratus and cumuli. While stratus cover is dependent on relative humidity and effective vertical velocity, cumuli coverage is a function of effective vertical velocity and surface specific humidity.
The existence of the large-scale circulation patterns (Hadley, Ferrel and Polar) is prescribed in the model as a parametrization of the zonally averaged component of the meridional velocity, but the intensity and extent of them is variable. This is based on the assumption that the structure of the zonally averaged circulation with three pairs of cells is a robust feature of the atmosphere that will exist under different climate conditions (Petoukhov et al. 2000).

The radiation scheme in the model is split up into a longwave and a shortwave part. In order to compute the radiation fluxes, the atmosphere is divided into 16 vertical levels. The longwave radiation scheme accounts for water vapor, CO_2 and ozone in

the atmosphere. The shortwave radiation is further divided into ultraviolet and visible radiation and near infrared radiation and accounts for water vapor, clouds, aerosols and ozone. Clouds are treated as black-body radiators and total longwave flux in each atmospheric grid cell is computed as a weighted sum of clear-sky and cloudy-sky flux.

For a detailed description of the equations used in POTSDAM-2 and CLIMBER-2 see Petoukhov et al. (2000) and Ganopolski et al. (2001) and the references used there.

Ocean Module (MUZON)

The ocean module of CLIMBER-2.3 is a multibasin zonally averaged ocean model based on the model of Wright and Stocker (1992). It resolves three oceanic sectors corresponding to the Atlantic, Indian and Pacific Ocean and has a latitudinal resolution of 2.5 degrees. Vertical resolution consists of 20 uneven vertical levels from 0 meters down to 5000 meters with an upper well-mixed layer of 50 m thickness. MUZON simulates only the zonally averaged temperature, salinity, meridional and vertical velocities for the individual ocean basins for latitudes where they are separated by continents because then no zonal mass transfer can occur between the basins. For the circumpolar oceans, which are latitudinal belts without meridional boundaries, the module also calculates the zonally averaged zonal component of the velocity based on the meridional density gradients and assuming zero pressure gradient at the bottom.

Since the module can only resolve zonally averaged oceans, the wind driven quasi-closed horizontal surface-systems called gyre and the meridional heat and salt transport associated with them cannot be explicitly simulated in the model. To account for them the freshwater transport in the North Atlantic associated with the subpolar gyre circulation is parameterized based on observational data (Ganopolski and Rahmstorf 2001). This parametrization is explained in the description of the factor FSB on page 34.

Sea Ice Module (ICE)

The sea-ice module is a one-layer thermodynamic sea-ice model based on Semtner (1976) with a simple treatment of horizontal transport via advection and diffusion. Sea-ice fraction and thickness are calculated based on the sea-ice mass balance and a relation between ice thickness and fraction. The effective coefficient of heat diffusion in the sea-ice depends on the thickness of the snow cover on top of the sea-ice. To account for spacial inhomogeneity due to the coarse resolution of the model, it is assumed that sea-ice can appear in a grid box when the SST drops below 0 °C. Between 0 °C and the sea water freezing point of −1.8 °C the sea-ice fraction increases linearly with the decrease of the SST. The fraction of open water is assumed to be inversely proportional to the sea-ice thickness for temperatures below −1.8° C. To account for the conditions in the Weddel and Ross sea near Antarctica, where Antarctic Bottom water is formed, a small northward velocity of 0.05 m/s is added to the ice velocity in the grid cells in

the latitudinal belt from 70–80 ° S in the Atlantic and Pacific. Outside of this area, the sea-ice is freely transported by advection and diffusion.

Vegetation Module (VECODE)

The vegetation module of CLIMBER-2.3 is VECODE (Brovkin et al. 1999, 2002a/b) and it is based on a continuous bioclimatic classification (Brovkin et al. 1997). It simulates the vegetation cover and its dynamics, the Leaf Area Index (LAI) and the terrestrial carbon cycle with an annual time step based on the annual mean precipitation and temperature fields (respectively growing degree days[2]) that it gets from the atmospheric module from CLIMBER. In turn, the simulated vegetation cover and the LAI are accounted for in calculating the surface albedo, roughness and evapotranspiration during the following year (see paragraph 'ASI', page 31).
VECODE was designed explicitly for interactive coupling to a coarse atmospheric resolution model. It simulates vegetation coverage using two Plant Functional Types (PFTs)[3]: grass and trees. They were chosen because only for them the bioclimatic parameters differ significantly and also because they have quite a different allocation function and residence time for carbon (for details see Brovkin et al. 1997). In contrast to some other vegetation models (e.g. BIOME (Prentice et al. 1992)), VECODE calculates the vegetation fractions continuously, allowing more than just one vegetation type to exist in each box and avoiding inconsistent jumps in vegetation cover within one grid box in time. The sum of tree fraction f and grass fraction g is always equal to the vegetation fraction v of each ice-free land gridbox. The rest $1 - v = d$ is the desert fraction.

If the climate changes, the model simulates a transition in vegetation coverage from the old equilibrium state towards a new equilibrium with a timescale that is determined by the carbon cycle model. Thereby, the timescale for the vegetation dynamic is of the order of decades to centuries for trees and of years for grass. Whenever vegetation fraction is below 0.1, the timescale for vegetation regrowth is set to the timescale of trees to account for the absence of soil and nutrients in desert or semi-desert regions. The simulation of the net primary production (NPP) follows the semi-empirical parametrization by Lieth (1975) and is a function of annual temperature and precipitation. To account for the biotic growth factor, a logarithmic dependence of NPP on CO_2 is also included. The carbon in the terrestrial system is divided into four compartments, two for living vegetation (including the "fast" pool of green biomass like leafs and the "slow" pool of structural biomass like roots) and two for dead organic matter (first the "fast" pool of

[2]The variable growing degree day is defined here in CLIMBER-2 as the annual sum of temperatures on days where temperature was above 0 ° C, therefore, being a measure for the accumulated heat available for plant growth. $GDD_{T_0} = \sum_{i=1}^{360} (T_a - T_0)_i$ with $T_a > T_0$ on days where the mean daily temperature T_a was above 0 ° C. The minimum growing degree number required for tree growth was set to $\mathrm{GDD}_{T_0} = 800\,^{\circ}\mathrm{C}$ while the minimum number for grass growth was set to $\mathrm{GDD}_{T_0} = 100\,^{\circ}\mathrm{C}$ (Brovkin el al. 2002b).

[3]Vegetation types that have similar characteristics are grouped into Plant Functional Types.

woody residues and then also a "slow" pool consisting of humus). The dynamics for these compartments are quite different for trees and grass (which was one of the reasons they were chosen in the first place) and, therefore, they are simulated separately for both of them with an annual time step. Overall, the carbon cycle dynamic is controlled by the NPP, which leads to an increase in green biomass when NPP increases. That is why the LAI for trees and grass is calculated as a function not only of temperature and precipitation like the vegetation fractions, but also as a function of the NPP. As a consequence, LAI is also dependent on CO_2 over the fertilization effect that is accounted for in the calculation of NPP. Since the model has an annual time step, no seasonal cycle of LAI is seen. For transpiration calculation a linear decrease of up to 80% in LAI for temperatures between 0–10 °C is parameterized in VECODE, reflecting the loss of leaves in fall and winter in reality (Kubatzki 2000).

Atmosphere-Surface Interface (ASI)

The atmosphere-surface interface (ASI) is the module in the model that links the other modules of CLIMBER-2 through the fluxes of energy and water and also describes the seasonal evolution of surface processes. The surface processes description used is based on the Biosphere-Atmosphere Transfer Scheme (BATS) that was developed by Dickinson et al. (1986). It was modified to fit the spatial and temporal resolution and complexity of CLIMBER-2.3 and has a time step of one day (Kubatzki 2000).

The six different surface types, grass, trees, desert, glacier, ocean and sea-ice, can coexist in one grid cell and change their fraction while the fractions of land and ocean in one cell in time are prescribed in this work. Changes in surface types directly affect the climate through albedo, roughness length and transpiration changes.
The roughness length is prescribed for each type of surface and determines effective wind speed, sensible heat flux and evaporation. If vegetation is partly snow-covered, its original roughness length is modified so that it approaches the roughness length of snow with increasing snowdepth.
On land, the surface albedo of bare soil (desert) is estimated to be 0.15 for visible and double that for infrared radiation. Based on satellite measurements (e.g. Knorr et al. 2001), the albedo of the Sahara desert is set to a higher albedo than in other desert areas (0.24 for visible light and 0.45 for infrared). The albedo for trees is set to 0.05 for visible light and 0.2 for infrared radiation. Grass albedo is 0.08/0.3 and the albedo of fresh snow is 0.6/0.9 for visible/infrared radiation, respectively. The albedo of snow is modified from the values of fresh snow according to its age and temperature. The surface albedo of land partly covered by snow is calculated as a weighted sum of the albedo of snow-free and snow-covered ground. The albedo for snow-covered ground is dependent on the different surface types covered by snow as well as the snow age. It is calculated by changing the original snow fraction of the model as a function of snow thickness, temperature and vegetation type following Dickinson et al. (1986), where the important feature of vegetation is the roughness length. Snow coverage of trees depends mainly on snow fall versus thawing and snow temperature, while for grass and

desert it depends also on orography; snow coverage of glaciers and sea-ice is accounted for implicitly. The calculation of the albedo of snow-covered ground in CLIMBER-2, therefore, makes it possible to simulate the important vegetation-snow-albedo effect (taiga-tundra effect) in winter and spring.
For the soil-moisture, ASI uses a two-layer soil model with a depth of 0.1 m and 0.9 m. Precipitation, evaporation, transpiration, interception, melting of snow, surface runoff and drainage determine the water balance in the soil. The surface runoff depends on the relative soil moisture of the upper layer and the precipitation, drainage is assumed to be only downwards and also depends on relative soil moisture. Evaporation is calculated taking into account the near surface windspeed, saturation level and soil moisture. The transpiration is mainly dependent on LAI, soil moisture, stomatal and root resistance and leaf conductivity, which again are a function of temperature and wind speed.

3.2.3 Evaluation of CLIMBER

CLIMBER-2 has been evaluated extensively in the past against data and GCM results in sensitivity studies for present day climate (Petoukhov et al. 2000) and for its response to different forcing such as insolation, CO_2, land cover change and freshwater flux (Ganopolski et al. 2001). Moreover, CLIMBER-2 has been successfully used in paleoclimate simulations of the Holocene (Claussen et al. 1999; Ganopolski et al. 1998a; Kubatzki 2000), the Last Glacial Maximum (Ganopolski et al. 1998b; Ganopolski and Rahmstorf 2001; Ganopolski 2003), the Eemian (Kubatzki et al. 2000) as well as for future climate scenarios (Rahmstorf and Ganopolski 1999).

In all these studies CLIMBER-2 showed that it is able, in spite of its coarse resolution and simplicity in the description of individual processes, to capture many features of atmosphere and ocean climate fairly realistically and that it is able to simulate the climatic response to changes in different types of forcing and boundary conditions in reasonable agreement with the results of state-of-the-art GCMs. Most of these studies were undertaken with CLIMBER-2.1, but Claussen et al. (2003b) and Fast (2002) repeated some of the studies with CLIMBER-2.3 and showed that in spite of quantitative changes the overall qualitative response of the model does not depend strongly on the version of CLIMBER-2 used. Because of that I believe that the credibility of CLIMBER-2 has been amply shown in the past and I want to refer to the cited publications for more information about these studies.

Chapter 4

Experiments

4.1 Last Glacial Maximum

To analyze the importance of vegetation effects and synergy effects with the vegetation in the climate system at the Last Glacial Maximum, equilibrium experiments for the LGM were performed. As reference state the present day climate with a preindustrial CO_2 concentrations of 280 ppm (part per million) was chosen[1].

The five factors that were analyzed in these experiments were the same ones also used by Ganopolski (2003), who already performed a factor analysis for these five factors for the LGM. Since he did not perform a factor separation the intention for this part of my thesis was to show a different approach of interpretation of simulations of the LGM climate. Therefore, a full factor separation, was carried out for the five following factors:

Astronomical: Insolation characteristics are set to the conditions for either 21,000 years BP or to the present day conditions as shown in table 4.1, calculated in the model following Berger (1978).

CO_2: The CO_2 concentration in the atmosphere is either set to the preindustrial value of 280 ppm or to 200 ppm for 21 ky BP as used in the Paleoclimate Model Intercomparison Project (PMIP 2000).

Inland-Ice and Orography: Either a land-sea distribution and orography for present day conditions (REF) or a land-sea mask for the LGM, with a sea-level drop of 115 m and ice sheets on the continents (following Peltier 1994), is used.

[1] It has been shown that it is more reasonable to use preindustrial CO_2 concentrations with otherwise present day boundary conditions instead of present day CO_2 levels (e.g. Kubatzki et al. 2000) for comparison with paleoclimate experiments. The reason for that is that the rapid, anthropogenically-caused increase of CO_2 in the atmosphere during the last hundred years has led to a present day climate that is not in equilibrium with its CO_2 concentration but is in the process of adapting to it. Since this CO_2 increase is not caused naturally it is more reasonable to use preindustrial CO_2 levels in order to investigate the natural state and behavior of the climate system.

	Present	LGM
Eccentricity	0.017	0.019
Obliquity	23.45°	22.95°
Day of Perihelion	January 3	January 15

Table 4.1: Orbital parameters after Berger (1978) for present day and the LGM at 21 ky BP.

FSB: FSB is the acronym for a parametrization for an Arctic freshwater bypass that was introduced into the model in order to take into account that at present about 0.08 Sv [2] of fresh water escapes from the Arctic via the Canadian Archipelago and the East Greenland current without mixing with the incoming salty Atlantic water. This stabilizes convection in the Nordic Seas and is, therefore, an important mechanism. In a zonally averaged ocean model, as the one used in CLIMBER-2.3, this process cannot be explicitly described, which leads to a unrealistically low threshold for the convective instability of the thermohaline circulation. To include this effect in CLIMBER, a parametrization was developed in order to account for this present day freshwater transport of 0.08 Sv (REF) (parametrization described in detail in Ganopolski and Rahmstorf 2001). For glacial conditions, the freshwater transport via this bypass was probably reduced, due to the closing of the Canadian archipelago and the partial closure of the Denmark Strait by ice sheets. In the parametrization the freshwater bypass-flux was, therefore, reduced by 50% to 0.04 Sv for glacial conditions (LGM).

Vegetation: The vegetation in the model was either fixed to the vegetation field from the reference run (REF) (vegetation "off") or the vegetation module VECODE was run interactively so that vegetation distribution could adapt to and interact with climate (vegetation "on").

These five factors are hereafter abbreviated in the following way: The astronomical factor is "A", the CO_2 factor "C", the inland ice and orography factor "I", FSB "F" and the vegetation factor "V".

To perform a complete factor separation for them, $2^5 = 32$ equilibrium runs were performed. Each run was integrated for 5000 years to make sure that even the slow components of the climate system (e.g. the ocean) were in equilibrium. I analyzed the equilibrium state at the end of the runs and for that the output over the last 100 model-years was averaged and then written to an output-file.

The reference run REF was a fully coupled equilibrium run for present day conditions with a preindustrial CO_2 level. The vegetation distribution computed at the end of this run was then used as the vegetation in all experiments where vegetation was fixed. The restart files for all runs came from REF as well.

[2] Sv stands for Sverdrup, with 1 Sv= $1 * 10^6$ m^3/s.

The 32 experiments were set up in a way so that all five factors were used in all possible combinations (without repetition) until the fully coupled run was achieved. Possible states for each factor were the REF or the LGM state, referred to as "0" and "1" in table 4.2 (on page 38) where the complete setup for all runs is shown. The simulations are all called LGM with a subscript consisting of the abbreviations introduced earlier ($A - C - I - F - V$) for all the factors where the specific factor was set to LGM (or "1" in the table).

The factor separation was performed for five factors so that from the 32 runs five factors, 26 synergy terms and one reference state were calculated. The factors and synergy terms are referred to by using the abbreviation introduced earlier ($A - C - I - F - V$) as subscripts, i.e. the pure effect of the astronomical forcing is $\hat{f}_A$, the CO_2 factor is $\hat{f}_C$ and the ice-orography factor is $\hat{f}_I$. Their synergy effects are addressed by adding the appropriate letter in the order $A-C-I-F-V$, so that the synergy between the orbital forcing and the CO_2 forcing is written as $\hat{f}_{AC}$, the synergy between orbital forcing, CO_2 and inland-ice forcing as $\hat{f}_{ACI}$ and the synergy between all five factors as $\hat{f}_{ACIFV}$ while the reference factor, called $\hat{f}_0$ before, is now called $\hat{f}_R$. The full set of the 36 equations used for the factor separation for five factors is derived from equation (2.12) on page 21 and can be found in the appendix A.1 on page 111.

It is important to note that the term "synergy effect" in this work refers to the interaction terms like $\hat{f}_{CI}$, even though neither the CO_2 nor the inland ice changes due to a feedback between them, as they are both forcings that are prescribed. As in my equilibrium experiments only one feedback is explicitly investigated (the vegetation), while the other factors are forcings, the use of the term "synergy" differs from its use in other publications where it often refers only to the interaction of two feedbacks. Hence, the term "synergy" is used in a more technical way here in this study to describe the results of the factor separation.

4.2 Glacial Period 60,000 to 20,000 Years BP

In order to estimate the importance and also the dynamic behavior of the atmosphere-vegetation feedback compared to the atmosphere-ocean feedback and to their synergistic effects in the climate system during the last glacial period from 60–20 ky BP, two sets of transient experiments with CLIMBER-2.3 were performed. The two sets differ in their reference states, but they both include the same four experimental setups needed in order to perform the transient Stein and Alpert Factor Separation (1993) for the 40,000 year long glacial period investigated here. The four runs are called A, AO, AV and AOV and these acronyms stand for the following simulations:

A: Simulation, where only the atmosphere module of CLIMBER-2 was used, while the ocean characteristics (SST, sea-ice fraction and thickness, circulation) and the vegetation distribution (vegetation fractions, LAI) were fixed on the results from the respective reference run with CLIMBER.

AO: Simulation, where the atmosphere and the ocean modules of CLIMBER-2 were used and coupled, while the vegetation distribution was fixed on the distribution from the respective reference state.

AV: Simulation, where the atmosphere and the vegetation module of CLIMBER-2 were used and coupled, while the ocean was fixed on the respective reference state.

AOV: Simulation, where the atmosphere, the ocean and the vegetation modules of CLIMBER-2 were all used, coupled and could interact.

As the results of the factor separation technique depend on the reference state and the factors chosen (see page 21), two very different reference states were chosen in order to compare the resulting factors and to find out how stable the features are, independent of the reference state. As reference state the present day climate (called "00") and the climate at 20,000 years BP (called "20") were chosen because they represent two fundamentally different climate states: at present the climate system is in an interglacial state, while at 20 ky BP the climate was at the maximum of the last glacial cycle.

The restart files and the fixed ocean- and vegetation characteristics for runs with the reference state of present day were produced by a full *AOV* equilibrium run with CLIMBER-2.3. Present day orbital parameters and land-sea mask were used while CO_2 was set to the preindustrial value of 280 ppm (the reason for that choice is the same as explained for the LGM experiments in the footnote on page 33). This *AOV* run was then integrated over 5000 model years and the output that I used was produced by averaging over the last 100 model years.

The reference state for 20,000 years BP was defined by the results from the end of a transient *AOV* run from 60–20 ky BP at 20 ky BP. The CO_2 concentration over the length of the run was prescribed according to CO_2 reconstructions (Petit el al. 1999). The reason for the choice of using the results of a transient simulation rather than the results of an equilibrium simulation was that climate was not in equilibrium around 20 ky BP, so that small differences exist between the results of a equilibrium run and a transient experiment for the same time. This is of course also true for present day climate, but here it is only important for 20 ky BP as the run does not extent to present day. For 20 ky BP the factors converge if ocean- or vegetation states from the transient run for 20 ky BP are prescribed while runs forced with vegetation- and ocean characteristics from an equilibrium run would not converge in one point at 20 ky BP. This would cause problems for the interpretation of the results as the offset is not constant in time. In order to avoid this problem, I used the transient vegetation and ocean distribution and the restart file from the end of the *AOV* run for 20 ky BP, averaged over the last 100 model years.

For each reference state the above described four experiments *A*, *AO*, *AV*, and *AOV* were performed. To differentiate between the runs for the two sets ,"00" and "20" are added as subscripts to the names: AOV_{20}, $AOV_{00}, \ldots$, A_{20}, A_{00}.

All runs were integrated for 40,000 from 60–20 ky BP with the following forcing:

- prescribed changing orbital parameters (Berger 1978),
- prescribed CO_2 changes as reconstructed from the Vostok Ice core (Petit et al. 1999),
- prescribed inland ice sheet changes,
- freshwater forcing to trigger Heinrich Events (HE) and Dansgaard/Oeschger (D/O) events in the model (see chapter 1 and Ganopolski and Rahmstorf (2001) and Claussen et al. (2003a) for a detailed description of effect, nature and reason of the freshwater forcing).

The shape of these forcings can be seen in figure 4.1.

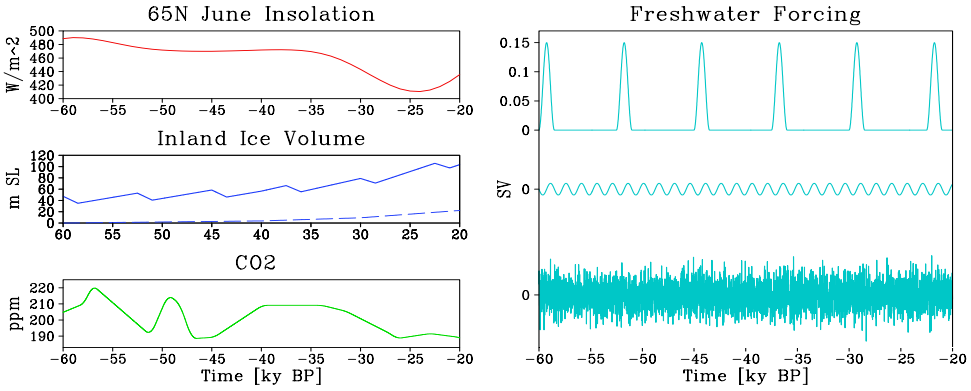

Figure 4.1: Forcing for the transient runs: Insolation in W/m^2, average for June in 65° N shown (but forcing is global), inland ice volume in meter of sea level change (m SL)(the dashed line is the ice volume in Eurasia, the solid line is the global ice volume); CO_2 variation in ppm; Freshwater forcing in SV (the top line is the freshwater forcing to trigger Heinrich Events, the middle curve is a small sinusoidal forcing (which itself is too weak to trigger D/O events but which is able to synchronize D/O events via the mechanism of stochastic resonance) and the lowest line is a random white noise forcing at high northern latitude which triggers D/O events). Part of the Figure adapted from Claussen et al. (2003a).

To analyze the results of these experiments the earlier introduced Stein and Alpert Factor Separation Method (1993) for two factors was used (see section 2.2 with equations (2.2–2.5)). For each of the two sets two factors, one synergy term and a reference state were calculated. The ocean factor is called $\hat{f}_{oce}$, the vegetation factor $\hat{f}_{veg}$, the synergy factor between them $\hat{f}_{syn}$ and the reference state is $\hat{f}_{ref}$. The exact equations used can be found in appendix B.1 on page 115. As already practised for the names of the experiments, "00" and "20" are used as subscripts for the factors (e.g. $\hat{f}_{syn_{(20)}}, \hat{f}_{oce_{(00)}}, \ldots$) to differentiate between the factors for the two sets.

Setup for all LGM runs

run	Astronomical	CO_2	Ice and Orography	FSB	Vegetation
REF	0	0	0	0	0
LGM_A	1	0	0	0	0
LGM_C	0	1	0	0	0
LGM_I	0	0	1	0	0
LGM_F	0	0	0	1	0
LGM_V	0	0	0	0	1
LGM_{AC}	1	1	0	0	0
LGM_{AI}	1	0	1	0	0
LGM_{AF}	1	0	0	1	0
LGM_{AV}	1	0	0	0	1
LGM_{CI}	0	1	1	0	0
LGM_{CF}	0	1	0	1	0
LGM_{CV}	0	1	0	0	1
LGM_{IF}	0	0	1	1	0
LGM_{IV}	0	0	1	0	1
LGM_{FV}	0	0	0	1	1
LGM_{ACI}	1	1	1	0	0
LGM_{ACF}	1	1	0	1	0
LGM_{ACV}	1	1	0	0	1
LGM_{AIF}	1	0	1	1	0
LGM_{AIV}	1	0	1	0	1
LGM_{AFV}	1	0	0	1	1
LGM_{CIF}	0	1	1	1	0
LGM_{CIV}	0	1	1	0	1
LGM_{IFV}	0	0	1	1	1
LGM_{ACIF}	1	1	1	1	0
LGM_{ACIV}	1	1	1	0	1
LGM_{ACFV}	1	1	0	1	1
LGM_{AIFV}	1	0	1	1	1
LGM_{CIFV}	0	1	1	1	1
LGM_{ACIFV}	1	1	1	1	1

Table 4.2: "0" means that the factor is set to preindustrial conditions or that vegetation is fixed to the output from REF. "1" means that the factor is set to LGM conditions or that the vegetation module is switched on.

Chapter 5

Results for the Last Glacial Maximum

In this chapter, I want to present the results from the equilibrium experiments for the LGM. I will start in section 5.1 by showing the most important simulated climatic features of the fully coupled LGM run compared to the reference run, followed by a comparison to the LGM run with fixed reference vegetation. Section 5.2 will then focus on how this climatic response can be attributed to individual factors using the Stein and Alpert Factor Separation Method (1993) presented earlier on.

5.1 Simulation of the LGM Climate

The LGM climate presented here was simulated in a fully coupled equilibrium experiment with CLIMBER-2.3, called LGM_{ACIFV}. The comparison of this simulation to the REF experiment is done in order to give an overview over the differences between the climate in the LGM and today. The influence of the interactive vegetation on the climate of the LGM is investigated through the difference between the run LGM_{ACIFV} and LGM_{ACIF}.

Inland Ice and Land Area

Inland ice area (shown in Figure 5.2) and sea-level were prescribed in accordance with reconstructions for the LGM (Peltier 1994) so that 4.3% of the earth surface was covered by ice in all experiments with LGM orography, as opposed to just 1.6% in the reference run. This includes the increase of inland ice on land areas that are not land in REF, as the land area fraction increases from 31% in REF to 34% in LGM (Fig. 5.1) due to the sea-level drop of about 115 m (Peltier 1994).

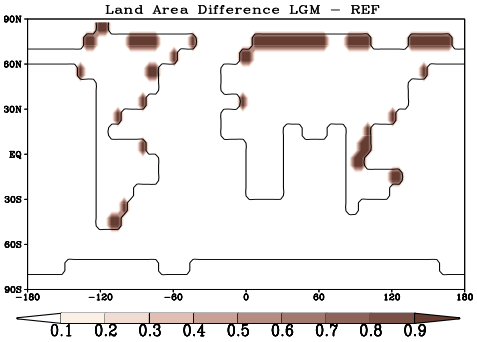

Figure 5.1: Land area difference between LGM and *REF*. "New" land areas in LGM are shaded in brown.

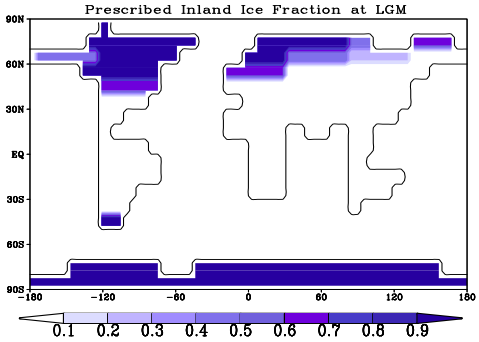

Figure 5.2: Prescribed inland ice fraction in LGM

Atmospheric Response

The global annual surface air temperature in LGM_{ACIFV} is simulated to be 9.1° C, which gives a temperature difference to the reference run *REF* of −4.9° C. This is a temperatures decrease for the LGM climate that is in the range of simulated changes from other climate models (e.g. Dong and Valdes (1998): −4.2 °C ; Hewitt et al. (2003): −3.8 °C ; Kim et al. (2002): −10 °C ; Wyputta and McAvaney (2001): −3.9 °C ; Crowley and Baum (1997): −4.2 °C ; Levis and Foley (1999): −4.3° C).

As expected, the simulated distribution of the cooling in LGM_{ACIFV} is neither uniform over the globe nor over the seasons. Figure 5.3 shows that the temperature decrease in LGM_{ACIFV} was much more pronounced over the NH and there especially over the inland ice shields of Eurasia and North America, where the temperature difference between LGM_{ACIFV} and *REF* reaches −21 °C on annual average.

On the seasonal scale the strongest temperature decrease over Eurasia and the North Atlantic is seen in winter[1] while in North America it is strongest during summer (Fig. 5.4). Summer is the coldest season in North America because the albedo effect caused by the inland ice cover has its strongest cooling effect in summer due to the insolation maximum. The fact that in Eurasia the winter is colder than the summer is due to the extended sea-ice cover over the Atlantic as well as to the change in the Atlantic circulation that leads to a reduced oceanic heat transport to Eurasia (will be discussed later on). The maximum of the influence on Eurasia of both sea-ice cover and oceanic northward heat transport is in winter, which leads to this further reduction in winter temperature compared to the pure albedo effect of the inland ice cover.

The LGM climate was not only colder but also drier than today, with a simulated precipitation reduction of 0.39 mm/day (140 mm/year) compared to *REF* with 2.68 mm/day.

[1]Seasons always refer to NH seasons unless otherwise noted. This means that spring is the average of March, April and May, summer of June, July and August, fall of September, October and November and winter of December, January and February.

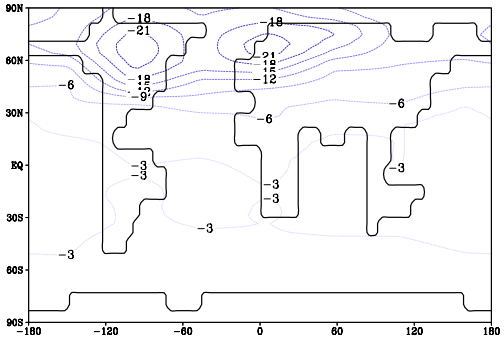

Figure 5.3: Annual mean surface air temperature difference between LGM_{ACIFV} and REF [in °C].

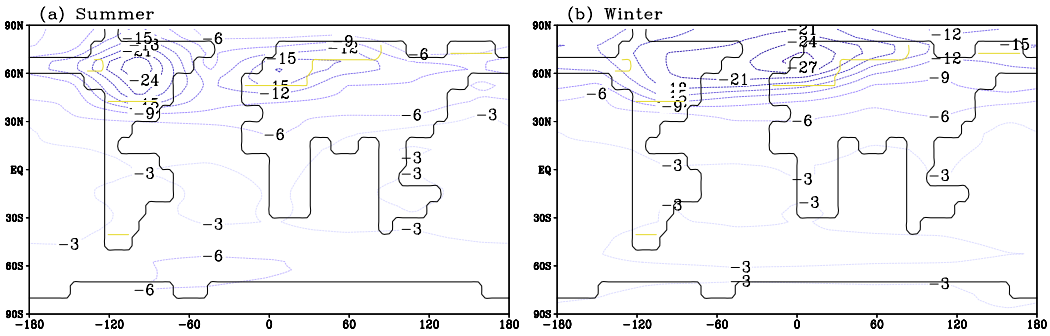

Figure 5.4: Surface air temperature difference [in °C] between LGM_{ACIFV} and REF for summer (a) and winter (b). For orientation the 60% inland ice line is plotted in yellow.

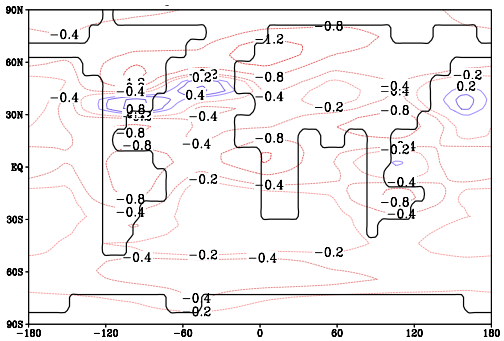

Figure 5.5: Annual mean precipitation difference between the LGM_{ACIFV} and REF run [in mm/day].

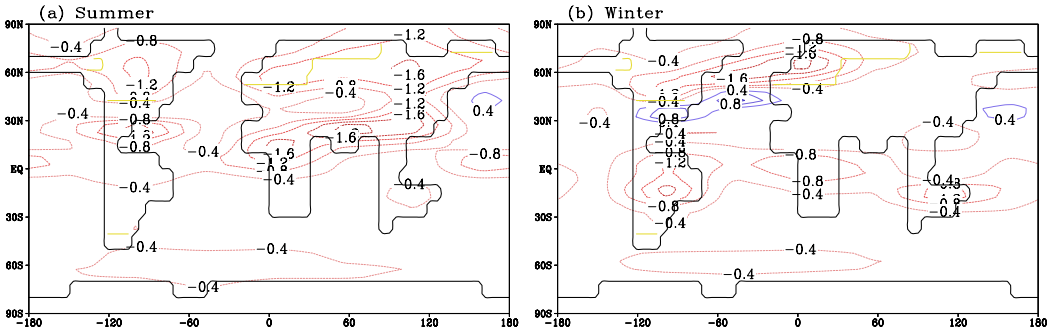

Figure 5.6: Precipitation difference [in mm/day] between LGM_{ACIFV} and REF for summer (a) and winter (b). For orientation the 60% inland ice line is plotted in yellow.

The precipitation decrease is most pronounced in the tropical regions around the Equator, over the ice shields of the NH and to a smaller extent also over the Southern Ocean around 60° S (Fig. 5.5). Over the Atlantic at 40° N, in North America at 30° N as well as over the Pacific at 30° N a local precipitation increase is simulated. On the seasonal scale the strongest precipitation decrease over eastern Eurasia and North America is seen in summer, while the reduction is largest in winter for the North Atlantic and the western part of Eurasia. A very similar pattern was also found for the seasonal temperature change earlier on. Over the North Atlantic and western Europe this is due to the shift of storm tracks as well as to the decreased evaporation caused by the extended sea-ice cover and reduced temperature. Even though precipitation and evaporation both decrease over the North Atlantic in LGM_{ACIFV}, evaporation decreases less, so that south of 65° N the North Atlantic is freshened. The region of precipitation reduction around the Equator consists of a region north of the Equator that experiences the strongest reduction in summer and a region south of the equator with its maximum in southern summer (Figure 5.6). This pattern is due to a weakening of the summer monsoon in the respective hemisphere.

The basic features of the atmospheric circulation are not changed in LGM_{ACIFV} compared to REF. This also means that atmospheric mass transport does not change significantly between them. In LGM_{ACIFV} a slight reduction of the mass transported by the Southern Hemisphere (SH) Hadley cell is seen while it slightly increases for the NH Hadley cell and NH Ferrel cell (Fig. 5.7 (b)). Due to the stronger cooling on the NH than on the SH, the Hadley cell and the thermal equator are slightly moved to the south. For the same reason, atmospheric meridional heat transport increases notably in LGM_{ACIFV} with a meridional averaged increase in of 0.45 PW (PW= 10^{15}W) compared to REF. On the NH LGM_{ACIFV} shows a stronger increase (+0.78 PW) than on the SH (+0.03 PW) (Fig. 5.8) due to a stronger temperature gradient between the polar region and the tropical region on the NH than on the SH. Hence, the increase in the outer-tropics is mainly caused by an increase in synoptic energy transport while in the tropical regions the advective energy transport is responsible for the small increase

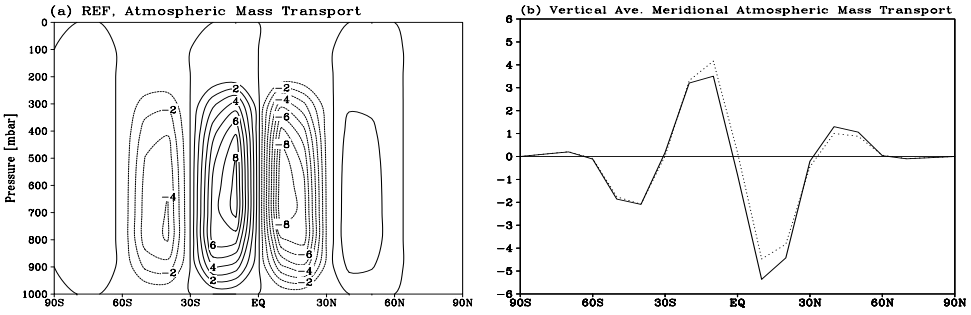

Figure 5.7: Annual mean atmospheric meridional mass transport [in 10^{10} kg/s]. In (a) its vertical distribution for REF is shown while in (b) the vertical averaged mass transport of LGM_{ACIFV} (solid) and REF (dotted) are shown. The vertical distribution for LGM_{ACIFV} is not shown because it is almost the same as for REF, as changes are only small compared to the absolute values.

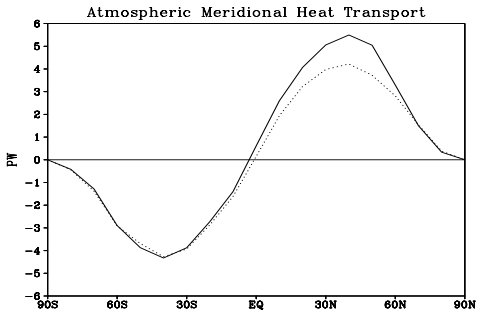

Figure 5.8: Meridional and annual averaged atmospheric heat transport [in PW]. Dotted line for REF and solid line for LGM_{ACIFV}.

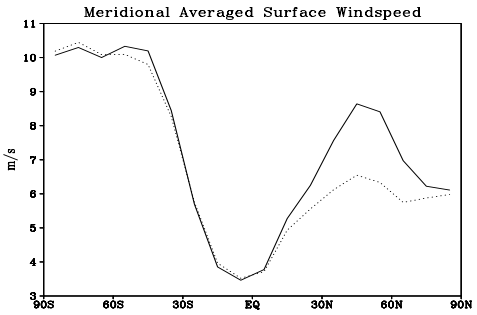

Figure 5.9: Meridional and annual averaged surface windspeed [in m/s]. Dotted line for REF and solid line for LGM_{ACIFV}.

compared to REF. Consistent with this is the increase in surface wind speed in the outer tropics where synoptic energy transport increases, with the main increase on the NH between 30–60° N (Fig. 5.9). Over the North Atlantic this increase reaches its maximum with about 4 m/s increase in LGM_{ACIFV} compared to REF.

Oceanic Response

The ocean circulation in the Atlantic is in a so-called glacial "cold" mode in the LGM_{ACIFV} simulation while it is in a "warm" interglacial mode in REF (Ganopolski and Rahmstorf 2001). The main differences between "cold" glacial and "warm" interglacial mode are the place of deep water formation, the stability of the circulation and the depth of it (Ganopolski and Rahmstorf 2001; summary in chapter 1). The

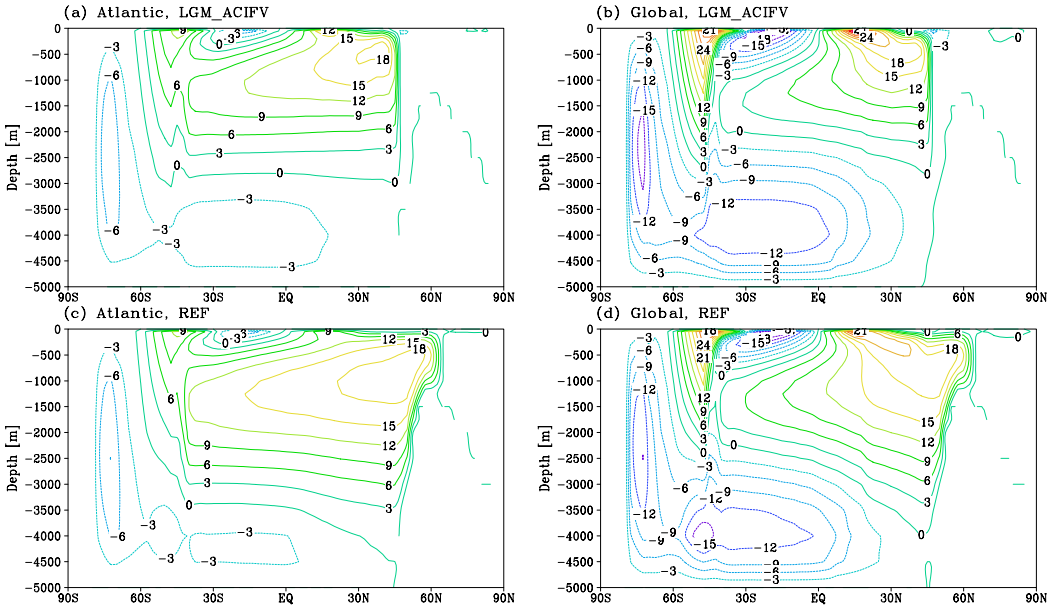

Figure 5.10: Annual averaged Atlantic (a, c) and global (b, d) overturning stream function [in Sv] for LGM_{ACIFV} (a, b) and REF (c, d). Circulation occurs around positive lines in clockwise direction and around negative lines counterclockwise. The NADW formation is represented by the large positive overturning cell on the NH in the Atlantic while the Antarctic Bottom Water (AABW) is represented by the negative overturning cell south of 60° S in the global overturning circulation. The northward outflow of AABW is represented by the negative cell below 3000 m in the Atlantic and also globally. The strong positive cell at 50° S in the global circulation is the Deacon cell, driven by Ekman divergence in response to the westerlies over the Southern Ocean.

Atlantic and global overturning stream function for LGM_{ACIFV} and REF is shown in Figure 5.10. Here, it is can be seen that in LGM_{ACIFV} the North Atlantic convection is shallower by about 500 m than in REF. This increases Antarctic Bottom Water (AABW) outflow into the Atlantic by 1.6 Sv in LGM_{ACIFV} since the NADW is less dense and, therefore, shallower. AABW formation itself decreases slightly in LGM_{ACIFV} (by 0.2 Sv). The stream function in the Atlantic is weaker in LGM_{ACIFV} than in REF (Fig. 5.11 and Fig. 5.10 (a), (c)), with a reduction of 0.7 Sv in maximum Atlantic overturning. The formation of NADW is associated with the maximum overturning stream function in the North Atlantic, so that the relative small decrease in maximum overturning in LGM_{ACIFV} means that also the NADW formation decreases slightly. More important than the weakening of the NADW formation in LGM_{ACIFV} is the southward shift in the NADW formation site by about 15° from the Nordic Seas to the south of Iceland at 45° N (Fig. 5.11 (a) shows this shift).

Due to the weaker overturning circulation, the northward heat transport in the Atlantic is reduced on meridional mean by 0.14 PW in LGM_{ACIFV} compared to REF. While

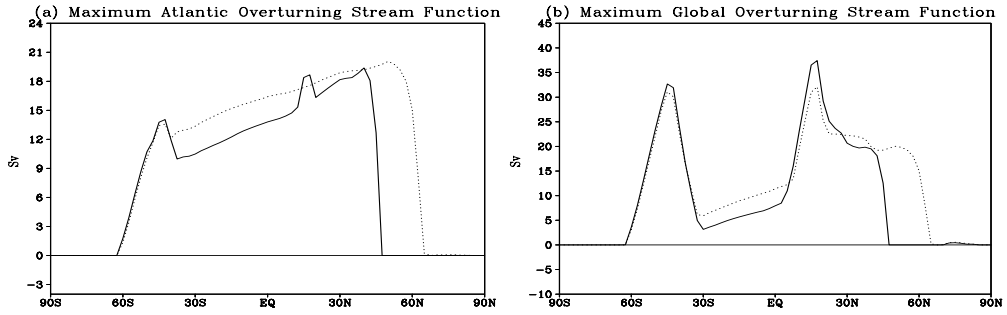

Figure 5.11: Atlantic (a) and global (b) annual maximum overturning stream function [in Sv]. The dotted line stands forREF and the solid line for LGM_{ACIFV}. Maximum overturning is zero south of 60° S due to the negative AABW formation there. The focus is on the shift of the NADW formation site.

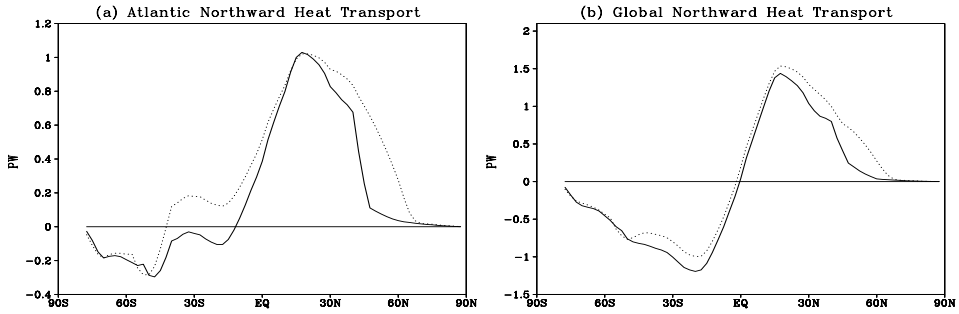

Figure 5.12: Latitudinal distribution of the annual vertically and zonally integrated northward heat transport in the Atlantic and the global ocean for the runs LGM_{ACIFV} (solid) and REF (dotted) [in PW].

this decrease in northward heat transport in LGM_{ACIFV} is especially strong north of the new NADW formation site at 45° N, the maximum Atlantic northward heat transport stays almost the same in LGM_{ACIFV} and REF, reaching 1 PW at about 15° N (Fig. 5.12 (a)). Globally, the mean oceanic northwards heat transport is also reduced in LGM_{ACIFV}, from 0.14 PW in REF to −0.02 PW in LGM_{ACIFV}. Hence, in LGM_{ACIFV} global mean oceanic heat transport is reversed to a slight southward heat transport due to a decrease in northward heat transport on the NH and an increase in southward heat transport on the SH in LGM_{ACIFV} (Fig. 5.12 (b)).

The global SST decreases by 2.3 °C in LGM_{ACIFV}, but locally the cooling is much stronger, reaching −10 °C in the North Atlantic at 50° N in LGM_{ACIFV} (Fig. 5.14). On the Southern Hemisphere the cooling reaches only about −4 °C in LGM_{ACIFV}. All this is due to the weaker northward heat transport in LGM_{ACIFV} compared to REF, that warms the Southern Ocean and cools the northern Atlantic and Pacific in LGM_{ACIFV} relative to REF. The SST decrease causes a substantial global increase in sea-ice cover for LGM_{ACIFV} (Fig. 5.13). The southward shift of the sea-ice margin

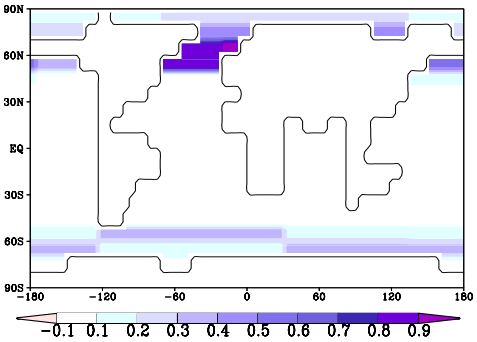

Figure 5.13: Annual averaged sea-ice fraction difference for $LGM_{ACIFV} - REF$.

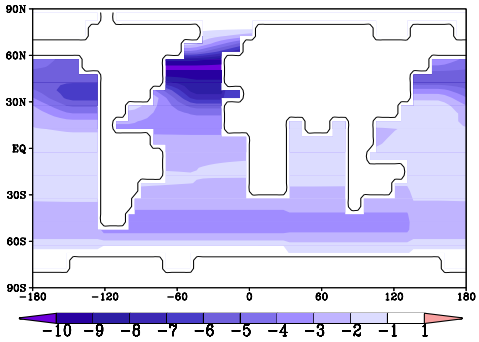

Figure 5.14: Annual averaged SST difference for $LGM_{ACIFV} - REF$ [in ° C].

in the Atlantic in LGM_{ACIFV} compared to REF is caused by the southward shift in NADW formation to 45° N and the, therefore, greatly reduced northward heat flux north of it in LGM_{ACIFV}.

Vegetation Response

The $LGM_{ACIFV} - REF$ difference map of vegetation distribution is affected by the dynamic vegetation response and the displacement of vegetation by the extended inland ice. To separate these responses, the total difference is split up into a "dynamic" response and a "displacement" response in Figure 5.15. The "displacement" response is the effect that is already included in LGM_I, as it is caused by imposing the inland ice cover, while the dynamic vegetation changes are caused by the interactive vegetation and, therefore, cause the difference between LGM_{ACIFV} and LGM_{ACIF}.

Due to the temperature reduction in LGM_{ACIFV} compared to REF the minimum growing degree day line (see page 30 for details on growing degree days) for trees shifts south from about 65–70° N in REF to 40° N in North America and to 45–55° N in Eurasia in LGM_{ACIFV}. This leads to the replacement of trees in these latitudes by grass, as also seen in vegetation reconstructions for the LGM (e.g. Crowley 1995).

Global grass fraction is reduced by 25% and the tree fraction by 35% in LGM_{ACIFV}, from which 91% are due to the dynamic response and 9% to the displacement. This makes the global dynamic grass decrease 23% and the tree reduction 32% in LGM_{ACIFV}. The replacement of trees in the northern latitudes leads to a cooling in LGM_{ACIFV} over the taiga-tundra feedback, while the decrease of grass in tropical and subtropical regions leads to a cooling mainly due to the hydrological feedback. The reduction of rainforest during the LGM is only small in LGM_{ACIFV}, while reconstructions suggest that the tropical rainforest has been reduced by about 2/3 of its present day area (Crowley 1995; Adams and Faure 1997). Therefore, vegetation reductions in the tropics for the LGM are probably underestimated in CLIMBER-2.3, with the consequence

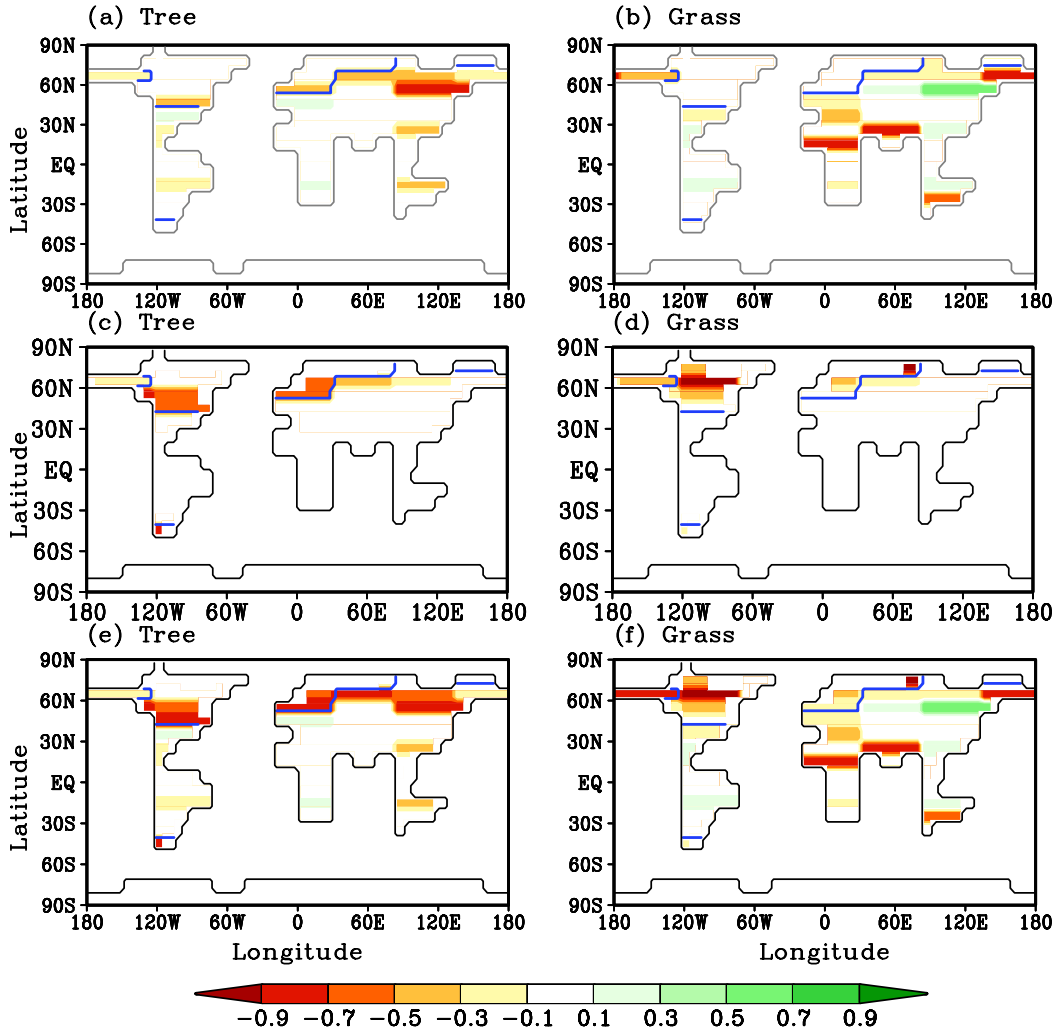

Figure 5.15: Vegetation distribution difference map for $LGM_{ACIFV} - REF$. The dynamic response of trees and grass is shown in (a), (b) while the "displacement" effect is shown in (c), (d) and the total difference is shown in (e), (f). For better comparison with the LGM_{ACIFV} vegetation distribution the vegetation from REF is transferred to the LGM_{ACIFV} land-mask. "New" land areas are thereby assigned vegetation according to the fractions valid in the specific grid box of REF.

that also no vegetation induced temperature changes in the tropics occur, while other studies find a warming of 1–4 °C in the Amazon Basin and some also a small cooling of up to 1 °C in the other tropical regions during the LGM due to the reduction of rainforest and the, therefore, weaker hydrological cycle (e.g. Crowley and Baum 1997; Levis and Foley 1999).

To investigate the effect of the above described vegetation changes on climate, the dif-

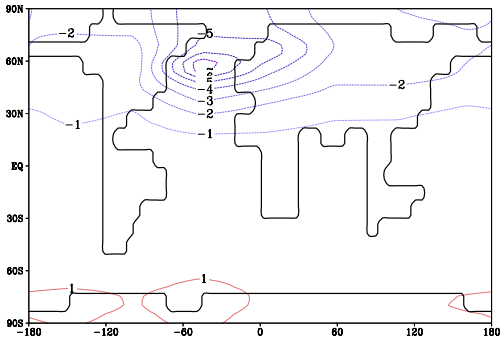

Figure 5.16: Annual averaged surface air temperature difference [in ° C] between LGM_{ACIFV} and LGM_{ACIF}.

ference between LGM_{ACIFV} and LGM_{ACIF} (that includes the effect of the atmosphere-vegetation feedback and its synergies) is now looked at: LGM_{ACIF} simulates a surface temperature of 9.8° C, showing a globally by 0.7 °C warmer climate for the Last Glacial Maximum than LGM_{ACIFV}. While the pattern of temperature change relative to REF is very similar for LGM_{ACIFV} and LGM_{ACIF}, a strong difference is seen over the North Atlantic where the cooling is up to −7 °C stronger for LGM_{ACIFV} than for LGM_{ACIF} (Fig. 5.16). This difference decreases down to −1 °C at 30° N and is also present over the continents of the NH with a temperature difference of about −2° C, with even stronger cooling in western Europe (up to −5° C). Even though LGM_{ACIFV} is globally colder than LGM_{ACIF}, the Southern Ocean and Antarctica are by 1.5 °C warmer in LGM_{ACIFV}.

The additional cooling over the Northern Hemisphere in LGM_{ACIFV} compared to LGM_{ACIF} is, thereby, mainly caused by the taiga-tundra feedback in the northern latitudes where the vegetation changes from trees to grass or desert, the sea-ice-albedo effect of the extended sea-ice cover in the North Atlantic (Fig. 5.18) and the reduced northward heat transport (Fig. 5.19) caused by a weaker overturning in the North Atlantic (Fig. 5.20). The temperature difference is, thereby, strongest in winter, second strongest in spring and weakest in summer (Fig. 5.17). The reason for this is that the cooling effect of the extended sea-ice cover and the decreased northward heat transport is strongest in winter (reaching −9 °C over the North Atlantic) while the effect of the changed vegetation is strongest in spring, where a widespread cooling of 3 °C is seen over Eurasia and the sea-ice still cools the air over the ocean (−6 °C over the ocean). The warming over the Southern Ocean in LGM_{ACIFV} compared to LGM_{ACIF} is also caused by the decreased northward heat transport in LGM_{ACIFV}, as more heat stays on the SH.

Overturning and northward heat transport are decreased in LGM_{ACIFV} compared to LGM_{ACIF} because the ocean is in the so-called "warm" glacial mode in LGM_{ACIF} while it is in the "cold" glacial mode in LGM_{ACIFV} (Fig. 5.20). This means that in LGM_{ACIF} the convection is intensified and reaches down below 5000 m, which is an increase by about 2000 m compared to REF. This drastically decreases the outflow of

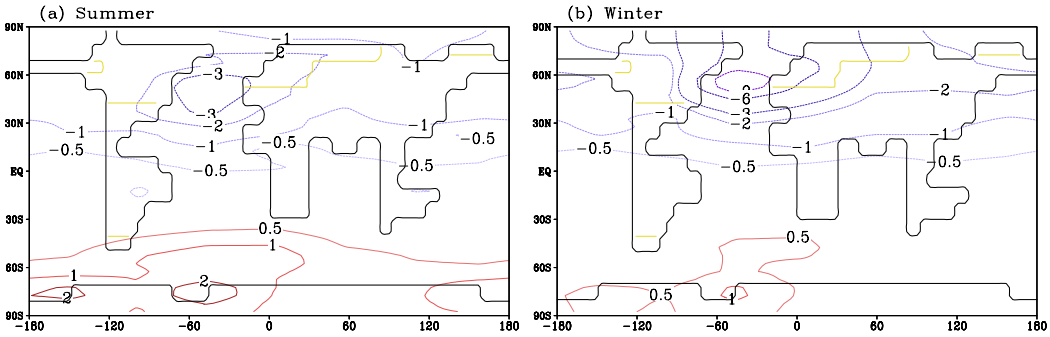

Figure 5.17: Surface air temperature difference [in ° C] between LGM_{ACIFV} and LGM_{ACIF} for summer (a) and winter (b). For orientation the 60% inland ice line is plotted in yellow.

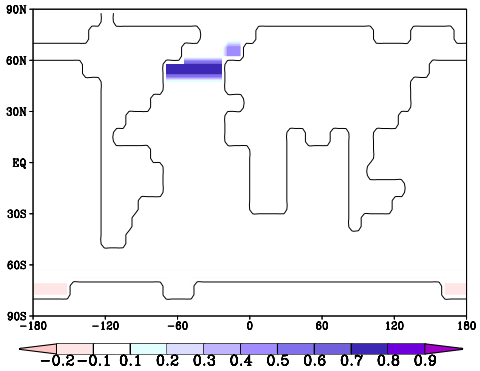

Figure 5.18: Annual averaged sea-ice fraction difference for $LGM_{ACIFV} - LGM_{ACIF}$. The southward shift of the sea-ice margin is caused by the southward shift in NADW formation to 45° N in LGM_{ACIFV}.

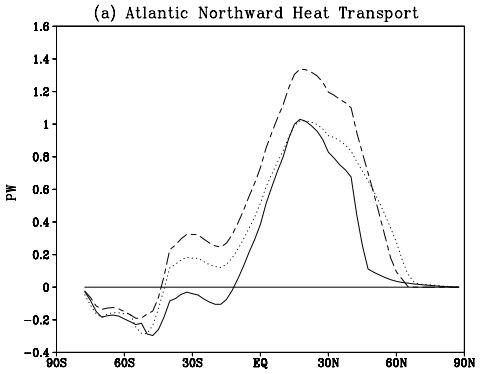

Figure 5.19: Latitudinal distribution of the annual vertically and zonally integrated northward heat transport [in PW] in the Atlantic for LGM_{ACIFV} (solid), LGM_{ACIF} (dashed) and REF (dotted).

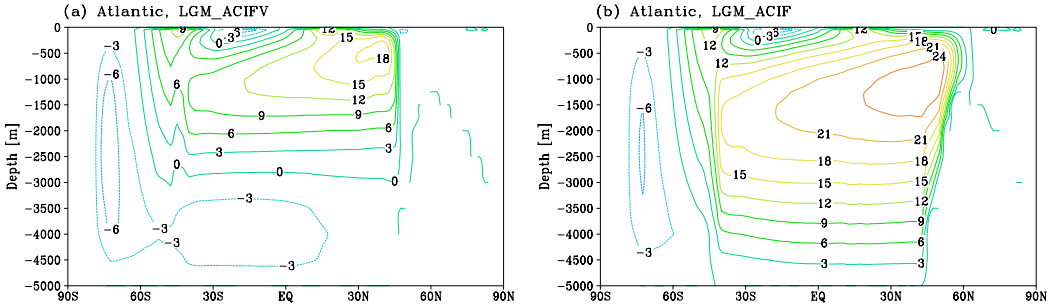

Figure 5.20: Annual averaged overturning stream function for the Atlantic [in Sv]. LGM_{ACIFV} is in the glacial "cold" mode (a) and LGM_{ACIF} in the glacial "warm" mode (b).

AABW into the Atlantic by 2.4 Sv in LGM_{ACIF} compared to REF, as well as AABW formation in the Southern Ocean (by 4.5 Sv). The maximum Atlantic overturning in LGM_{ACIF} shows an increase by 5.6 Sv compared to REF and 6.3 Sv compared to LGM_{ACIFV}, so that NADW formation in the Nordic Seas is increased in LGM_{ACIF}. Due to the stronger oceanic overturning in LGM_{ACIF}, the northward heat transport in the Atlantic is increased by 0.15 PW compared to REF and by even 0.29 PW compared to LGM_{ACIFV}. All this is in contrast to the ocean circulation seen in LGM_{ACIFV}, with decreased northward heat transport, a weaker and shallower overturning and a southward shift in NADW formation.

The switch from the "warm" mode in LGM_{ACIF} to the "cold" mode in LGM_{ACIFV} is caused by the use of the interactive vegetation because its use leads to an additional cooling and drying of the climate so that the threshold of the ocean circulation is crossed. The fact that a small change as the atmosphere-vegetation feedback and its synergies can cause this large change in the ocean is the result of the non-linear behavior of the ocean circulation (Ganopolski and Rahmstorf 2001). It shows that already in LGM_{ACIF} the circulation was close to its threshold where it would jump to the "cold" mode.

In addition to temperature differences and changes in the ocean circulation also precipitation changes occur between LGM_{ACIFV} and LGM_{ACIF}. The simulation LGM_{ACIF} yields a by 0.07 mm/day (25 mm/year) moister climate than LGM_{ACIFV}. This difference between LGM_{ACIFV} and LGM_{ACIF} is limited to the NH, with the largest difference centered over two areas: Over the North Atlantic, where precipitation decreases by up to 0.8 mm/day, and over southern North America around 40° N, where an increase in precipitation of up to 0.4 mm/day is found. Besides that, precipitation is reduced in the tropics by up to 0.2 mm/day (Fig. 5.21). The precipitation reduction in the tropics is a feature of summer and fall, while the decrease over the North Atlantic and over southern North America is least pronounced during this time and reaches its maximum in winter and spring (Fig. 5.22). This seasonal distribution is due to the different causes of the precipitation change: In the tropics the effect is caused by a weaker hydrological cycle due to vegetation changes that are strongest in summer and fall when temperatures are highest. Over the North Atlantic and southern South America the decrease is caused by the shift in storm tracks due to extended sea-ice and inland ice cover. Thus, it is at its maximum in the storm season from fall to spring.

Comparison of the Vegetation Effect with other Studies

Ganopolski et al. (1998b) already performed a simulation for the LGM with an earlier version of CLIMBER-2 (CLIMBER-2.0) and with prescribed present day vegetation. In their study they found a global LGM cooling of 6.2 °C and an ocean that was in the "cold" glacial mode. These earlier results differ from my results, which is most obvious in the temperature change as LGM_{ACIFV} causes a 4.8° C cooling and LGM_{ACIF}, which corresponds to their experiment, a cooling of 4.1° C. However, not only the temperature change is different in Ganopolski et al. (1998b), as LGM_{ACIF} shows the ocean in the

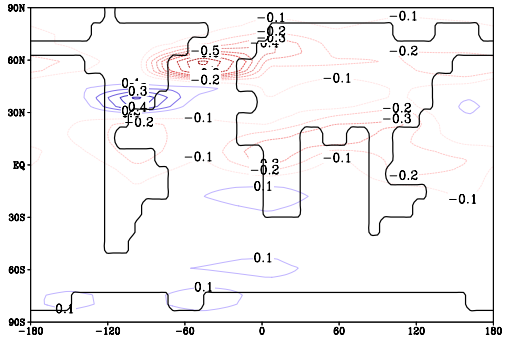

Figure 5.21: Annual averaged precipitation difference [in mm/day] between LGM_{ACIFV} and LGM_{ACIF}.

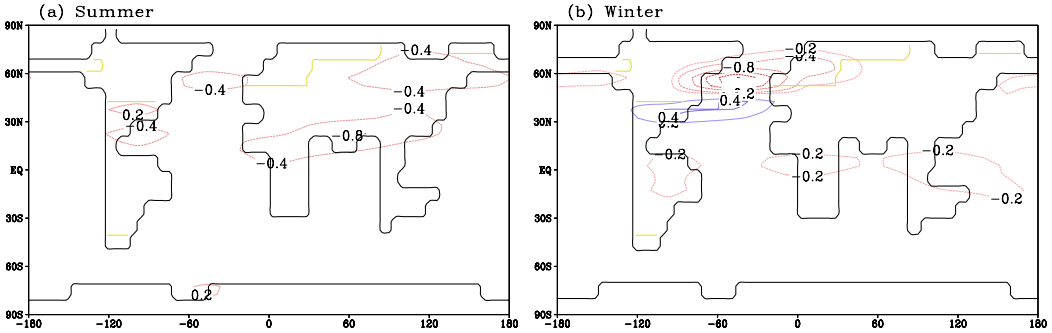

Figure 5.22: Precipitation difference [in mm/day] between LGM_{ACIFV} and LGM_{ACIF} for summer (a) and winter (b). For orientation the 60% inland ice line is plotted in yellow.

"warm" glacial mode that is only transformed to the "cold" glacial mode (that they found) when the interactive vegetation is added in LGM_{ACIFV}.

Part of the reason for the differences is that the climate sensitivity of the model is lower in the current version of CLIMBER-2 than in the earlier version, which accounts for about one degree stronger cooling in the study of Ganopolski et al. (1998b). Another part of the difference is due to an improvement in ocean parametrization and the increase of ocean levels. The different ocean state in the two studies is again explained by the non-linearity of the ocean circulation and the stability of the glacial ocean circulation: Due to the lower climate sensitivity in my model version, the additional cooling caused by the interactive vegetation was needed for the system to cross the threshold of the ocean circulation towards the "cold" glacial mode. It is important to note that, even though the ocean circulation change occurs when vegetation is switched on, it is not the vegetation itself that "changes" the ocean circulation! Rather, the additional cooling effect of the interactive vegetation and its feedbacks provided the small change that was still missing in LGM_{ACIF} in order to cross the threshold of the circulation, as the ocean circulation is very close to the bifurcation point in the glacial

climate state (Ganopolski and Rahmstorf 2001).

In their study, Ganopolski et al. (1998b) differentiated between a slab ocean and a full ocean to determine the role of the deep ocean circulation in glacial climate and found that with a slab ocean the cooling was only 4.2° C, so that the ocean circulation had an additional cooling effect on the glacial climate. Even though temperatures cannot be directly compared as they differ considerably, it can be inferred form the study of Ganopolski et al. (1998b) that the deep ocean circulation amplifies the global LGM cooling in CLIMBER-2 by about 30%.

The decrease in northward heat transport simulated in LGM_{ACIFV} agrees with results from some modeling studies (e.g. Weaver et al. 1998; Kim 2004, 2003) but is in disagreement with others (e.g. Hewitt et al. 2003; Kitoh et al. 2001). The weaker and shallower overturning and its shift to the south simulated with CLIMBER-2.3 in LGM_{ACIFV} is consistent with findings from Kim (2003) and Weaver et al. (1998) but is contrary to others (Hewitt et al. 2001, 2003; Kitoth et al. 2001). Hewitt et al. and Kitoth et al. explain their increased overturning and northward heat transport with an increase in buoyancy flux to the surface waters across the North Atlantic and the Labrador Sea. Paeleodata is rather in favor of a weaker circulation and less northward heat transport though (Lynch Stieglitz et al. 1999, Duplessy et al. 1988).

Due to the different ocean circulation in LGM_{ACIFV} and LGM_{ACIF}, LGM_{ACIF} agrees with exactly the studies that LGM_{ACIFV} and the study by Ganopolski et al. (1998b) disagrees with. As the ocean circulation is a threshold system and in CLIMBER-2 a change in climate sensitivity or the use of an interactive or fixed present day vegetation made the difference in whether the ocean stayed on the "warm" side of the bifurcation point or whether it crossed it to the "cold" side, it can be suspected that similar reasons cause the difference among the model results and that small changes in the models setup could yield different results.

Comparison of the Atmosphere-Vegetation Feedback with other Studies

If concentrating only on the temperature change caused directly by the vegetation (without including the strong non-linear cooling effect of the changed ocean circulation), these results can be compared to the results of other studies that have also investigated the effect of either an interactive or a prescribed LGM vegetation distribution. I want to shortly present and compare the results of three often cited examples with my results, but it should be noted that there are many more studies dealing with the vegetation influence in the LGM (e.g. Levis and Foley 1999).

Wyputta and McAvaney (2001) investigated the importance of different vegetation distributions on the atmospheric circulation during the Last Glacial Maximum. They used the atmospheric general circulation model BMRC with vegetation reconstructions for the LGM and today and prescribed modern day SST. They find that the LGM vegetation makes the LGM climate globally 0.3 °C colder, with the strongest decrease over

land on the NH where cooling reaches −6 °C over Siberia and −4 °C over North America and an increase over Alaska due to a strengthened jet stream. Vegetation changes alter the surface albedo by 4% in their experiment. Compared with the vegetation effect in my study, the cooling of Wyputta and McAvaney (2001) is really large, as CLIMBER-2.3 only shows a cooling due to vegetation changes of about 1.5–2 °C over northern Eurasia and Siberia. The reason for this smaller change in CLIMBER-2.3 is probably a much smaller albedo change caused by the modeled vegetation changes in my study.

Crowley and Baum (1997) investigated the effect of vegetation changes during the LGM with the GENESIS GCM. They used a LGM vegetation reconstruction by Crowley (1995) and CLIMAP SST and sea-ice distributions for the LGM. With their experiments they found a 3–7 °C change over Siberia and western Europe compared to today. This was a decrease of 2–4 °C compared to LGM simulations with present day vegetation but otherwise LGM conditions. This cooling of 2–4 °C is larger than the 1.5–2 °C cooling over Sibiria found in my model, but it is closer than the results of Wyputta and McAvaney (2001). Large differences between the study of Crowley and Baum (1997) and my study are found in the tropics, as they prescribed a reduction of about 65% in tropical rainforest area (based on Crowley 1995), while in my study the tropical rainforest is only reduced by about 20–30%. As a consequence, Crowley and Baum (1997) find an additional cooling over Australia and Africa while the Amazon Basin warms by 2–4 °C compared to present day. None of these changes can be seen in my study, due to the much smaller change in tropical rainforest area that is probably an underestimation of the vegetation changes in the tropics.

Kubatzki and Claussen (1998) performed an experiment with the coupled ECHAM-BIOME model to investigate the influence of a modeled vegetation in contrast to a prescribed present day vegetation for the LGM. In their experiment, SST, CO_2 concentration, sea-ice distribution and orography were prescribed from CLIMAP (1981) and inland-ice coverage from Tushingham and Peltier (1991). They found the most striking differences in the high northern latitudes and especially in Siberia, with an additional cooling of 1–2 °C and 5° C, respectively, due to the taiga-tundra feedback that can work when the interactive vegetation is used. In sensitivity studies they also found that in North Africa two equilibrium states exist, depending on the initial conditions. Hence, they concluded that the African monsoon region and the high northern latitudes are "hot-spots" regarding atmosphere-vegetation feedbacks. As in the other presented studies, the cooling effect of vegetation over Siberia is much larger in Kubatzki and Claussen (1998) than in my study, while the averaged cooling in the high northern latitudes in Kubatzki and Claussen (1998) agrees quite well with my results.

This short comparison with other studies regarding the effect of the vegetation shows that the cooling caused by the vegetation changes simulated by CLIMBER-2.3 is smaller than the cooling calculated by other models if they use a prescribed reconstructed vegetation (as Wyputta and McAvaney (2001) and Crowley and Baum (1997)). Compared to the study of Kubatzki and Claussen (1998), who used a dynamic vegetation model, my study differs less. This shows that the results differ not only among models, but

that also a reconstructed or modeled vegetation makes a difference. The region where vegetation changes cause an additional cooling in the LGM, the high northern latitudes and especially Siberia, is the same in all above summarized studies so that it can be concluded that this region is the most sensitive region for the atmosphere-vegetation feedback during the LGM.

5.2 Contribution of Individual Factors

The climatic differences between LGM_{ACIFV}, LGM_{ACIF} and REF presented in the previous section can be attributed to individual factors and synergies. In order to separate their influence, I used the Stein and Alpert Factor Separation (1993) and looked at five different factors: The astronomical forcing, CO_2 forcing, inland ice sheets and orography forcing, FSB forcing and the vegetation feedback (see also section 4.1). The first four factors are forcings, while the last one, the vegetation, is a feedback. This has the consequence that the factor $\hat{f}_V$ is zero because without changed boundary conditions an interactive vegetation obviously leads to no effect. However, vegetation reacts to the changed forcings so that $\hat{f}_{AV}, \hat{f}_{CV}, \hat{f}_{IV}$ and $\hat{f}_{FV}$ are the "synergistic" terms between various changed forcings and the vegetation feedback.

From the 30 factors that I calculated for a number of climatic variables seven factors proved to be of some importance in order to explain the final result, globally or regionally. These seven factors are: $\hat{f}_F, \hat{f}_C, \hat{f}_I, \hat{f}_{CI}, \hat{f}_{CV}, \hat{f}_{IV}, \hat{f}_{CIV}, \hat{f}_{CIFV}$. I will discuss the effects of these seven factors for temperature and precipitation on the following pages. Only the factors for temperature and precipitation will be investigated in detail as they are the most important atmospheric climatic variables, but the factors for other climatic variables are also mentioned when necessary in order to explain the reaction of the climate system and to complete the picture. The acronyms for the factors (like $\hat{f}_I$) always stand for the change caused by this specific factor for the variable named in the context, e.g. in case of $\hat{f}_I$ for sea-ice it is the difference in sea-ice area between the run LGM_I and the run REF (see section 2.2 for the calculation of factors).

The astronomical factor and its synergies turned out to have only small and rather insignificant effects, as it was expected since the astronomical forcing was not very different from today. If summing up $\hat{f}_A$ and all synergistic terms that include astronomical forcing, it makes up only 0.3% of the temperature change $LGM_{ACIFV} - REF$ and 1.6% of the precipitation difference[2]. Therefore, they are not discussed any further in this work, neither are all the other factors that do not belong to the above seven mentioned important ones. A table with the values of global temperature and precipitation factors for all 32 factors is shown in appendix A.2 on page 113.

[2]If summing up all synergistic terms for each individual forcing separately, as done here for the astronomical forcing, this would lead to an overall sum that is larger than 100% of $LGM_{ACIFV} - REF$ as all synergy terms would be counted twice, three times, four times or even five times, depending how many factors they include. This sum is, therefore, not giving the absolute individual contribution of the astronomical factor, but mixes it with the synergistic effects with others. It is, nevertheless, used here to demonstrate how small the astronomical effect is.

5.2.1 Temperature

The global surface air temperature (SAT) decrease of 4.9 °C is caused to 60% by the factor $\hat{f}_I$ and to 26% by $\hat{f}_C$. The remaining 13% are explained by $\hat{f}_{IV}$ which causes 9.7% of the cooling and $\hat{f}_{CIV}$ and $\hat{f}_{CV}$ which cause another 2.8% and 1.5% respectively. Another factor worth while considering is $\hat{f}_{CI}$ as it shows temperature changes on NH and SH that are larger than $\hat{f}_{CV}$, but globally it is small due to the different direction of the changes on SH and NH. The same is true for $\hat{f}_{CIFV}$ which causes even higher absolute temperature changes on the respective hemisphere.

In table 5.1 the annual mean temperature change caused by all the above mentioned factors is shown while on page 56 the spatial distribution of all these factors is shown. The discussion of the individual factors and also some additional figures to them follow on pages 55–67.

Factor	Global	NH	SH
$\hat{f}_I$	−2.96	−4.00	−1.93
$\hat{f}_C$	−1.32	−1.21	−1.43
$\hat{f}_{IV}$	−0.48	−0.59	−0.36
$\hat{f}_{CIV}$	−0.14	−0.68	+0.40
$\hat{f}_{CV}$	−0.07	−0.10	−0.04
$\hat{f}_{CI}$	+0.03	−0.08	+0.13
$\hat{f}_{CIFV}$	+0.02	−0.12	+0.15

Table 5.1: The important annual averaged surface air temperature factors [in °C] with their global, NH and SH values, in the order of their relative global importance.

Inland Ice and Orography Factor $\hat{f}_I$

The global temperature change caused by the factor $\hat{f}_I$ is −2.96° C, which accounts for 60.1% of the total $LGM_{ACIFV} - REF$ cooling and even 70.5% of the $LGM_{ACIF} - REF$ change. This temperature change is mainly due to the change in albedo and orography caused by the imposed inland ice sheets (Fig. 5.2 on page 40). In North America and northern Eurasia, the orography is changed by 1500–2000 m and 1000–1500 m, thus changing the surface air temperature because of the higher elevation[3]. The global averaged surface albedo is increased by 3% due to $\hat{f}_I$, but over the new inland ice areas of North America and Eurasia the albedo increase is much larger (40–50% from the value in REF). Since these changes are mainly concentrated on the Northern Hemisphere, it is not surprising that the factor $\hat{f}_I$ causes its most pronounced effect there as well,

[3]With a lapse rate of 0.65 K/100 m, a change in orography by 1000 m causes a local change in surface air temperature of 6.5 K, for 1500 m of 9.75 K. The orography effect is, therefore, smaller than the albedo effect, but is responsible for about 1/3 of the decrease over Northern America and Eurasia

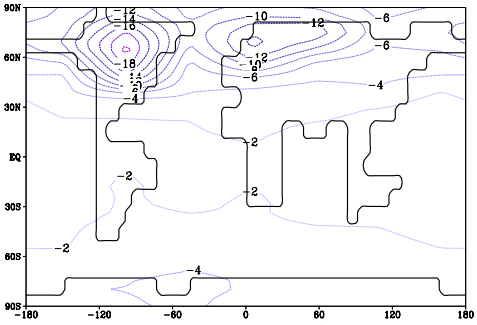

Figure 5.23: $\hat{f}_I$

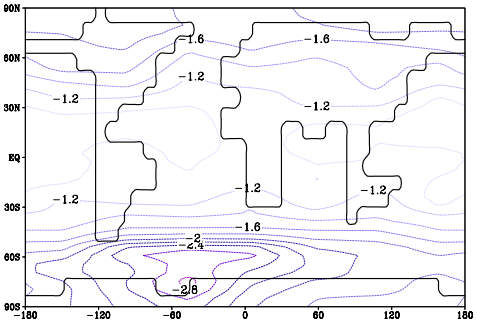

Figure 5.24: $\hat{f}_C$

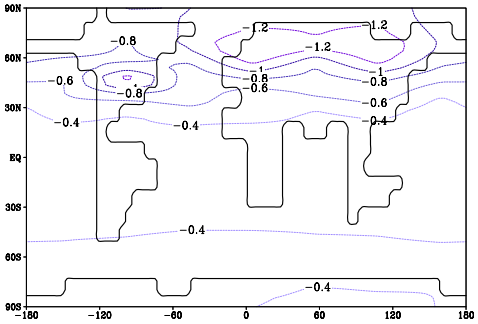

Figure 5.25: $\hat{f}_{IV}$

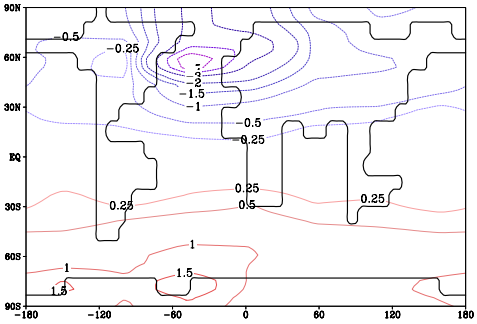

Figure 5.26: $\hat{f}_{CIV}$

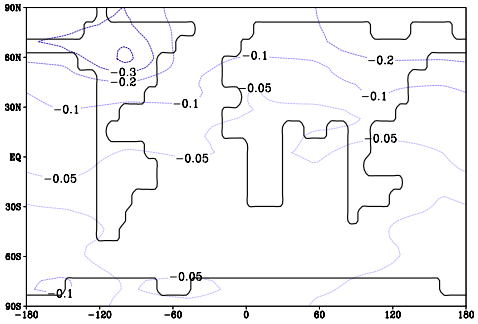

Figure 5.27: $\hat{f}_{CV}$

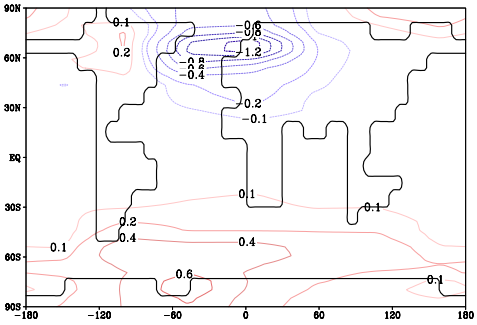

Figure 5.28: $\hat{f}_{CI}$

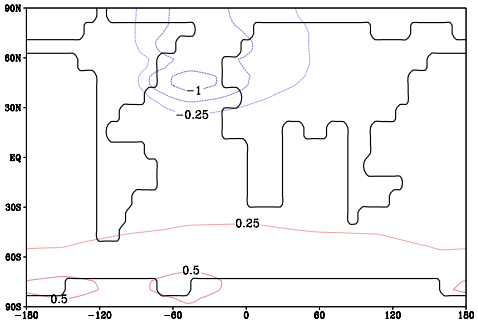

Figure 5.29: $\hat{f}_F + \hat{f}_{CIFV}$

Fig. 5.23–5.29 show the annual averaged surface air temperature changes for the named factors [in $^\circ$ C] .

with temperatures over central North America decreasing by up to $-20\,^{\circ}$C on annual average and over northern Europe by -14° C.

From the northern high latitudes the SAT change decreases towards the equator, reaching less than $-2\,^{\circ}$C in the tropical regions and only a maximum of $-4\,^{\circ}$C over parts of Antarctica and the Southern Ocean. The cooling over the tropical and subtropical regions can be explained by the water vapor feedback[4]. Atmospheric water content decreases by $0.29\,\mathrm{kg/m^3}$, which is a 12% decrease compared to REF and makes up 60% of the total $LGM_{ACIFV} - REF$ reduction, reducing the greenhouse effect and thus leading to a global cooling, also in regions where no substantial change in albedo or orography is simulated. All this leads to a radiative effect at the top of the atmosphere of $-3.97\,\mathrm{W/m^2}$, which are 64% of the $LGM_{ACIFV} - REF$ reduction.

The cooling over the Southern Ocean is due to the increase of sea-ice area (by 25%) there, as well as to the by 0.23 PW increased northward heat transport (which is an increase of 56% relative to REF) that reduces the heat in the Southern Hemisphere (Fig. 5.30). This increase in northward heat transport is due to the increase of 7.25 Sv in

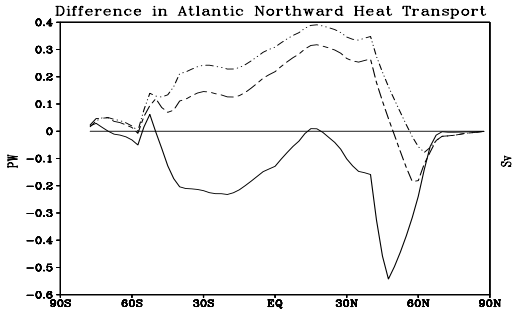

Figure 5.30: Difference in annual averaged northward heat transport for the factor $\hat{f}_I$ (dot-dot-dashed), $LGM_{ACIFV} - REF$ (solid) and $LGM_{ACIF} - REF$ (dashed)

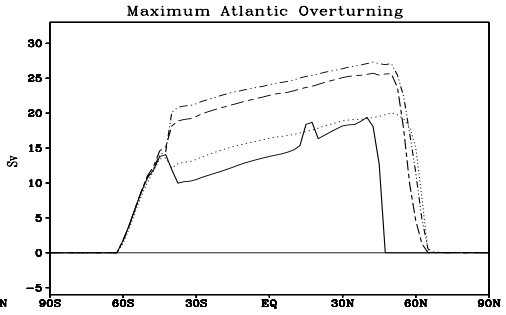

Figure 5.31: Annual maximum overturning stream function in Atlantic for $\hat{f}_I + REF$ (dot-dot-dashed), LGM_{ACIFV} (solid), LGM_{ACIF} (dashed) and REF (dotted).

maximum North Atlantic overturning (Fig. 5.31) and thus in increased NADW formation. The convection in the North Atlantic intensifies and reaches down to the bottom of the Atlantic (Fig. 5.32 (a)), thus greatly reducing the outflow of Antarctic bottom water into the Atlantic (by 2.7 Sv, which is equal to a reduction of 87%). AABW formation is also decreased by 28% (4.6 Sv), as can be seen in Figure 5.32 (b). These changes in the ocean are a result of the change in the Atlantic circulation, from the "warm" interglacial state in REF to the so-called "warm" glacial mode (Rahmstorf and Ganopolski 2001) in LGM_{ACIF}. The factor $\hat{f}_I$, therefore, is the main factor that governs the change in ocean circulation for the LGM_{ACIF} run, with $\hat{f}_I$ even causing greater changes than seen in LGM_{ACIF} so that other factors will dampen the effect of

[4]This feedback can add to the "pure" albedo and orography effect since water vapor is not a factor I investigated here, thus it can interact with and react to the forcings (see also section 2.1).

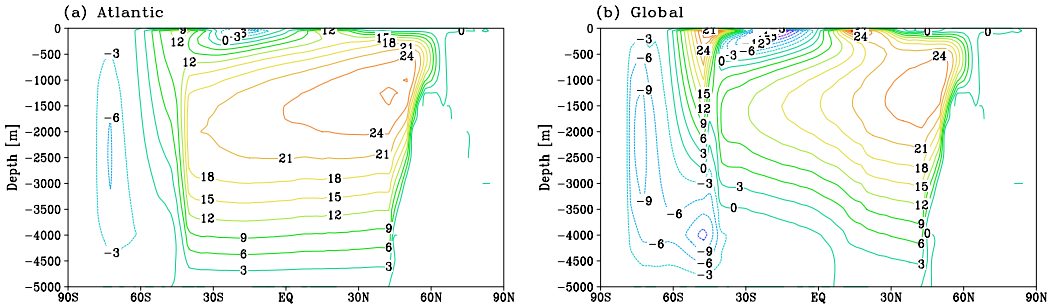

Figure 5.32: Annual averaged Atlantic (a) and global (b) overturning stream function [in Sv] for $REF+\hat{f}_I$. The Atlantic is in the "warm" glacial mode.

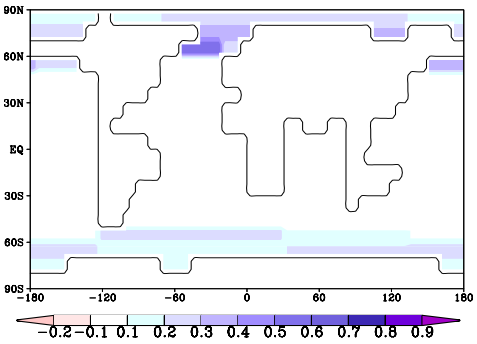

Figure 5.33: Difference in annual averaged sea-ice caused by $\hat{f}_I$.

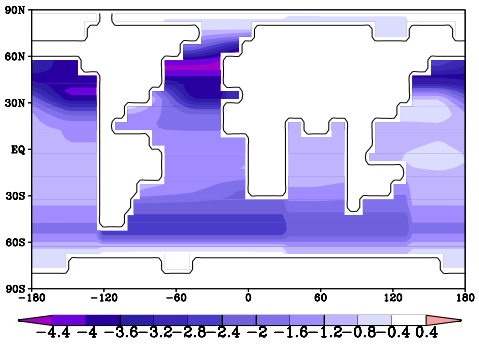

Figure 5.34: Difference in annual averaged SST caused by $\hat{f}_I$.

$\hat{f}_I$ slightly.
SST is also reduced (Fig. 5.34), globally by 1.3 °C (56% of the $LGM_{ACIFV} - REF$ change)and regionally by 2.5–3 °C in the southern Atlantic ocean and also in the northern Atlantic and Pacific Ocean. This leads to an extension of sea-ice fraction by overall 59% (Fig. 5.33), which is already 60% of the $LGM_{ACIFV} - REF$ increase in sea-ice fraction. Due to the greatly intensified temperature gradient between the polar regions and the tropics the surface wind speed increases by 0.35 m/s, which makes up 81% of the LGM_{ACIFV} increase.

The earlier so-called "displacement" response of the vegetation is formally also due to the factor $\hat{f}_I$, because the inland ice replaces the vegetation in the northern latitudes, thus causing a global 2.1% decrease of grass fraction and a reduction of global tree fraction by 3.3%. This reduction is limited to the area of extended inland ice, which are the northern latitudes and the southern tip of South America (as shown in Figure 5.15 (e) and (f) on page 47).

Overall, with respect to atmospheric reactions, the ice and orography effect has the greatest impact on the climate from the factors looked at. It alone is already respon-

sible for about 60% of the $LGM_{ACIFV} - REF$ change in SAT, radiative effect and atmospheric water vapor (and also for the SST change), while its effect on surface wind speed is even larger (81%). For the response of the oceanic circulation its influence is also very important, as $\hat{f}_I$ causes large changes in overturning, northward heat transport and AABW formation, but in the opposite direction to the overall $LGM_{ACIFV} - REF$ change.

CO_2 Factor

The global temperature change caused by the factor $\hat{f}_C$ is $-1.32°$ C. This is 26.8% of the total $LGM_{ACIFV} - REF$ cooling and 31% of the $LGM_{ACIF} - REF$ change. In general, the CO_2 cooling is caused by the reduced greenhouse warming due to the 80 ppm reduction in atmospheric CO_2 concentration. The decrease in atmospheric water content by 6% (relative to REF and 32% of the $LGM_{ACIFV} - REF$ reduction) leads to an even further decrease of the greenhouse effect. As CO_2 changes influence the atmospheric composition in general, its effect is always a global one. Nevertheless, the effect can be intensified by processes at the earth surface so that in the end the surface air temperature changes turn out to be stronger in the polar regions than in the tropics (Figure 5.24). This is due to an 5% increased snow cover there as a reaction to the colder temperatures, with a, therefore, higher albedo in the high latitudes of both hemispheres (see detailed description of the ice/snow-albedo feedback in chapter 2.1), while the albedo in the tropics does not change. Globally, the albedo increases by 0.8%. The magnitude of the temperature change increases from less than $-1\,°$C in the tropics and subtropics to $-1.5\,°$C in the Arctic and $-2.5\,°$C over the Southern Ocean and Antarctica.

The more pronounced cooling over the southern polar region is consistent with the overall stronger southern hemispheric CO_2 cooling (see table 5.1). It is caused by the increase in sea-ice in the Southern Ocean by almost 20% (Fig. 5.35). The cooling over the sea-ice is strongest in the Southern Hemisphere winter and spring (June–November) while it is weakest in Southern Hemisphere summer (December–February). Since the incoming radiation is low during southern winter, the main cooling effect is due to the isolating effect of the sea-ice that prevents the heat flux from the relative warm ocean to the cold air and not so much to the sea-ice albedo effect.

Surface wind speed increases by 0.05 m/s globally due to the increased temperature gradient between the poles and the tropics. This increase makes up 13% of the $LGM_{ACIFV} - REF$ increase of 0.4 m/s.

The cooling pattern for the SST (Fig. 5.36) is basically the same as for the air temperature, only the amplitude of the cooling is smaller, reaching $-0.9\,°$C globally, $-0.6\,°$C in the tropics, $-1.2\,°$C in the North Atlantic and $-1.5\,°$C in the Southern Ocean. On the global scale the CO_2 factor is responsible for 40% of the total SST decrease in LGM_{ACIFV}. The global annual radiative effect of the CO_2 factor at the top of the atmosphere is -0.94 W/m^2, compared to the pure astronomical effect of $+0.02$ W/m^2

it is rather large. The total radiative difference between LGM_{ACIFV} and REF is -6.18 W/m^2, so that $\hat{f}_C$ makes up 15% of this decrease.

In the ocean, the AABW formation weakens by 2 Sv (12%) due to $\hat{f}_C$ and NADW formation increases slightly by 0.3 Sv, which are 5.8% of the $LGM_{ACIF} - REF$ increase. Also mean Atlantic overturning increases and reaches down to 3400 m, 400 m deeper than in REF. The northward heat transport is not notably changed, its increase makes up only 1.7% of the $LGM_{ACIF} - REF$ change and -1.6% of the $LGM_{ACIFV} - REF$ decrease. However, as already seen for $\hat{f}_I$, these effects of $\hat{f}_C$ in the ocean are opposite to the total $LGM_{ACIFV} - REF$ change.

Overall, in respect to temperature changes, $\hat{f}_C$ has a strong influence on SAT and SST change causing 26.7% and 40% of the total LGM_{ACIFV} SAT and SST reduction, respectively. Its impact is also important for the surface wind, the sea-ice and the radiative effect, accounting for 13%, 30.5% and 15% of the respective $LGM_{ACIFV} - REF$ change, while its influence on the ocean circulation is rather small (below 10%) but opposite to the $LGM_{ACIFV} - REF$ change.

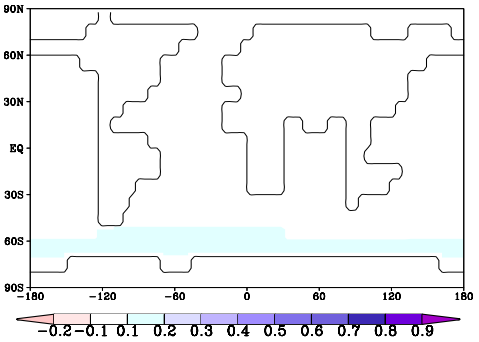

Figure 5.35: $\hat{f}_C$ annual averaged sea-ice effect

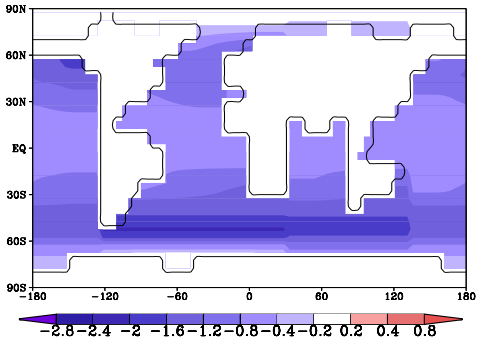

Figure 5.36: $\hat{f}_C$ annual averaged SST effect [in $^\circ$ C]

Synergy of Inland Ice/Orography and Vegetation ($\hat{f}_{IV}$)

The global mean temperature decrease is -0.48° C, which is 9.7% of the global difference between LGM_{ACIFV} and REF and 68.6% of the change between $LGM_{ACIFV} - LGM_{ACIF}$. Formally it is the cooling caused by the "synergism" between inland ice and vegetation, but since $\hat{f}_V = 0$ (explained before) and inland ice is prescribed, it mainly is the cooling caused by the reaction of the vegetation to the cooling induced by the factor $\hat{f}_I$. This reaction consists primarily of the albedo change due to vegetation reduction, but also in the decrease of transpiration and, therefore, atmospheric water content by 2.3% compared to REF, which are 11.6% of the $LGM_{ACIFV} - REF$ reduction. The SAT reduction is largest over land areas, especially in the northern latitudes where it reaches its maximum magnitude of -1.2° C. The cooling is smallest in the tropics and subtropics and much larger over the NH than over the SH (Fig. 5.25).

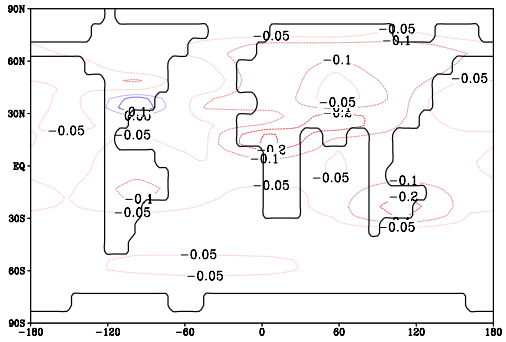

Figure 5.37: Annual averaged evaporation change caused by $\hat{f}_{IV}$.

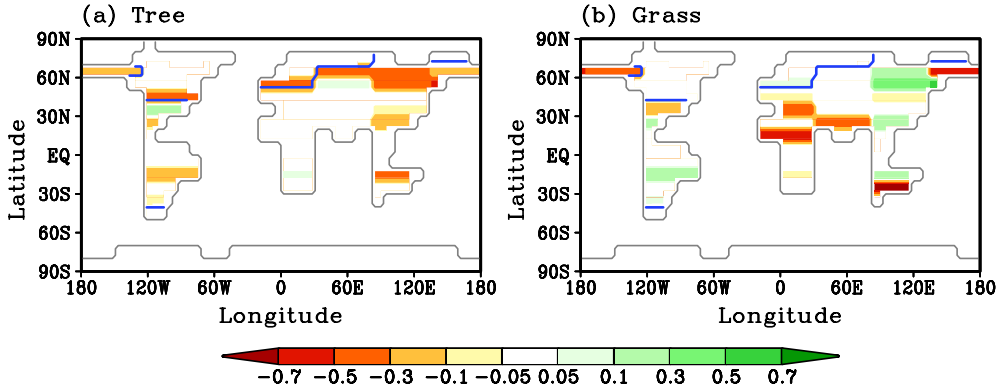

Figure 5.38: Vegetation change caused by $\hat{f}_{IV}$. Shown are the differences in tree fraction (a) and grass fraction (b). The blue line is the 60% inland ice border.

This cooling over land over northern Eurasia and central North America is caused mainly by the taiga-tundra feedback, as trees are replaced by grass or desert (Fig. 5.38). The effect is largest in spring with 1.5–2° C, due to the increased albedo of these regions when snow-covered. In summer, the temperature reduction over the northern latitudes decreases to −1° C, as the snow cover disappears, decreasing the albedo difference of trees and grass so that the temperature effect is smaller.

Over the areas where grass is replaced by desert (southern Europe, the Sahel, over northern India and over Australia), the cooling effect of $\hat{f}_{IV}$ is weakened during summer season (summer on the respective hemisphere), with temperature decrease reduced to −0.1 °C over these regions in this time. This is caused by the decrease in evaporative cooling over these regions due to the change in surface type from grass to desert (Fig. 5.37). This decrease in evaporation is strongest during summer and fall (reaching −0.3 mm/day) when temperatures are highest. The radiative effect at the top of the atmosphere is reduced by 0.9 W/m^2 due to $\hat{f}_{IV}$ (14.4% of $LGM_{ACIFV} - REF$).

On global average, tree fraction is reduced by 13% due to $\hat{f}_{IV}$, which is 82.9% of the total ($LGM_{ACIFV} - REF$) and 91,6% of the dynamic reduction. Grass fraction is

reduced by 5%, accounting for 56% of the total decrease and 62% of the dynamic change. The snow fraction is increased (8.4% of $LGM_{ACIFV} - REF$), especially in the northern latitudes, thus increasing the effect of the vegetation-snow-albedo effect there.

In the ocean, the effect of $\hat{f}_{IV}$ is small, only a small reduction in northward heat transport as well as a slight decrease in NADW formation and an also small weakening in AABW formation is simulated. SST is reduced globally by $-0.3\,^{\circ}$C on annual average, which are 12.5% of the $LGM_{ACIFV} - REF$ decrease.

Overall, $\hat{f}_{IV}$ is the third most important factor for many atmospheric variables in order to explain the change between LGM_{ACIFV} and REF. Since $\hat{f}_{IV}$ causes 90% of the dynamic tree reduction and 60% of the grass reduction it causes the strongest vegetation induced cooling from all considered factors.

Synergy of Inland Ice/Orography, CO_2 and Vegetation ($\hat{f}_{CIV}$)

On global average, the temperature reduction caused by the synergy term $\hat{f}_{CIV}$ is -0.14° C, which is 2.8% of the $LGM_{ACIFV} - REF$ change but 20% of the $LGM_{ACIFV} - LGM_{ACIF}$ decrease. Already in the table 5.1 one could see that the temperature change caused by $\hat{f}_{CIV}$ is negative on the Northern Hemisphere (-0.68) and positive on the Southern Hemisphere ($+0.40^{\circ}$ C). The temperature change thereby increases from the tropics, where it is only $0.05\,^{\circ}$C large (positive on SH, negative on NH), to the high latitudes of both hemispheres where it reaches its maximum over the ocean (Fig. 5.26). That already gives an indication that the temperature change pattern is caused mainly by the ocean and not the land. Indeed, mean northward heat transport decreases by 0.24 PW, which is a change of 60% compared to REF and makes up 169% of the $LGM_{ACIFV} - REF$ change and 83% of the decrease between LGM_{ACIFV} and LGM_{ACIF} (Fig. 5.39). Therefore, the effect of $\hat{f}_{CIV}$ is larger but opposite to $\hat{f}_I$, which caused -160% of the $LGM_{ACIFV} - REF$ change. This reduction in northward heat transport is caused by the reduction of the maximum overturning stream function by 5.6 Sv (Fig. 5.40). In other words, it causes a decrease of 830% compared with the $LGM_{ACIFV} - REF$ difference, while it makes up 99.5% of the difference between LGM_{ACIFV} and LGM_{ACIF}. This reduces NADW formation while AABW formation increases by 4.2 Sv, increasing the amount of Antarctic bottom water outflow by 4 Sv.

SST increases by only $0.08\,^{\circ}$C on global scale, but this small number is misleading as SST, like SAT, increases in the SH and decreases in the NH (Fig. 5.41). This can also be explained by the decreased mean northward heat transport, since now more heat stays in the Southern Ocean and on the Southern Hemisphere in general while the Northern Hemisphere is colder due to the lack of heat transported northwards. This is especially the case north of 50° N, where the temperature decrease is most pronounced, reaching 4° C, because the NADW formation site moves southward to 45° N. This leads to an increased sea-ice area in the North Atlantic (Fig. 5.42), which expands southward to 50° N on annual average and even to 40° N in winter and spring. The sea-ice albedo feedback together with the effect of reduced northward ocean heat transport finally leads to the strong reduction in surface air temperature over the North Atlantic, which is strongest during winter and spring when sea-ice cover is at its maximum extent and

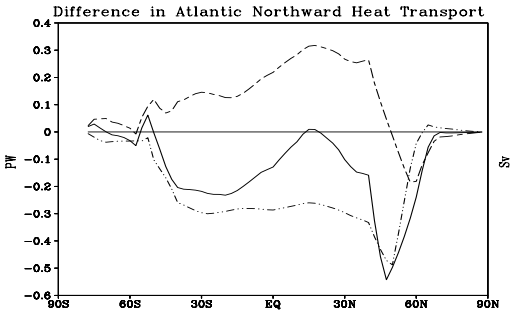

Figure 5.39: Difference in annual averaged northward heat transport for factor $\hat{f}_{CIV}$ (dot-dot-dashed), $LGM_{ACIF} - REF$ (dashed) and $LGM_{ACIFV} - REF$ (solid).

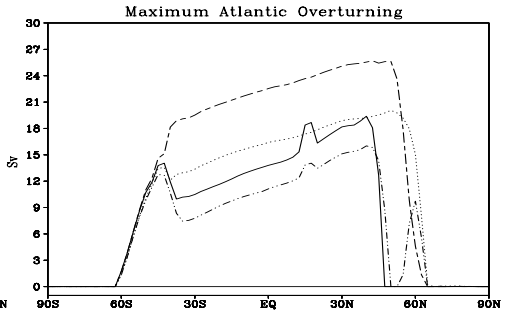

Figure 5.40: Annual maximum overturning stream function in Atlantic for $\hat{f}_{CIV} + REF$ (dot-dot-dashed), LGM_{ACIF} (dashed), LGM_{ACIFV} (solid) and REF (dotted).

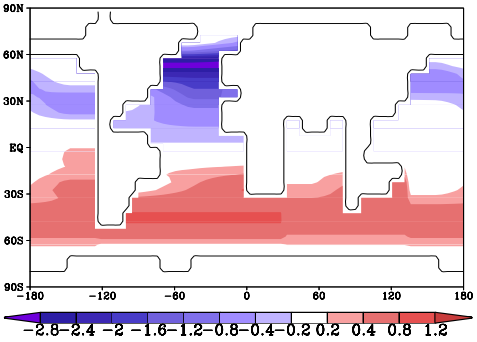

Figure 5.41: Annual averaged SST change caused by $\hat{f}_{CIV}$ [in $^\circ$ C]

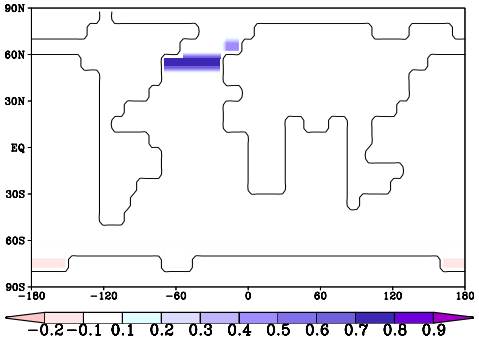

Figure 5.42: Annual averaged sea-ice fraction change caused by $\hat{f}_{CIV}$

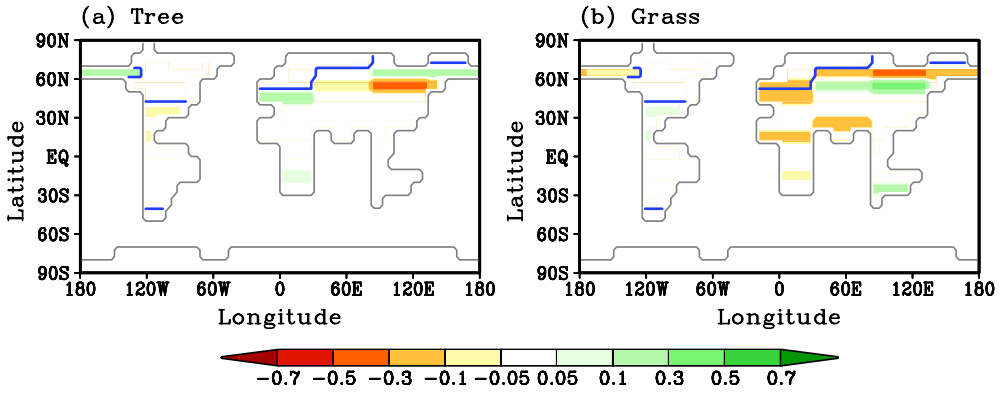

Figure 5.43: Vegetation change caused by $\hat{f}_{CIV}$. Shown are the differences in tree fraction (a) and grass fraction (b). The blue line is the 60% inland ice border.

the oceanic heat transport has the strongest effect on climate in this region (Rahmstorf 2000).

The vegetation change caused by the synergy factor $\hat{f}_{CIV}$ is smaller than the change caused by $\hat{f}_{IV}$, but it is still is the second most important factor in reducing vegetation. Grass fraction is reduced by 3% (38% of the dynamic response and 35% of total reduction) and tree fraction by 1% (7.4% of $LGM_{ACIFV} - LGM_{ACIF}$ and 6.7% of total reduction). Where trees are retreating (Fig. 5.43), the temperature decrease is largest during spring, the season when the snow-vegetation-albedo effect is strongest. The overall radiative effect of $\hat{f}_{CIV}$ at the top of the atmosphere is $-0.28\ \mathrm{W/m^2}$, which is 4% of the $LGM_{ACIFV} - REF$ change.

Overall, $\hat{f}_{CIV}$ has some influence on atmospheric variables, but this change is governed by the changes in the ocean circulation caused by $\hat{f}_{CIV}$ so that vegetation effects only add to it. In the ocean, $\hat{f}_{CIV}$ is responsible for the shift in Atlantic ocean circulation from the "warm" glacial mode found in LGM_{ACIF} to the "cold" glacial mode seen in LGM_{ACIFV} (Fig5.44 (b)). For the ocean circulation, $\hat{f}_{CIV}$ is, therefore, more important as $\hat{f}_I$, which was the factor mainly responsible for the shift from the "warm" interglacial to the "warm" glacial mode. However, $\hat{f}_I$ caused an increase in overturning that was even larger than the increase seen in LGM_{ACIF} so that $REF + \hat{f}_I$ leads to a too strong overturning compared to LGM_{AVIF} (Fig. 5.44 (a), (d)). If $\hat{f}_{CI}$ and $\hat{f}_C$ are also added they compensate the additional increase, so that their sum resembles LGM_{ACIF} (Fig. 5.44 (f)). The sum of $REF + \hat{f}_I + \hat{f}_{CI} + \hat{f}_{CIV}$ (Fig. 5.44 (g)) then resembles LGM_{ACIFV} almost completely (all this can be seen in Figure 5.44).

Synergy of CO_2 and Vegetation ($\hat{f}_{CV}$)

The global effect of $\hat{f}_{CV}$ is a decrease of SAT by 0.07° C, which is 3.32% of the global temperature reduction $LGM_{ACIFV} - REF$ and 18.5% of the $LGM_{ACIFV} - LGM_{ACIF}$ change. The effect is stronger on the NH than on the SH, with a NH cooling of 0.10 °C and of 0.04 °C on the SH.

This is due to the vegetation changes that occur mainly on the NH. The largest temperature decreases (Fig. 5.27) are seen exactly over the areas with the strongest decrease in vegetation cover (Fig. 5.45), with the strongest cooling during spring, due to the snow-vegetation-albedo effect. Since there is no extended inland ice cover yet for $\hat{f}_{CV}$, it is not a mistake that the strongest vegetation changes and consequently temperature changes are seen over North America (−0.04° C) and in Siberia (−0.2° C). South of these regions towards the southern polar regions, the cooling decreases, with only a slight increase in cooling over Antarctica. On global average, the tree fraction decreases due to $\hat{f}_{CV}$ by 2%, which are 14.7% of the dynamic response and 13.3% of the total difference of $LGM_{ACIFV} - REF$. For grass fraction a decrease of 1% is seen, causing 7.8% of the total and 8.6% of the dynamic response. Some part of the global cooling is also caused by the decrease in greenhouse warming due to the reduction in atmospheric water content by 2% of $LGM_{ACIFV} - REF$. At the top of the atmosphere $\hat{f}_{CV}$ causes a radiative effect of $-0.12\ \mathrm{W/m^2}$ (1.9% of $LGM_{ACIFV} - REF$).

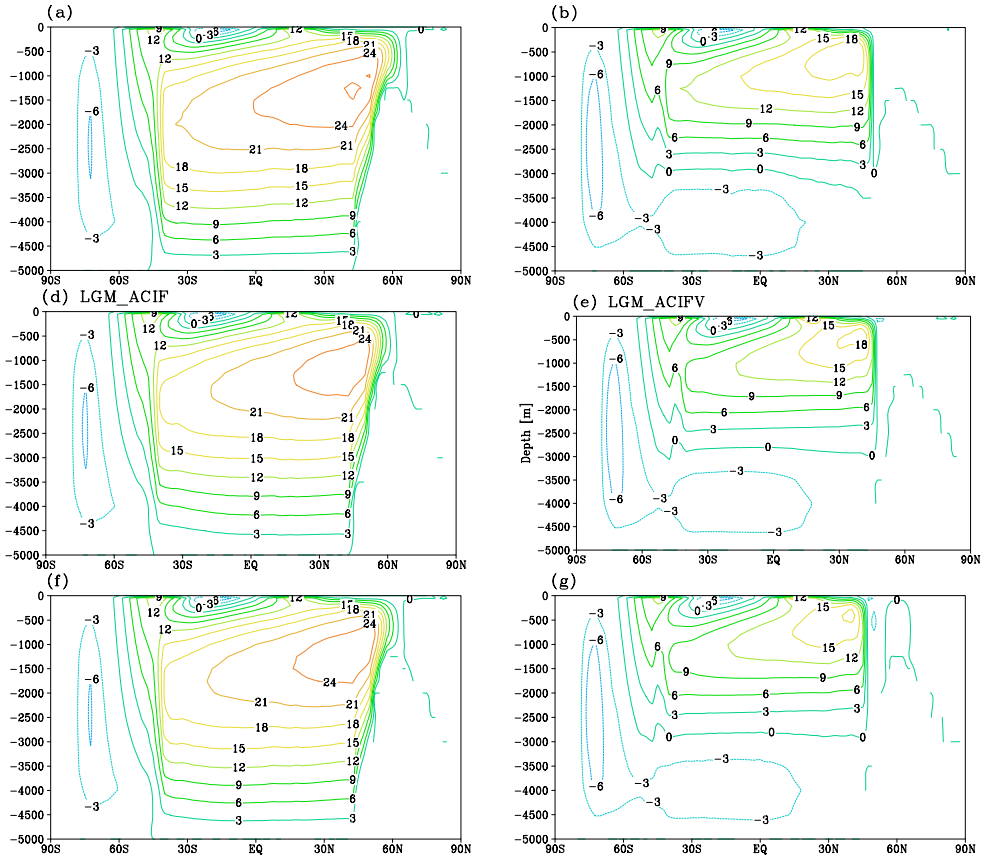

Figure 5.44: Annual averaged Atlantic overturning stream function [in Sv]. In the top row $REF + \hat{f}_I$ (a) and $LGM_{ACIF} + \hat{f}_{CIV}$ (b) are presented, while LGM_{ACIF} (c) and LGM_{ACIFV} (d) are shown in the middle row for comparison. In the bottom row $REF + \hat{f}_I + \hat{f}_C + \hat{f}_{CI}$ (e) and $REF + \hat{f}_I + + \hat{f}_C + \hat{f}_{CI} + \hat{f}_{CIV} + \hat{f}_{CIFV}$ (f) are shown, which resemble LGM_{ACIF} and LGM_{ACIFV} from the middle row.

SST only cools slightly by 0.3 °C over the northern Pacific and Atlantic, which adds up to a global SST decrease of 0.05° C, only accounting for 2% of the $LGM_{ACIFV} - REF$ decrease. Due to this small SST change, also no important sea-ice effect is seen. Ocean circulation also does not change much.
Overall, $\hat{f}_{CV}$ causes a cooling mainly over land areas on the NH due to the reduction in trees by 14.7% and of grass by 8.6% of the total dynamic decrease.

Synergy of CO_2 and Inland Ice/Orography Factor ($\hat{f}_{CI}$)

Globally, the effect of $\hat{f}_{CI}$ is not under the most important factors, causing only a global temperature decrease of 0.5° C. The temperature changes becomes larger, however, when looking at the two hemispheres separately, as $\hat{f}_{CI}$ causes a temperature decrease of −0.08 °C on the NH while causing an increase of 0.13 °C on the SH (Fig. 5.28). The

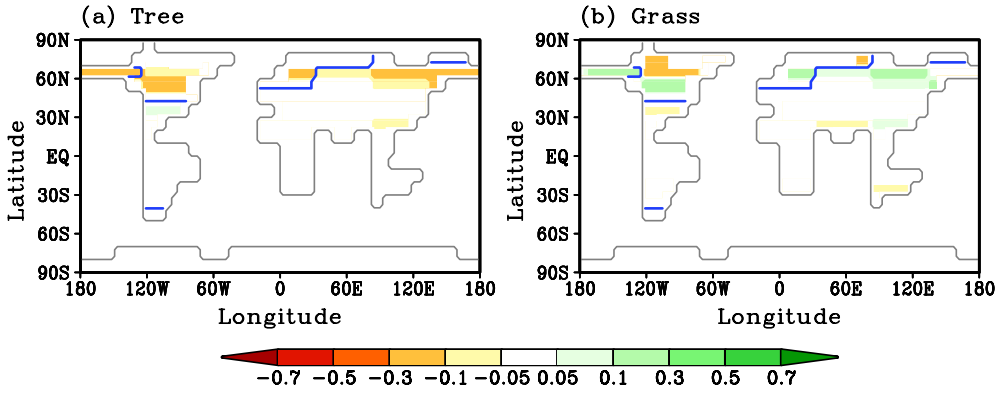

Figure 5.45: Vegetation change caused by $\hat{f}_{CV}$. Shown are the differences in tree fraction (a) and grass fraction (b). Since here no inland ice change is prescribed, the blue line representing the 60% inland ice border in other Figures about the vegetation change is missing here. Green colors indicate an increase in the respective vegetation fraction, while yellow–red indicate a decrease.

SAT cooling reaches −1.2 °C over the North Atlantic and north-west Europe, while a warming of 0.1–0.2 °C is seen over parts of North America. The strongest warming on the SH is located over the southern Atlantic, reaching up to 0.5° C. The cooling over the North Atlantic and warming over the southern Atlantic ocean are mainly caused by a change in ocean circulation, with a decreased maximum overturning in the North Atlantic of 1.7 Sv (makes up −31% of $LGM_{ACIF} - REF$ change) and an intensified formation of AABW by 1.4 Sv (−30% of $LGM_{ACIF} - REF$). This is followed by a decrease of 0.07 PW in northward heat transport (50% of $LGM_{ACIFV} - REF$ and −48% of $LGM_{ACIF} - REF$) that leads to a SST decrease in the North Atlantic and an otherwise overall increased SST. Due to the decreased SST in the North Atlantic, an increase in sea-ice is seen which also contributes to the cooling there over the sea-ice-albedo effect. Part of the warming is due to an increase in atmospheric water content by 0.02 kg/m^3, which is −4.6% of $LGM_{ACIFV} - REF$. This leads to a small increase in the radiative effect of $\hat{f}_{CI}$ by 0.007 W/m^2.
It is important to note that all these effects of the synergy factor $\hat{f}_{CI}$, besides the increase in sea-ice and the associated cooling over the North Atlantic, are in the opposite direction than the effects of both of $\hat{f}_C$ and $\hat{f}_I$. The reason for this opposite effect of $\hat{f}_C$ is not known, but it has also been found in a study by Berger et al. (1996) (shown later on page 71) so that it can be suspected that it is a robust feature.

FSB Factor $\hat{f}_F$ and Synergy Term $\hat{f}_{CIFV}$

The FSB factor $\hat{f}_F$ and the synergy $\hat{f}_{CIFV}$ are both not globally important with regard to temperature (0.1-0.6% of $LGM_{ACIFV} - REF$), but since they show an effect over the Atlantic and Southern Ocean that is comparable to other factors discussed here, they will be briefly discussed as well. $\hat{f}_F$ shows a cooling of up to 0.3 °C over the North

Atlantic around 70° N and a small warming of 0.1 °C over the Southern Ocean. This is due to a decrease in overturning in the Nordic Seas by 3 Sv due to the destabilizing effect of the reduction in freshwater bypass flux, which leads to a decrease in northward heat transport, cooling the Nordic Seas and warming the Southern Ocean.

The factor $\hat{f}_{CIFV}$ leads to a warming over the Southern Ocean and to a cooling over the Atlantic, but with its center much further south (at 50° N) than $\hat{f}_F$. This shift is due to the already by $\hat{f}_{CIV}$ shifted place of NADW formation, so that a weakening of the northward heat transport shows its effect further south now. With up to $-1°$ C, the cooling is stronger than for $\hat{f}_F$, due to the much stronger decrease in northward heat transport.
Overall, these two factors lead to a warming of the Southern Hemisphere and a cooling of the Nordic Seas and the North Atlantic. Their sum is shown in Figure 5.29.

5.2.2 Precipitation

The precipitation decreases globally by 0.39 mm/day or 140 mm/year between the runs LGM_{ACIFV} and REF and by 0.07 mm/day or 25 mm/year between LGM_{ACIF} and LGM_{ACIFV}. The global change between LGM_{ACIFV} and REF is caused to 51% by $\hat{f}_I$, the other half of the decrease is accounted for by $\hat{f}_C$ to 32%, $\hat{f}_{CV}$ to 16%, $\hat{f}_{CV}$ to 3.3% and $\hat{f}_{CI}$ to 1.8% . The values of global, NH and SH change for these factors are listed in table 5.2. In addition, other factors are also of importance on the regional scale to fully explain the spatial difference between LGM_{ACIFV} and REF, especially in the North Atlantic. Therefore, $\hat{f}_{CIV}$ and $\hat{f}_{CIFV}$ are added to the table 5.2 and will also be discussed later on together with the other factors (on pages 69–71). The spatial distribution of all of these factors is shown on page 68.

Factor	Global	NH	SH
$\hat{f}_I$	−0.200	−0.225	−0.174
$\hat{f}_C$	−0.125	−0.124	−0.126
$\hat{f}_{IV}$	−0.064	−0.082	−0.046
$\hat{f}_{CV}$	−0.013	−0.018	−0.008
$\hat{f}_{CI}$	+0.007	+0.005	+0.009
$\hat{f}_{CIV}$	+0.002	−0.031	+0.034
$\hat{f}_{CIFV}$	+0.002	−0.009	+0.012

Table 5.2: The annual averaged precipitation effect of the five most important precipitation factors and in addition two more factors are shown [in mm/day] with their global, NH and SH values, in the order of their relative global importance.

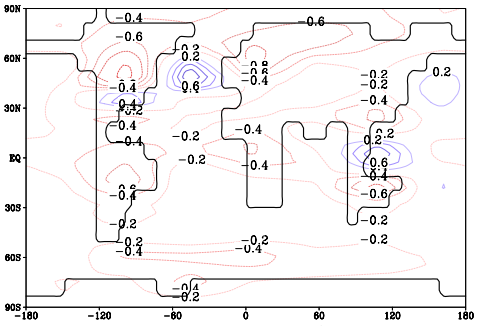

Figure 5.46: $\hat{f}_I$

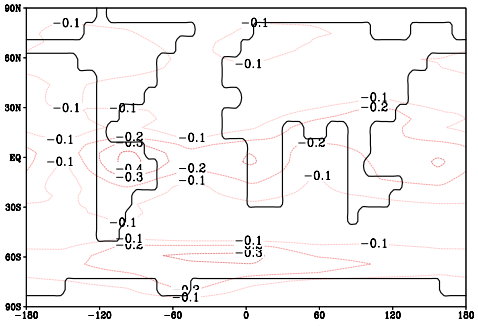

Figure 5.47: $\hat{f}_C$

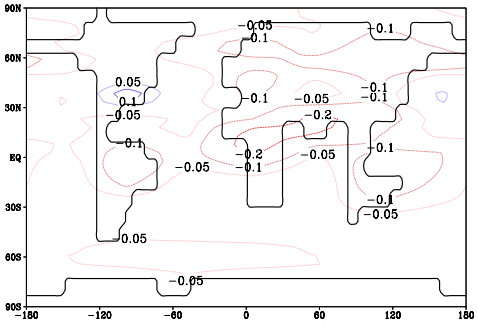

Figure 5.48: $\hat{f}_{IV}$

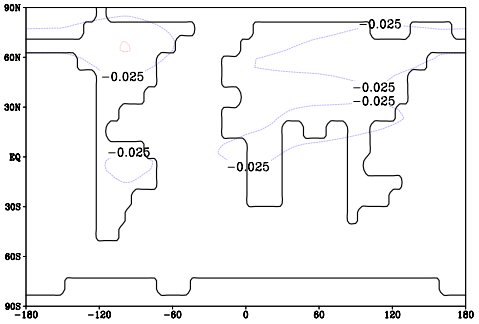

Figure 5.49: $\hat{f}_{CV}$

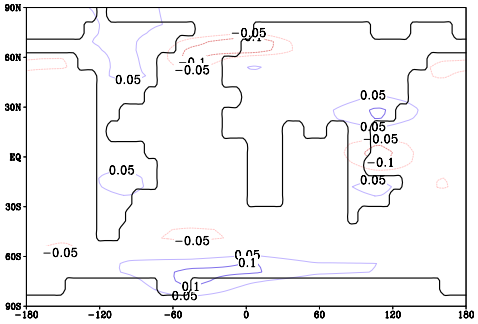

Figure 5.50: $\hat{f}_{CI}$

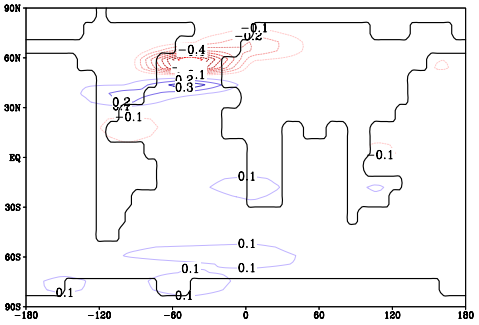

Figure 5.51: $\hat{f}_{CIV}$

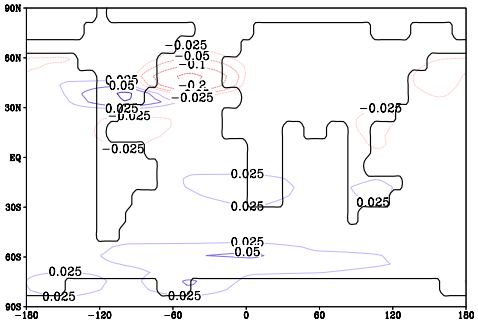

Figure 5.52: $\hat{f}_{CIFV}$

Fig. 5.46–5.52 show the annual averaged precipitation changes [in mm/day] caused by the above named factors.

Inland Ice and Orography Factor $\hat{f}_I$

Globally, $\hat{f}_I$ causes a reduction in precipitation by -0.2 mm/day, but it can be seen in Figure 5.46 that this reduction is most pronounced over the ice sheets of North America and Eurasia, reaching -0.8 mm/day. Over the North Atlantic, southern North America at 35° N as well as north of Australia (at 120°E/5° N), precipitation is increased by up to 0.8 mm/day. These increases are mainly due to the shift of precipitation area due to the imposed inland ice sheets which have a vertical extent of 1000–2000 m in North America and up to 1000–1500 m in Eurasia, thus greatly influencing the atmospheric circulation and leading to a southward shift of the storm tracks. Due to an increase in wind speed by 1.5 m/s, evaporation also increases over the North Atlantic. North of Australia evaporation and precipitation increase due to the additional land area that is exposed and covered with vegetation according to the surrounding grid boxes. The precipitation change caused by $\hat{f}_I$ accounts for 51% of the $LGM_{ACIFV} - REF$ change and for 65% of the $LGM_{ACIF} - REF$ change, making it the globally most important factor.

CO_2 Factor $\hat{f}_C$

The factor $\hat{f}_C$ is the second most important factor globally with regards to precipitation, accounting for 32% of the precipitation decrease from REF to LGM_{ACIFV}. This decrease is especially pronounced in the tropics with -0.4 mm/day and decreases towards the Arctic regions while it has a second maximum with -0.3 mm/day on the Southern Hemisphere at 60° S/10°W. The precipitation decrease is overall due to the temperature decrease caused by $\hat{f}_C$, with the strongest effect in the tropics. The strong decrease over the Southern Ocean is due to the increase in sea-ice area in this region that leads to less evaporation.

Synergy of Inland Ice/Orography Factor and Vegetation ($\hat{f}_{IV}$)

The synergy factor $\hat{f}_{IV}$ causes 16% of the global precipitation decrease of $LGM_{ACIFV} - REF$. The effect of $\hat{f}_{IV}$ is strongest over land areas, especially over the tropical regions around the equator, over Australia and over the land areas of Eurasia around 60° N. In the northern part of Eurasia and in Australia, this decrease in precipitation is due to the reduction of trees there which are replaced partly by grass, but mainly by desert. This weakens the hydrological cycle, leading to less precipitation. The decrease in precipitation is especially pronounced in summer in regions north of the equator and in northern winter in regions on the Southern Hemisphere, due to a weakening of the respective summer monsoon. Over southern North America precipitation increases slightly (Fig. 5.48) at 35° N, which is due to an increase in trees there by 10% (Fig. 5.38) that intensifies evaporation and precipitation, leading to a precipitation increase of 0.2 mm/day.

Synergy of CO_2 and Vegetation ($\hat{f}_{CV}$)

The synergy factor $\hat{f}_{CV}$ reduces precipitation globally by 0.013 mm/day, which accounts for 3.3% of the overall $LGM_{ACIFV} - REF$ reduction. This reduction is centered over the land areas where trees are replaced by grass or desert or grass is replaced by desert (Fig. 5.49 and map of vegetation change shown earlier 5.45). The precipitation changes are strongest during summer and fall when changes in evaporation are also strongest.

Synergy of CO_2 and Inland Ice/Orography Factor ($\hat{f}_{CI}$)

The synergy factor $\hat{f}_{CI}$ between inland ice and CO_2 is interesting to look at as it causes an opposite effect to the effect of both $\hat{f}_C$ and $\hat{f}_I$ on global and hemispheric mean. On global average, the change of +0.007 mm/day caused by $\hat{f}_{CI}$ accounts for 1.83% of the absolute change, thus in the opposite direction than the difference between LGM_{ACIFV} and REF. It shows the strongest increase in precipitation over the Southern Ocean (Fig. 5.50), where $\hat{f}_{CI}$ also causes a warming as discussed earlier. This increase in precipitation is just opposite to the effect of $\hat{f}_C$, but since it is smaller it only compensates about 1/3 of the local effect of $\hat{f}_C$. The strongest reduction caused by $\hat{f}_{CI}$ can be seen over the North Atlantic, where SAT as well as SST decrease and sea-ice area increases, thus greatly reducing evaporation. Another area with a decrease of 0.1 mm/day is the region north of Australia, where $\hat{f}_I$ showed an increase of 0.6 mm/day. The synergy term thus compensates about 15% of the effect of $\hat{f}_I$ in this area. The decrease here is due to a local decrease in evaporation over this area.

Overall, it can be noted that, as already for temperature, $\hat{f}_{CI}$ acts in the opposite direction than $\hat{f}_C$ and $\hat{f}_I$ alone in all areas beside the North Atlantic, where it reinforces their effects.

Synergy of Inland Ice/Orography, CO_2 and Vegetation ($\hat{f}_{CIV}$)

The synergy factor $\hat{f}_{CIV}$ contributes only −0.43% of the global absolute $LGM_{ACIFV} - REF$ change. On the regional scale though it is very important, as it is responsible for about 2/3 of the precipitation reduction in $LGM_{ACIFV} - LGM_{ACIF}$ over the North Atlantic at 60° N and about 1/2 of the precipitation increase south of this area of decrease. This pattern is due to the increased sea-ice cover in the North Atlantic that reduces the evaporation over the sea-ice and shifts the storm tracks to the south of its southern margin.

It is important to note that evaporation over the North Atlantic north of 50° N is decreased by 1.5 mm/day while precipitation only decreases by 0.8 mm/day, so that, overall, the region north of 45° N is freshened, even though precipitation decreases north of 50° N (Fig. 5.53). If this is part of the cause or the result of the switch of the ocean circulation into the "cold" glacial mode, cannot be determined here, but it can be suspected that a large part is the reaction to the change in ocean circulation and the

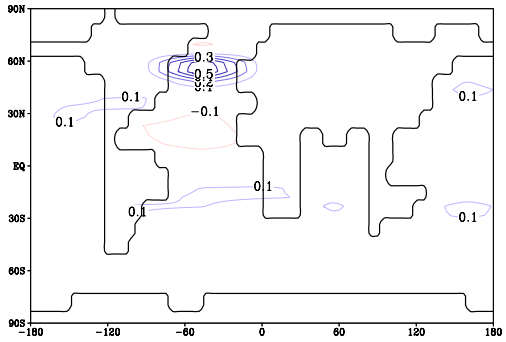

Figure 5.53: Difference between annual averaged evaporation and precipitation for $\hat{f}_{CIV}$ [in mm/day].

following increase of sea-ice area to the south (see paragraph about temperature effect of $\hat{f}_{CIV}$ on page 62). The synergy factor $\hat{f}_{CIV}$ also increases precipitation over the Southern Ocean (Fig. 5.51), but here this increase is due to the warming of this region, which in turn enhances evaporation, leading to stronger precipitation. The precipitation increase south of the inland ice area in North America with up to 0.2 mm/day is due to a small increase in tree fraction there, thus especially in summer and fall evaporation and precipitation increases due to a stronger hydrological cycle.

Synergy of CO_2, Inland Ice/Orography, FSB and Vegetation ($\hat{f}_{CIFV}$)

Globally, the influence of $\hat{f}_{CIFV}$ is very small (only 0.51% of the absolute change $LGM_{ACIFV} - REF$), but this is also due to the opposite signs of its effect on Northern and Southern Hemisphere. It causes a small widespread precipitation increase of 0.03 mm/day on the Southern Hemisphere and a substantial local reduction of 0.2 mm/day over the North Atlantic. This decrease is caused by a decrease in evaporation due to a local decrease in SST by 1.3° C. Over southern North America an precipitation increase of 0.05 mm/day is seen, which is due to a small increase in trees there so that the hydrological cycle is intensified a bit. $\hat{f}_F$, that was discussed for temperature together with $\hat{f}_{CIFV}$, is almost zero, so it is not discussed here.

5.3 Comparison of the Inland Ice and CO_2 Factors with other Studies

Berger et al. (1996): Berger et al. (1996) performed equilibrium experiments for the LGM with a 1-D radiative convective climate model. They performed their experiments to separate the effects of an astronomical-albedo forcing and a CO_2 forcing. They found a LGM cooling of −4.5° C compared to today. I found an overall $LGM_{ACIFV} - REF$ cooling of −4.9° C, but this is due to the interaction of five factors. They do not include

a dynamic vegetation model and also do not change the ocean parametrization, so that the experiment LGM_{ACI} is closest to their experiments.

In order to compare my results with their results, I have to add up the effects of my astronomical and my inland ice/orography factor as well as the synergy term $\hat{f}_{AI}$ in order to arrive at a new factor "albedo+astro" that refers to about the same changes as their astronomical-albedo effect. The CO_2 factor remains unchanged, but for the synergy between these two I have to add up the following of my factors: $\hat{f}_{AC} + \hat{f}_{CI} + \hat{f}_{ACI}$. The results from both studies are shown in table 5.3.

Factor	Berger et al.	CLIMBER-2
Albedo+Astro	−2.99/66.3%	−2.94/68.4%
CO_2	−1.57/34.8%	−1.32/30.9%
Synergy	+0.05/1.1%	+0.05/1.2%
LGM cooling	−4.50	−4.20

Table 5.3: Temperature change in degree Celsius due to the factors in Berger at al. (1996) the results from this work with CLIMBER-2.3. The LGM cooling and the percentages for CLIMBER-2 refer to the cooling caused by the run LGM_{ACI}

The by 0.25 °C larger CO_2 effect in the study of Berger et al. (1996) is due to their larger CO_2 decrease (−136 ppm) compared to mine (−80 ppm). This difference in CO_2 reduction is large enough to cause a stronger temperature decrease in Berger et al. (1996) in spite of a larger sensitivity to a doubling of CO_2 in CLIMBER-2.3 (2.6° C) than in Berger et al. (1996) (1.8° C). The albedo+astro effect is quite similar in both studies, even though in CLIMBER-2 the surface albedo change is larger and $\hat{f}_I$ also includes the effect of the orography, so that it would be expected that CLIMBER-2 shows a larger albedo+astro effect. The synergy term is only small and compares well for both studies, which shows that the two factors interact without causing strong non-linear effects in both models. The synergy effect they do cause is in the opposite direction than the effect of the factors alone for both studies. Overall, my results for the factors ice, astronomical forcing and CO_2, therefore, compare quite well with the results form Berger et al. (1996).

Broccoli and Manabe (1987): Broccoli and Manabe (1987) used an atmospheric GCM coupled to a mixed layer ocean model to simulate the LGM climate. They found that 90% of the global mean cooling can be explained by expanded inland ice together with reduced CO_2 concentrations. They also found that the effect of ice sheets is mainly restricted to the NH while the CO_2 effect also cools the SH. The influence of the CO_2 effect also on the SH is in agreement with my results, but the effect of the inland ice is not just limited to the NH in my results, probably because I used a model with a dynamic ocean module while Broccoli and Manabe (1987) prescribed SST, not allowing for heat exchange through the ocean.

Hewitt and Mitchell (1997): Hewitt and Mitchell (1997) used the UKMO Hadley Center Atmospheric GCM[5] HADSM2 with a mixed layer ocean model to investigate the influence of the different glacial boundary conditions CO_2, insolation and continental ice sheet. They found that about 2/3 of the global LGM cooling is due to ice sheets. The ice sheets thereby dominate the temperature decrease on the NH while the cooling on the SH is controlled by the lowering of CO_2 and the cooling effect of sea-ice. These results were obtained by the difference between runs with one forcing at a time turned on and the control simulation. In my study the inland ice causes 60% of the global cooling which agrees well with the 2/3 cooling found by Hewitt and Mitchell (1997). The stronger cooling of CO_2 on the SH that Hewitt and Mitchell (1997) find does not agree with my results because even though the inland ice cools the SH much less than the NH it still is stronger on the SH than the CO_2 cooling there.

Kim (2004): Kim (2004) used the Canadian Center for Climate Modeling and Analysis coupled general circulation model CGCM2 to investigate the effect of CO_2 change and ice-sheet-orography change on the simulation of the LGM climate. With this model, Kim (2004) found a LGM cooling that with 10.6 °C is much larger than the LGM cooling I found. About 60% of this cooling Kim (2004) attributes to the effect of lowered CO_2 (by 95 ppm), while the effect of ice sheets only accounts for 40%. This is a contrary result to the Hewitt and Mitchell (1997) and to my results. The reason for these at first glace very different results can probably be found in the calculation of the CO_2 effect and the ice-sheet-orography effect: The CO_2 effect was calculated from the difference between the run with lowered CO_2 and the present day control run while the effect of the inland ice was calculated as the difference between the full LGM run and the lowered CO_2 run. Ocean circulation is in the "cold" glacial mode already after imposing the lowered CO_2, which in this model is obviously enough to cross the threshold of the ocean circulation towards the "cold" circulation. Therefore, the CO_2 effect includes the cooling effect by the changed ocean circulation, while the inland ice effect only intensifies it a bit more. If the experiment had been performed differently by first introducing the inland ice and then lowing the CO_2 in a second step with the same calculation method, it can be suspected that results might differ and maybe inland ice would then cause the larger effect. To really be able to compare the effects, the difference between an experiment with prescribed inland ice but present day CO_2 and the reference run should be computed and compared to the effect of CO_2. Therefore, the calculation method might be the reason why the CO_2 effect in Kim (2004) dominates over the inland ice effect while in other studies the effect of the inland ice dominates.

Conclusion The comparison of the CO_2 and inland ice effect with other studies shows that the important aspects of my results are in agreement both with AGCMs results and simple 1-D model studies. It has also become apparent that the calculation of the factors is important, as the study by Kim (2004) has shown.

[5]Atmospheric GCMs are also-called AGCMs, while ocean GCMs are called OGCMs

Chapter 6

Results for 60-20 ky BP

In this chapter, the results of the experiments for part of the glacial period from 60–20 ky BP are presented. The first section is dedicated to the description of the climatic features of the fully coupled simulation *AOV*[1] over time. In the second section, the results of the transient factor separation for 60–20 ky BP will then be presented, with the focus on the climatic variables temperature and precipitation.

6.1 Climate Dynamics in 60-20 ky BP

As explained in chapter 1, the period from 60–20 ky BP is part of the last glacial period. It is also referred to as MIS 3 (60–30 ky BP) and MIS 2 (29-12.5 ky BP). Due to the decreasing solar insolation and the increasing inland ice sheets (both prescribed in the model) a slow cooling trend of about 1 °C globally is seen from 60–20 ky BP in *AOV* (Fig. 6.1). The most prominent feature of this period, however (in *AOV* as well as in the data) are the rapid climate changes, the so-called Dansgaard/Oeschger events (D/O events) and Heinrich events (HE) (see chapter 1) that punctuate the slow cooling from 60–20 ky BP (Fig. 6.1).

Also in agreement with paleodata is that in the simulation the influence of D/O events on the temperature and precipitation pattern is seen mainly on the NH, with the strongest signal over the North Atlantic. The temperature difference between the warm, interstadial phase of a D/O event and its cold, stadial phase reaches up to 6 °C over the North Atlantic and Greenland and about 1 °C over North America and northern Eurasia (Fig. 6.2 (a)), which is in reasonable agreement with data. Precipitation changes are also caused, mainly over the North Atlantic (Fig. 6.2 (b)). These changes occur because the ocean circulation flips from the "cold" glacial mode to the "warm" glacial mode

[1]The runs AOV_{00} and AOV_{20} are virtually the same, apart from the first 1000-2000 years where the influence of the different restart files is seen because the runs are in the process of adapting to the applied forcings (Fig. 6.1). Due to their similarity, I will from now on only refer to the run *AOV* instead of differentiating between both runs.

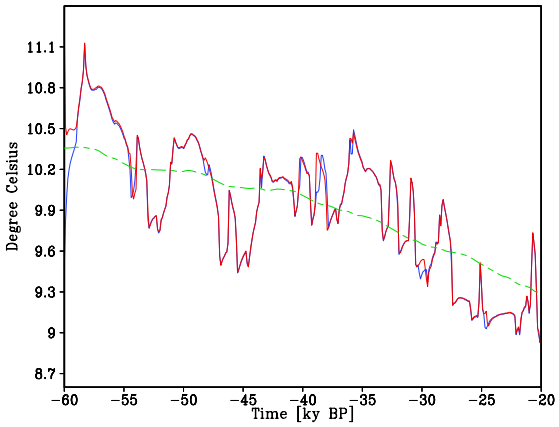

Figure 6.1: Globally averaged annual mean surface air temperature for $AOV20$ (blue) and $AOV00$ (red) [in °C]. The green dashed line is the trend line smoothed using a 10.000 year running mean in order to show the cooling trend over this period toward the LGM without the fluctuations caused by the D/O and Heinrich events.

during D/O events (Fig. 6.3 (a), (b)) (Ganopolski and Rahmstorf 2001; chapter 1), leading to an intensified northward heat transport and a northward shifted NADW formation that warms the North Atlantic. Hence, sea-ice area is reduced during D/O events, which further amplifies the warming and also leads to more evaporation from the ocean and a northward shift of the storm tracks so that precipitation over the North Atlantic increases. As the warm glacial mode is not stable in the glacial climate, it decays over time until a threshold is crossed again and the circulation flips back to the "cold" glacial mode with NADW formation further south and less northward heat transport (Ganopolski an Rahmstorf 2002; summarized in chapter 1).

Heinrich Events in the run AOV cause an additional cooling of about 1–2 °C over the Atlantic compared to the stadial phase of a D/O event. For HE the maximum cooling is, thereby, found around 35° N, which is further south than the cooling in the cold phase of a D/O event that is centered around 60° N. Another difference to the D/O events is found on the SH, where HE cause a widespread warming of up to 2 °C (Fig. 6.2 (c)), which makes HE much more apparent in SH data (Blunier et al. 1998) than D/O events (Fig. 6.4).

The freshwater input that causes the HE in AOV leads to a collapse of the thermohaline circulation in the Atlantic (Fig. 6.3 (c)), which in turn greatly reduces oceanic northward heat transport, so that the SH warms while the NH cools (see-saw effect (Stocker 1998)). This is in accordance with data (Broecker et al. 1992; see chapter 1). What is also in agreement with data is that the cooling on the NH associated with HE is not as large as the cooling between the interstadial and stadial phase of a D/O event. The cooling is also found further south because HE occur when the circulation is already in the stadial mode so that the northward heat transport is already reduced and shifted

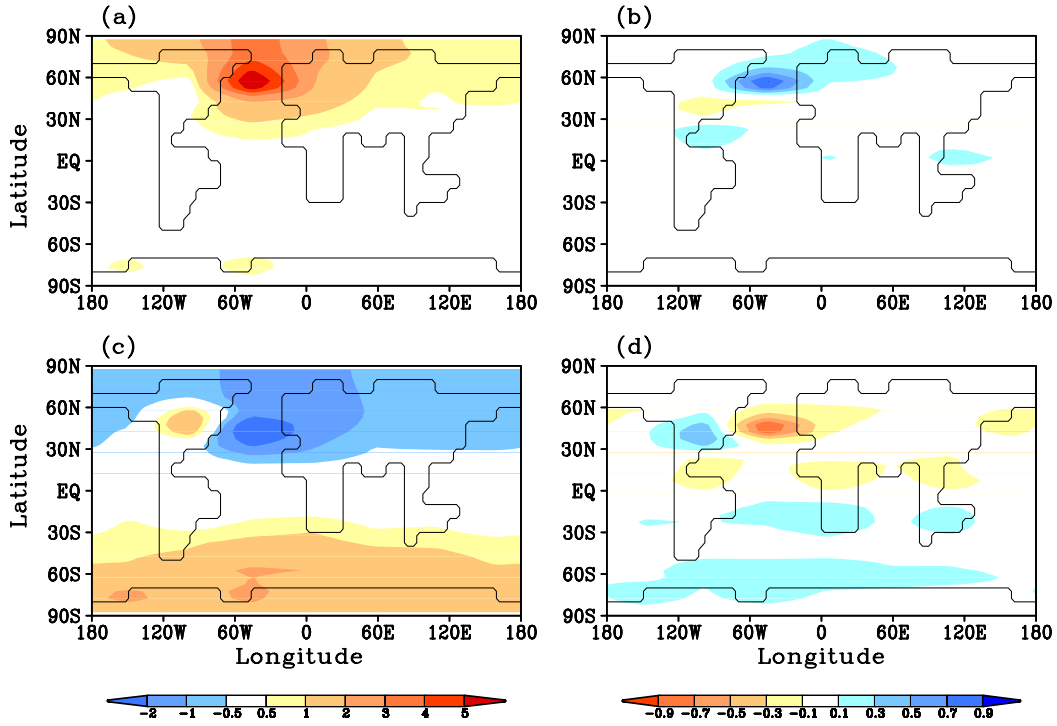

Figure 6.2: In (a) the typical warming of a D/O event in *AOV* is shown (annual surface air temperature difference between the warmest phase of a D/O event and its cold phase before) and in (b) the precipitation change for the same difference is shown. Figures (c) and (d) show the temperature and precipitation difference between the peak of a HE and the coldest point of the preceding D/O event, therefore, showing the additional cooling effect of a HE compared to the stadial phase before. Temperature changes are given in °C, precipitation changes in mm/day.

southwards. Only south of the stadial NADW formation site a further weakening of the northward heat transport is, therefore, able to cause a strong additional cooling (Ganopolski and Rahmstorf 2001). The collapsed thermohaline circulation is not a stable state of the ocean in the glacial climate (Ganopolski and Rahmstorf 2001), so that circulation starts up again as soon as the freshwater pertuberation that caused the HE stops, which leads to the warming to interstadial conditions after the HE.

The temperature and precipitation change caused by the D/O events and HE also cause vegetation changes and, thereby, mainly changes in grass fraction (Fig. 6.5) which are stronger for the HE than for the D/O events. The strongest response is thereby seen in Australia and in 40–50° N over North America, with an increase of grass during the peak phase of a HE by about 40% and 20%, respectively. These two areas are both regions where HE cause a warming and an increase in precipitation (Fig. 6.2), hence improving conditions for vegetation growth. Over the whole period from 60–20 ky BP

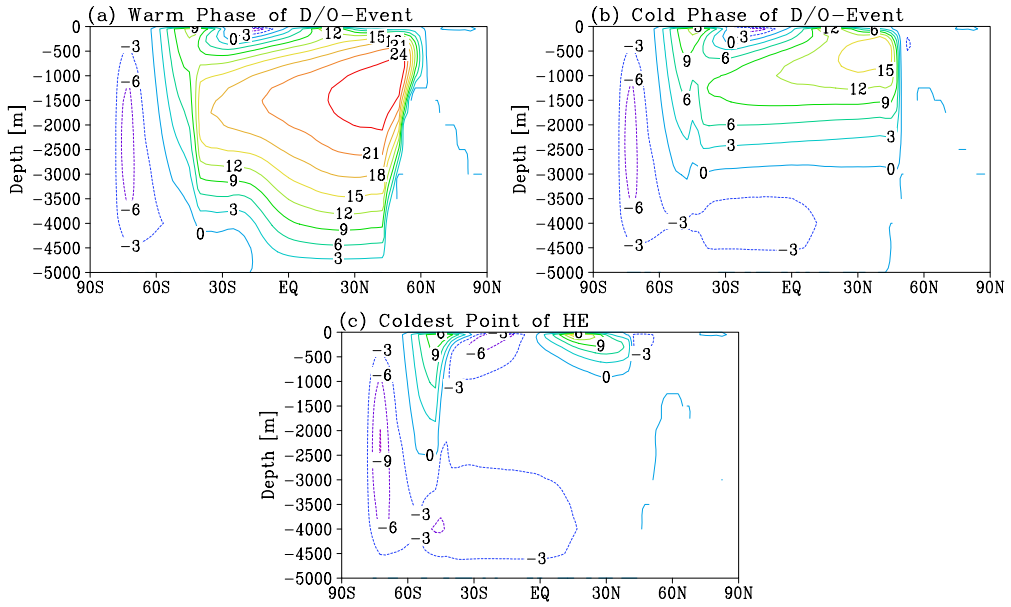

Figure 6.3: Annual averaged Atlantic overturning [in Sv] for the warm phase of a D/O event (a), the cold phase of a D/O event (b) and the coldest phase of a HE (c). In (a) the ocean is in the "warm" glacial mode, in (b) it is in the "cold" glacial mode and in (c) the circulation in the North Atlantic has collapsed ("off" mode).

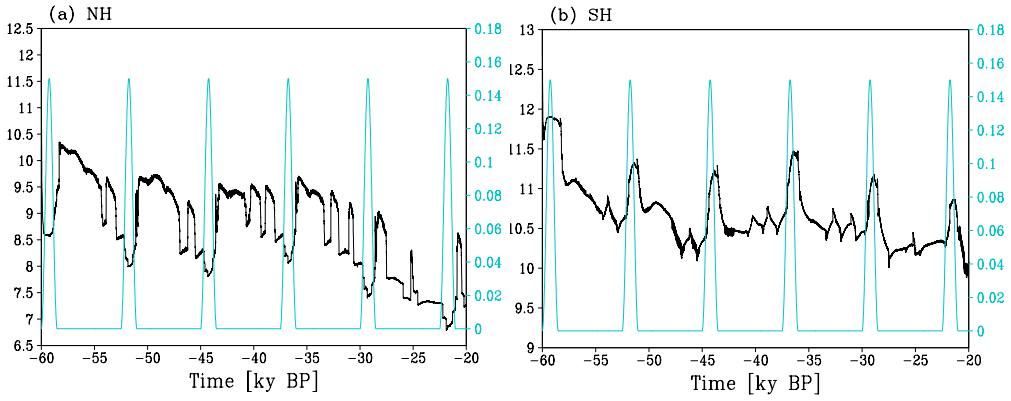

Figure 6.4: Annual averaged NH (a) and SH (b) surface air temperatures in °C (in black) plotted together with the freshwater forcing in Sv (in turquoise) that causes the HE in the model. NH and SH temperatures are plotted separately to show the different response of the temperature on the two hemispheres to this freshwater forcing (the so-called see-saw effect (Stocker 1998)).

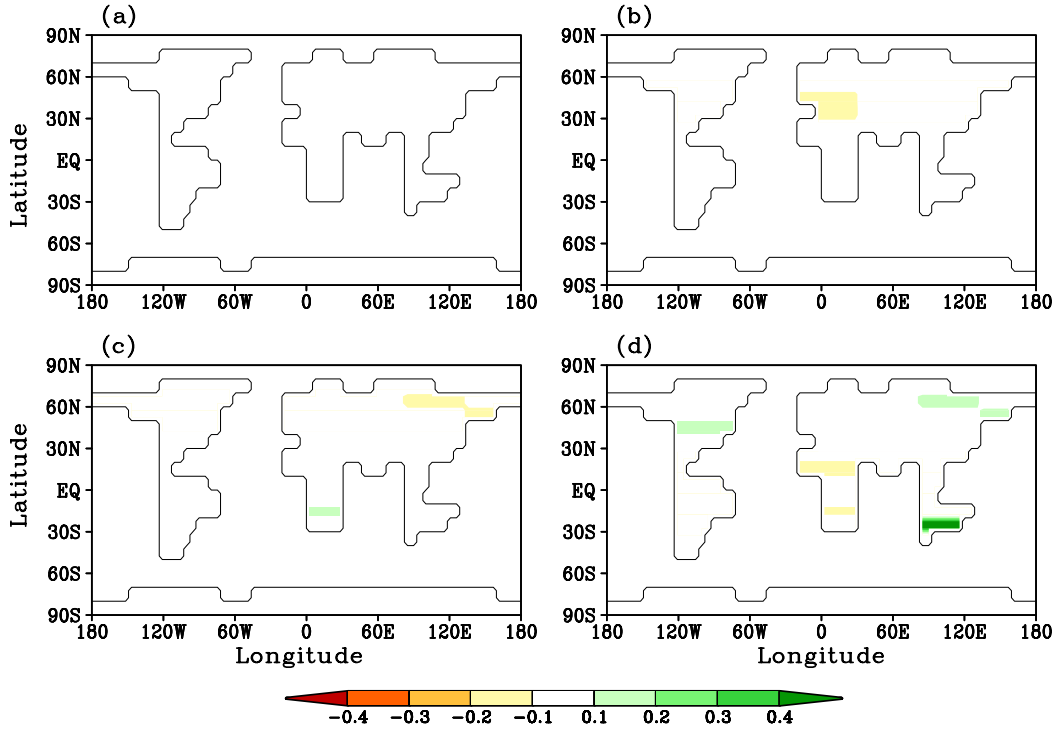

Figure 6.5: Tree (a) and grass (b) fraction change between the warm phase of D/O event and the previous cold phase of a D/O event (no changes in tree fraction are seen). In the second row the tree (c) and grass (d) change between the coldest point of a HE and the cold phase of a D/O events before is shown.

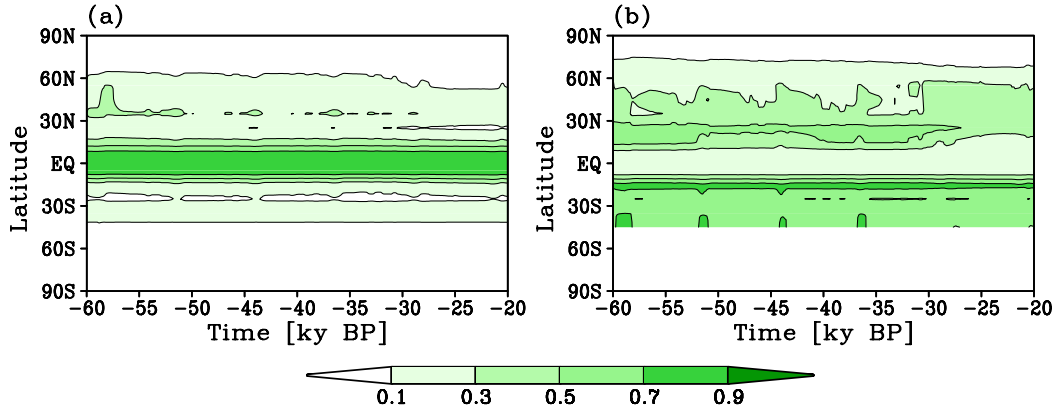

Figure 6.6: Zonally averaged tree (a) and grass (b) fractions for *AOV* over the period from 60–20 ky BP.

vegetation fraction decreases, with tress decreasing in the northern latitudes (around 60° N) and grass decreasing mainly in the subtropics (10–30° N) (Fig. 6.6), as a reaction to the overall cooling over this period.

6.2 Influence of Factors

To investigate the influence of a fixed or interactive ocean and fixed or interactive vegetation during glacial times, also AO, AV and A experiments for both reference states have been performed (see section 4.2). Using the Stein and Alpert Factor Separation Method (1993) described in section 2.2 the difference between these runs can be attributed to the influence of the ocean factor, the vegetation factor and their synergy term. The run A is the reference run to which the other runs are compared to. This

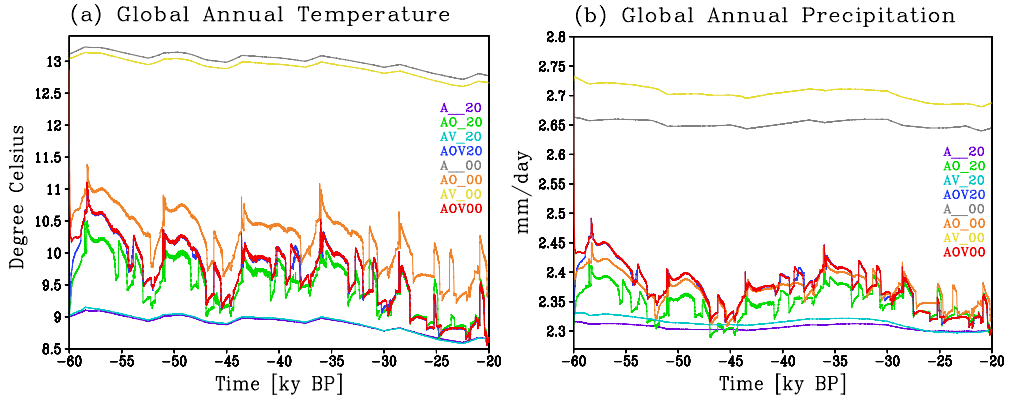

Figure 6.7: Annual averaged global surface air temperature (a) and precipitation (b) for the runs AOV_{00}, AO_{00}, AV_{00}, A_{00}, AOV_{20}, AO_{20}, AV_{20} and A_{20}. Temperature in °C and precipitation in mm/day.

means that for the "00" factors all changes are relative to A_{00}, which is with an averaged annual air temperature of 13.2° C, averaged over the 40,000 years of the model run, about 0.8 °C colder than the simulated present day climate (e.g. the run REF in the previous chapter). This difference from a present day run is due to the changes in astronomical forcing, the change in atmospheric CO_2 concentration and the imposed ice sheets. As these factors are not analyzed in this work, they were already included in the experiments A so that their effect would not be mixed up with the ocean and vegetation factor analyzed here

For the "20" factors the reference run that they are compared to is A_{20}, which is a run with the annual averaged global temperature of 8.2° C (averaged over the period of the run). This run is also influenced by the insolation and CO_2 changes and the imposed inland ice sheets, which explains the difference to the LGM equilibrium experiment LGM_{ACIFV} from the previous chapter, that had an annual averaged global temperature of 9.1° C.

Figure 6.7 shows that the temperature and precipitation difference is small between the runs A and AV and also between AO and AOV for both reference states, while it is large between these two pairs. What is also apparent is the different shape of the temperature curve for runs with an interactive ocean as opposed to a fixed ocean, the latter being flat and the earlier showing strong fluctuations, due to the D/O and Heinrich events. This already shows the dominant influence of the ocean in the glacial climate compared to the relative small vegetation influence. It can also be seen that the runs with prescribed "20" ocean or/and vegetation converge with AOV at 20 ky BP because for 20 ky BP the ocean and vegetation in AOV are the same as the prescribed "20" ocean and vegetation. The runs with "00" vegetation and/or ocean end in different temperatures and precipitation values than AOV, because they would only converge when AOV reaches the prescribed present day vegetation and ocean state, which does not happen in the period investigated here. This has the consequence that the factors for "20" become smaller toward 20 ky BP and become zero for 20 ky BP while the "00" factors do not converge (Fig. 6.8).

On the following pages the influence of the ocean, vegetation and synergy factors will be shown and explained in detail for the two climatic variables temperature and precipitation.

6.2.1 Temperature

In Figure 6.8 the global factors are shown over the period from 60–20 ky BP. There it becomes obvious that the ocean is by far the dominant factor and that the vegetation factor is barely visible while the synergy factor is larger than the vegetation factor, for both "00" and "20" factors.

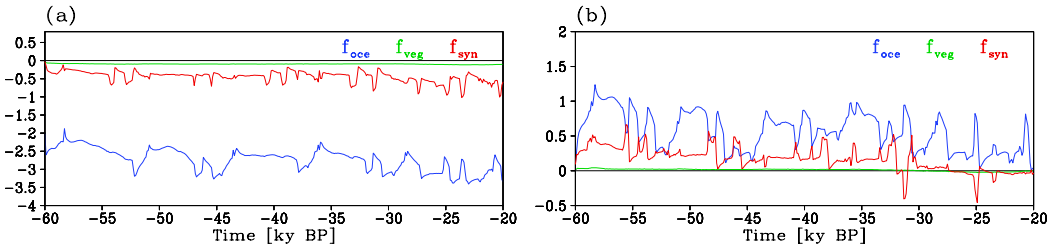

Figure 6.8: Annual and globally averaged temperature factors [in °C], for "00" (a) and "20" (b). The ocean factor is the blue line, the vegetation factor green and the synergy factor red.

Averaged over the whole period from 60–20 ky BP, the factor $\hat{f}_{oce_{(00)}}$ makes up 83.5% of the cooling between A_{00} and AOV_{00}, which are $-2.8°$ C, while $\hat{f}_{oce_{(20)}}$ makes up 77% ($+0.6°$ C) of the warming between A_{20} and AOV_{20}. The vegetation factor $\hat{f}_{veg_{(00)}}$ makes up only 3% ($-0.1°$ C) and $\hat{f}_{veg_{(20)}}$ even only 1.3% ($+0.01°$ C) of the difference. The

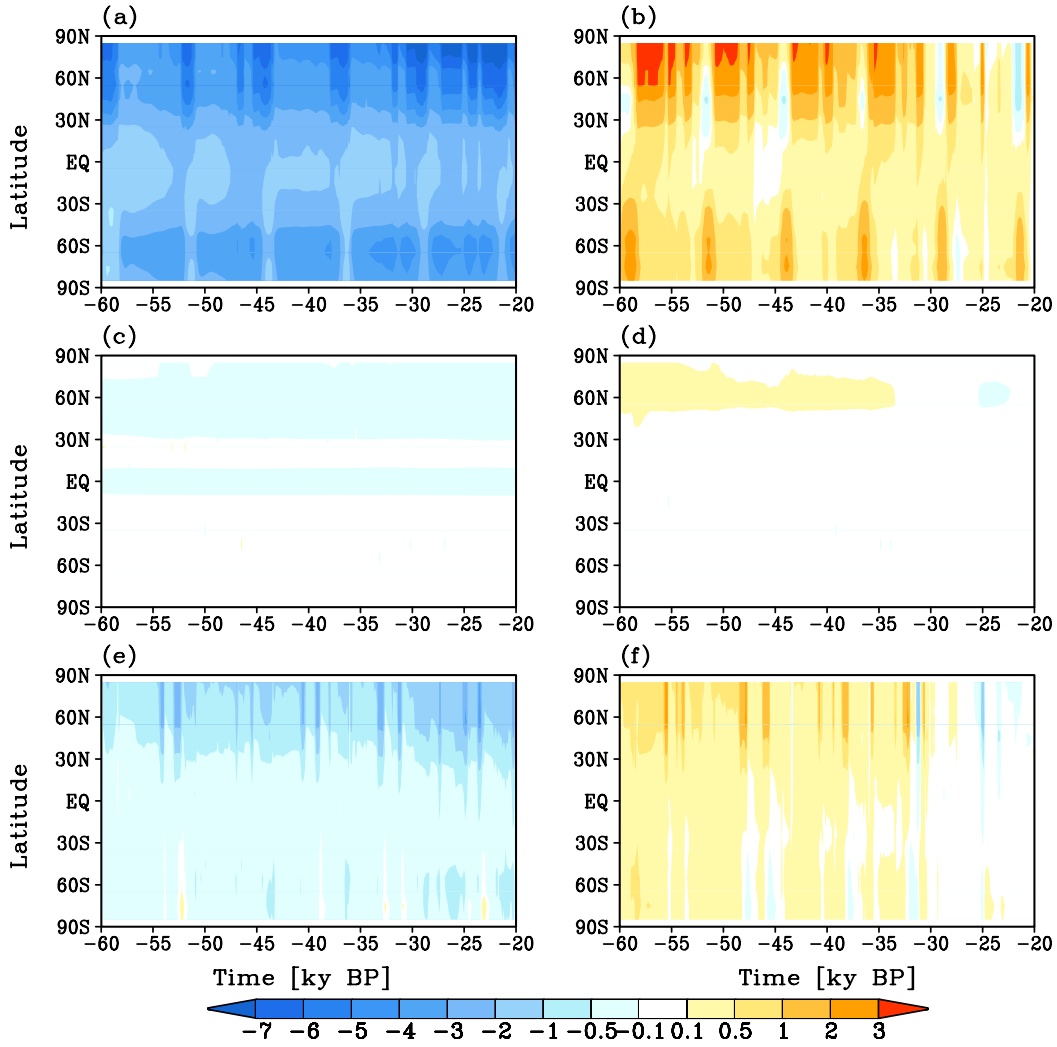

Figure 6.9: Zonally and annually averaged temperature factors $\hat{f}_{oce_{(00)}}$ (a), $\hat{f}_{oce_{(20)}}$ (b), $\hat{f}_{veg_{(00)}}$ (c), $\hat{f}_{veg_{(20)}}$ (d), $\hat{f}_{syn_{(00)}}$ (e) and $\hat{f}_{syn_{(20)}}$ (f) with temperature changes in ° C.

synergy factor is larger again, with 13.5% (−0.45° C) for $\hat{f}_{syn_{(00)}}$ and 21.7% (+0.17° C) for $\hat{f}_{syn_{(20)}}$.

Another important thing to note is that the "00" factors are larger than the "20" factors and also that the "20" factors are positive while the "00" factors are negative[2]. The larger changes for "00" than for "20" are caused because the fixed vegetation and ocean from "00" are from a very different climate state, an interglacial, while the ones from "20" are also from a glacial state and, therefore, not totally different

[2]Factors are calculated relative to the reference state, here the runs A_{00} and A_{20}, and not compared to *AOV*!

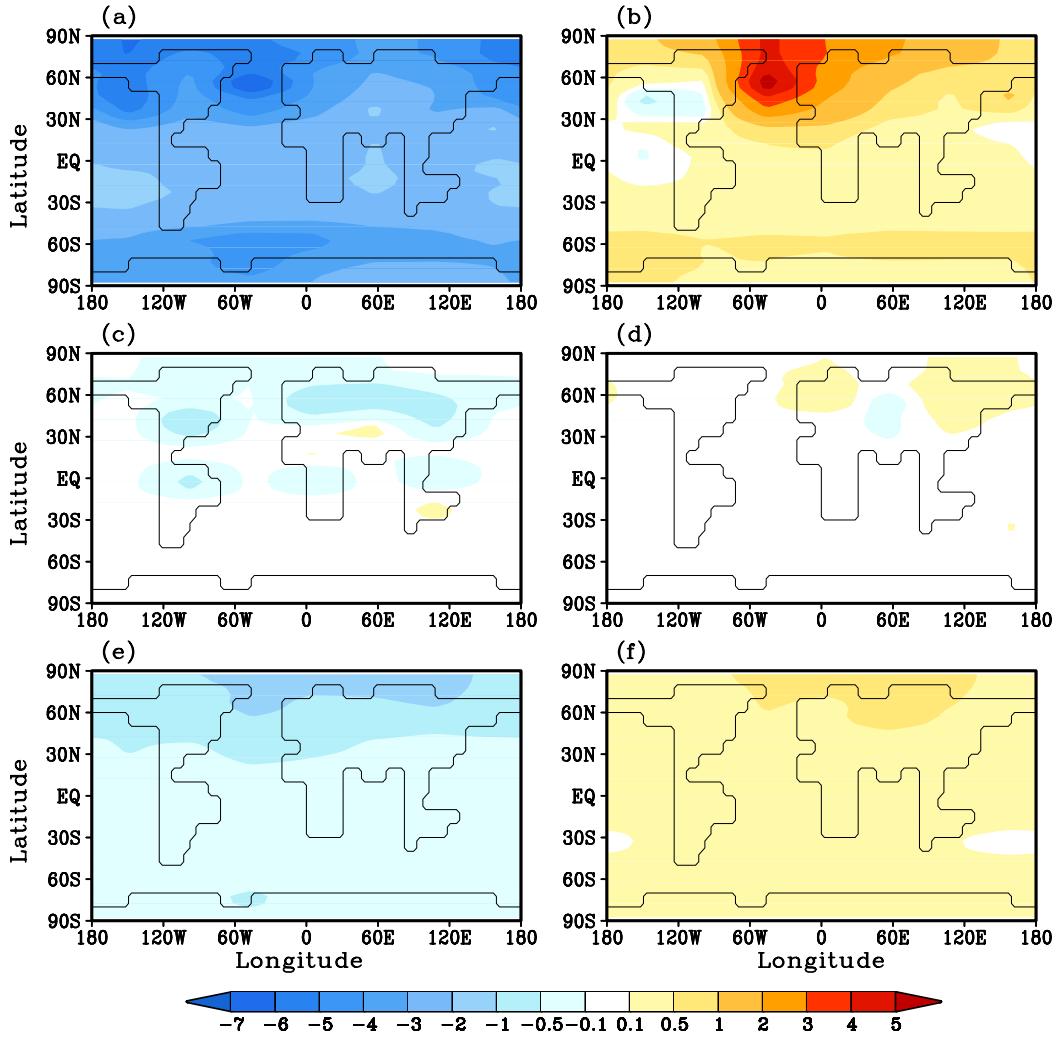

Figure 6.10: Between stadials and interstadials averaged temperature factors from about 45 ky BP. The area where changes occur stays the same during the period from 60–20 ky BP. $\hat{f}_{oce_{(00)}}$ (a), $\hat{f}_{oce_{(20)}}$ (b), $\hat{f}_{veg_{(00)}}$ (c), $\hat{f}_{veg_{(20)}}$ (d), $\hat{f}_{syn_{(00)}}$ (e) and $\hat{f}_{syn_{(20)}}$ (f) with temperature changes in ° C.

from the ones simulated interactively in *AOV* for 60–20 ky BP. The most important characteristics of the prescribed ocean and vegetation states for "00" and "20" can be found in appendix B.2 on page 116. The different direction of the reaction is also due to the difference between the two prescribed ocean and vegetation states, as the "00" ocean is much warmer than simulated for *AOV* and the "00" vegetation contains more trees than simulated in *AOV* for 60–20 ky BP while the "20" ocean is colder than the *AOV* ocean and the "20" vegetation has less trees than simulated in *AOV* for 60–20 ky BP. This leads to warmer temperatures compared to *AOV* for A_{00}, AO_{00} and AV_{00} and colder temperatures for A_{20}, AO_{20} and AV_{20} compared to *AOV*.

Ocean Factor $\hat{f}_{oce}$

The ocean factor $\hat{f}_{oce}$ is by far the largest factor of the two factors and the synergy term looked at. Especially the D/O and Heinrich events, the main features of the glacial climate, are not present when the ocean is fixed. Globally $\hat{f}_{oce_{(00)}}$ causes a cooling of $-2.73\,^{\circ}$C (compared to A_{00}) when averaged over the period 60–20 ky BP, with an even stronger cooling over the ocean (-3.03° C) and a weaker cooling over land (-2.55° C). The global effect of $\hat{f}_{oce_{(20)}}$ averaged over the same period is a warming of $+0.56\,^{\circ}$C which are 76% of the warming between AOV and A. Over the ocean the warming is again more intense ($+0.78^{\circ}$ C) than over land ($+0.54^{\circ}$ C).

The effect of the ocean factor $\hat{f}_{oce_{(00)}}$ on temperature is strongest in winter and spring (Fig. 6.11), due to the largest extent of sea-ice then and the largest influence of the northward heat transport on temperatures on the NH in winter. For $\hat{f}_{oce_{(20)}}$ the largest increase in temperature is seen in fall, due to the smallest extent of sea-ice area in fall so that the warming through heat transfer from the ocean to the air is strongest.

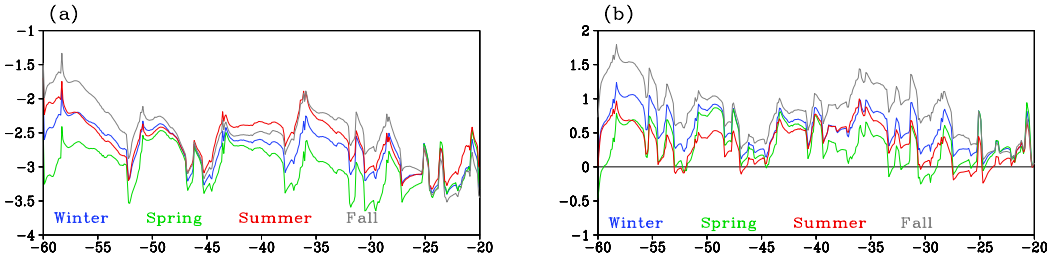

Figure 6.11: Globally averaged temperature factors [in $^{\circ}$ C] for the four different seasons. In (a) $\hat{f}_{oce_{(00)}}$ is shown and in (b) $\hat{f}_{oce_{(20)}}$.

Even though the effect of $\hat{f}_{oce}$ is large, it is not globally uniform. Figure 6.9 (a) and (b) show that the cooling caused by an interactive ocean instead of the fixed "00" ocean and also the warming caused by the interactive ocean compared to the fixed "20" ocean is largest in the polar regions and smallest in the tropics. This is mainly due to the strong feedback with the sea-ice in polar regions, that causes an increase in sea-ice area in the high latitudes when the temperature drops and a decrease when temperatures increase (Fig. 6.12). Hence, the sea-ice-albedo feedback and the isolating effect of the sea-ice on the ocean-air heat transfer are the reasons for the stronger cooling and warming in the polar regions compared with the tropics.

HE show up on the NH as increased cooling events in $\hat{f}_{oce_{(00)}}$ and small cooling events in $\hat{f}_{oce_{(20)}}$ (against the there prevailing warming), while on the SH they have a much weaker cooling effect in $\hat{f}_{oce_{(00)}}$ and a warming effect in $\hat{f}_{oce_{(20)}}$ (Fig. 6.9 (a), (b)), due to the bipolar-see-saw effect (Stocker 1998).

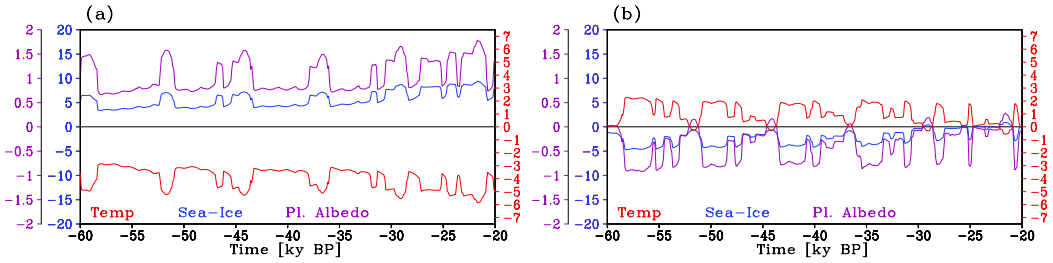

Figure 6.12: Zonally and annually averaged temperature, sea-ice fraction and planetary albedo factors for the region 30–90° N. In (a) $\hat{f}_{oce_{(00)}}$ is shown and in (b) $\hat{f}_{oce_{(20)}}$. Temperature changes are in °C while albedo and sea-ice fractions are in percent.

Vegetation Factor $\hat{f}_{veg}$

In Figure 6.8 it could be seen that globally the vegetation factor for both "00" and "20" is very small. This is due to the dominant effect of the fixed ocean in the glacial that defines the climate state. For AV_{00} the climate is still in an interglacial climate state with annual global mean temperatures of 13 °C due to the warm SST and the small sea-ice area because the ocean is fixed to the "warm" interglacial mode. In AO_{20}, on the other hand, the climate is in a glacial state, with an annual global mean temperature of 9° C, caused by a prescribed ocean that is in a "cold" glacial state and that has considerably colder SST and a larger sea-ice area than AO_{00} (see appendix B.2 for the prescribed vegetation and ocean characteristics). Averaged over the period 60–20 ky BP, the cooling caused by $\hat{f}_{veg_{(00)}}$ is −0.09 °C globally, but −0.18 °C over land and only −0.04 °C over the ocean. $\hat{f}_{veg_{(20)}}$ causes a warming of +0.01 °C globally and the effect is almost the same over land and ocean.

For $\hat{f}_{veg_{(00)}}$ the temperature decrease that occurs is concentrated on the northern latitudes from 30–70° N and on the tropical regions from 10° N to 10° S (Fig. 6.9 (c)). In the tropics, the temperature is decreased year-round while in 30–70° N and also globally the temperature decrease is strongest in summer (Fig 6.15 (a)). This is due to the increase in planetary albedo in summer over the northern region (by 1–2%), due to increased cloud cover and decreased trees there (Fig. 6.16 (a)). The increased cloud cover is caused by increased evapotranspiration in summer in this area, which is due to increased soil-moisture and increased windspeed (Fig. 6.16 (b)). The increased evapotranspiration leads to less latent heat flux so that evaporative cooling together with the increased albedo cool the region in summer. In winter and spring, the change in vegetation cover in this region (Fig. 6.13, 6.14) from trees to grass increases the surface albedo by 2%, so that the region cools by 0.1 °C due to the taiga-tundra feedback.

The described increase in evapotranspiration in this region is at first surprising, as trees are decreasing and this should weaken the hydrological cycle. However, the opposite is happening. Due to increased surface wind speed, evapotranspiration increases in

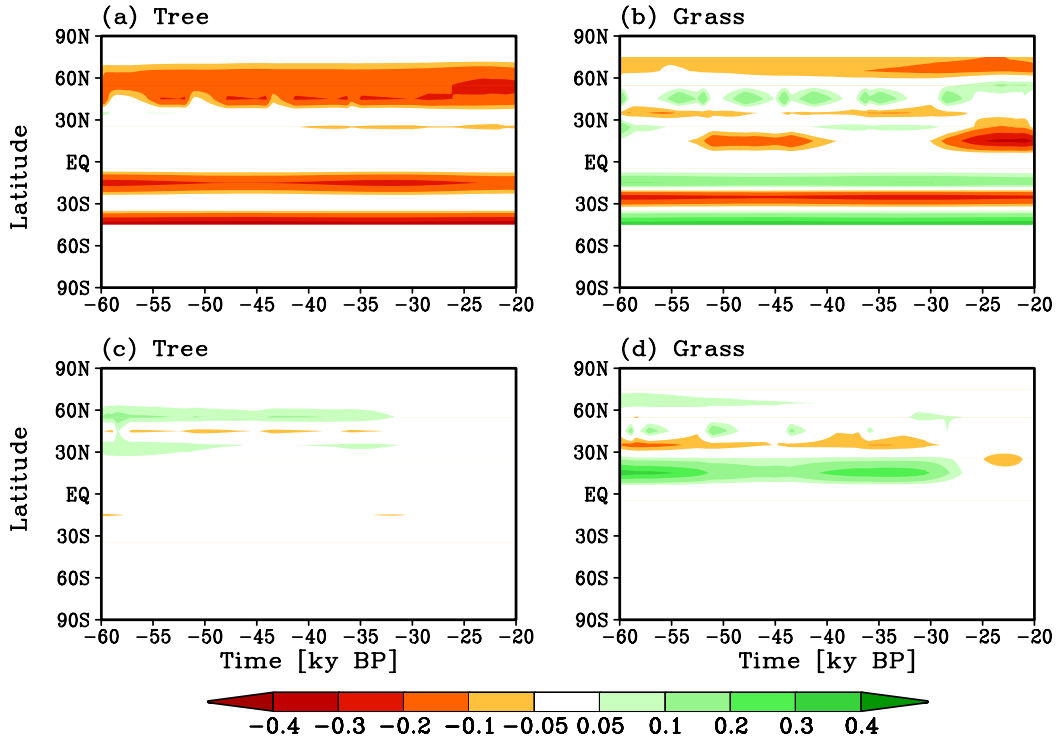

Figure 6.13: Zonally averaged change of tree fraction (a, c) and grass fraction (b, d). $\hat{f}_{veg_{(00)}}$ is shown in the top row (a, b) and $\hat{f}_{veg_{(20)}}$ (c, d) in the second row.

summer, even though trees are replaced by grass and desert (Fig. 6.16 (b)). The cooling in the tropics caued by $\hat{f}_{veg_{(00)}}$ is also caused by increased evaporative cooling and increased cloud cover year-round (not shown).

For $\hat{f}_{veg_{(20)}}$ the temperature effect is a very small warming effect between 50–70° N, with the strongest warming occurring in summer and spring and the weakest in fall (Fig 6.15). The warming in spring is due to the taiga-tundra feedback, caused by the increase of trees by about 10% in 50–60° N (Fig. 6.13 (c), (d)) that decreases the surface albedo locally by about 5% and, therefore, increases spring temperatures. Albedo changes are small in summer (Fig. 6.16) so that the warming in summer is caused through an intensified greenhouse warming due to higher atmospheric water vapor content. This warming overcompensates the increased evaporative cooling and leads to a warming in summer in 50–70° N by 0.1–0.2° C. From 28 ky BP on, $\hat{f}_{veg_{(20)}}$ causes a cooling and not a warming, due to the decrease in tree fraction from that time on, which leads to the cooling over the increased albedo (Fig. 6.16 (c), (d)).

Overall, it can be noted that the small temperature changes caused by $\hat{f}_{veg}$ occur mainly in regions where tree cover changes considerable while changes in grass cover do not cause a notable effect. It is interesting to note that the taiga-tundra effect contributes only a small part of the warming in $\hat{f}_{veg_{(20)}}$ and the cooling in $\hat{f}_{veg_{(00)}}$ and

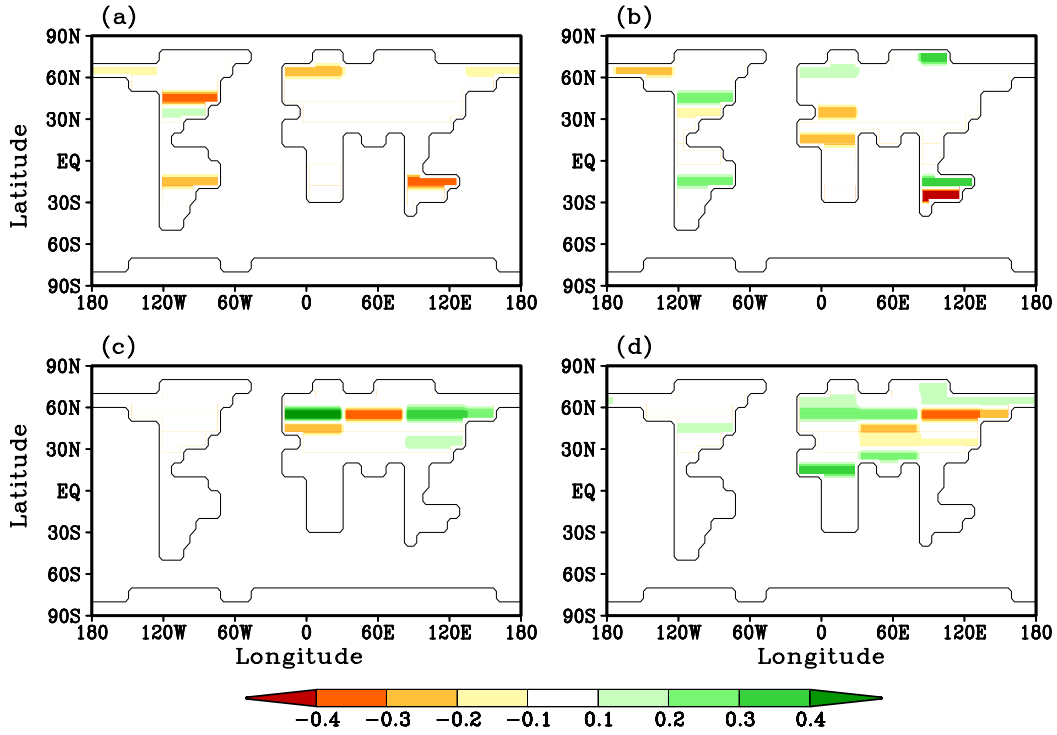

Figure 6.14: Vegetation change between AV and A around 45 ky BP. The area where changes occur stays the same during the period from 60–20 ky BP (see Fig. 6.13), only the magnitude of the vegetation change changes slightly. In (a) the tree fraction change and in (b) the grass change for $\hat{f}_{veg_{(00)}}$ is shown, while in (c) the tree fraction change and in (d) the grass fraction change for $\hat{f}_{veg_{(20)}}$ is shown.

that evaporative cooling and the increase in cloud cover (in $\hat{f}_{veg_{(00)}}$) or increase in greenhouse effect (in $\hat{f}_{veg_{(20)}}$) are more important.

Synergy Factor $\hat{f}_{syn}$

It has been noted already that $\hat{f}_{syn}$ has a larger effect than $\hat{f}_{veg}$ but that it is also much smaller than $\hat{f}_{oce}$ (Fig. 6.8). That $\hat{f}_{syn}$ is larger than $\hat{f}_{veg}$ is due to the feedbacks of vegetation changes with the ocean that are allowed to work for $\hat{f}_{syn}$ but not for $\hat{f}_{veg}$. While for $\hat{f}_{veg}$ the effect of evapotranspiration and clouds caused the largest changes in summer, $\hat{f}_{syn}$ now shows changes that are about equally large in all seasons (Fig.6.17). This is the result of the combined effect of the evaporative effect (with its maximum in summer and fall), the taiga-tundra effect (with its maximum in spring) and the sea-ice-albedo feedback (with its maximum in winter and spring) (Fig. 6.18). It is important to note that, overall, the $\hat{f}_{syn}$ temperature change is dominated by the effects from the

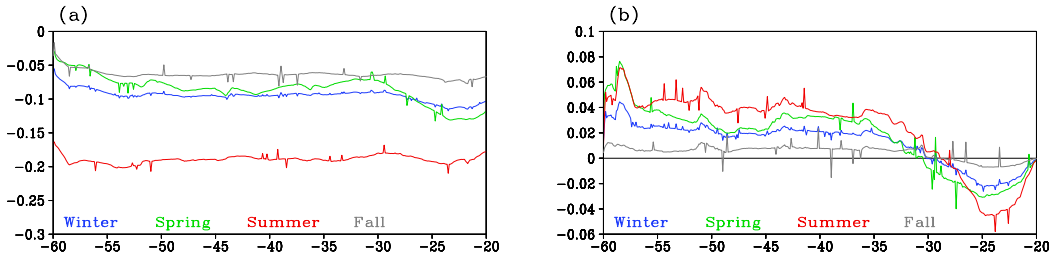

Figure 6.15: Globally averaged temperature factors [in °C] for the four different seasons. In (a) $\hat{f}_{veg_{(00)}}$ is shown and in (b) $\hat{f}_{veg_{(20)}}$.

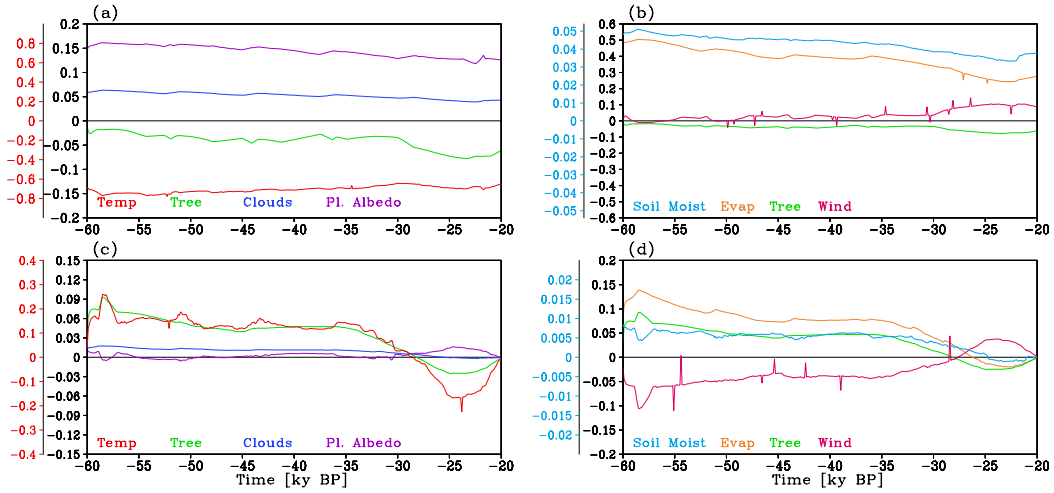

Figure 6.16: Differences between AV and A in summer, zonally averaged over 30–70° N, for cloud cover fraction, planetary albedo (∗10), temperature and tree fraction are shown in (a) for $\hat{f}_{veg_{(00)}}$ and in (c) for $\hat{f}_{veg_{(20)}}$ over time 60–20 ky BP. In (b) and (d) differences for surface wind speed, soil moisture (top 150mm), tree fraction and evapotranspiration are shown for $\hat{f}_{veg_{(00)}}$ and $\hat{f}_{veg_{(20)}}$, respectively.

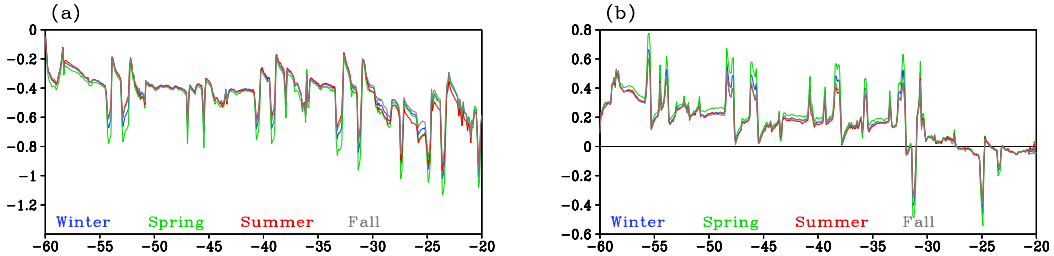

Figure 6.17: Globally averaged temperature factors [in °C] for the four different seasons. In (a) $\hat{f}_{syn_{(00)}}$ is shown and in (b) $\hat{f}_{syn_{(20)}}$.

ocean, namely the effects of sea-ice changes and changes in northward heat transport. This dominance is especially pronounced in spring and winter (Fig. 6.18), while in summer it can be seen that the sea-ice and, therefore, planetary albedo change is smaller, so that evapotranspiration changes due to vegetation changes have a stronger influence than in other seasons. The importance of the effects caused in the ocean is also the reason for the slightly stronger temperature change over the ocean than over land in $\hat{f}_{syn}$. $\hat{f}_{syn_{(00)}}$ cools the climate, averaged over the period 60–20 ky BP by −0.49 °C globally

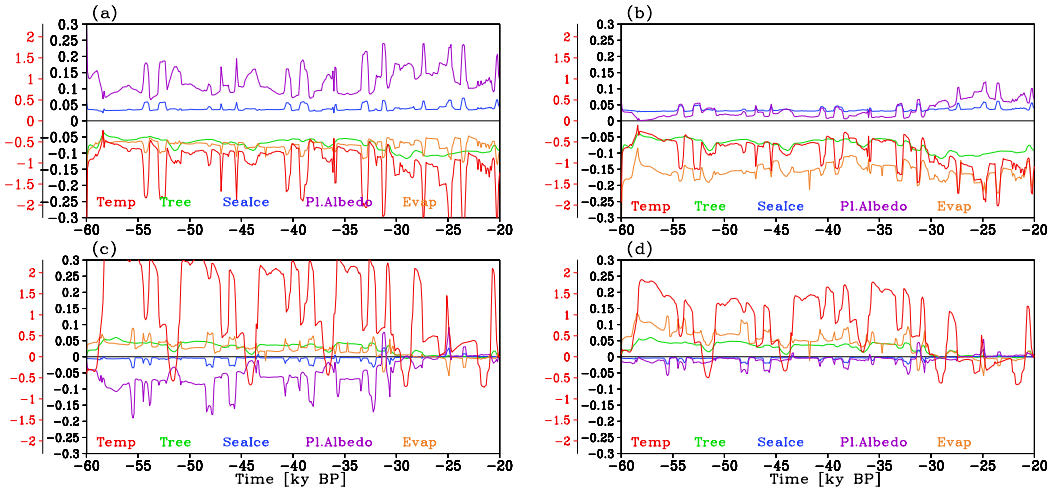

Figure 6.18: Albedo-, vegetation-, sea-ice-, evapotranspiration- and temperatures changes for $\hat{f}_{syn_{(00)}}$ (a, b) and $\hat{f}_{syn_{(20)}}$ (c, d) for spring (a, c) and summer (b, d), zonally averaged over 30–70° N.

on annual average. Averaged only over land the cooling is −0.44 °C and only over the oceans −0.49 °C . Globally, this makes up about 14% of the cooling between AOV and A_{00} averaged over this period.

Vegetation changes for $\hat{f}_{syn_{(00)}}$ (Fig. 6.19 (a), (b); Fig. 6.20 (a), (b)) are located between 20–65° N and between 25° S and 40° S. While trees mainly decrease, grass increases south of 60° N. The decrease in trees between 30–70° N causes a cooling due the taiga-tundra feedback and also a cooling due to the reduced greenhouse warming, caused by the decreased evapotranspiration. The reduction of trees in other regions south of 30° N and the changes of grass cover in general do not show a notable $\hat{f}_{syn_{(00)}}$ effect for temperature.

The effect of $\hat{f}_{syn_{(20)}}$ is a global warming effect (Fig. 6.9 (f)). Over the period from 60–20 ky BP it warms the climate by 0.17 °C globally on annual average, with 0.17 °C warming over land and 0.18 °C over the ocean. Globally, this are about 22% of the warming between AOV_{20} and A_{20} caused over this period.

Trees increase in $\hat{f}_{syn_{(20)}}$ in the northern regions from 45–60° N on the expense of grass and desert (Fig. 6.19 (a), (b)). Besides this decrease of grass due to extended tree cover, grass fraction increases as well, especially around 20–40°on both hemispheres.

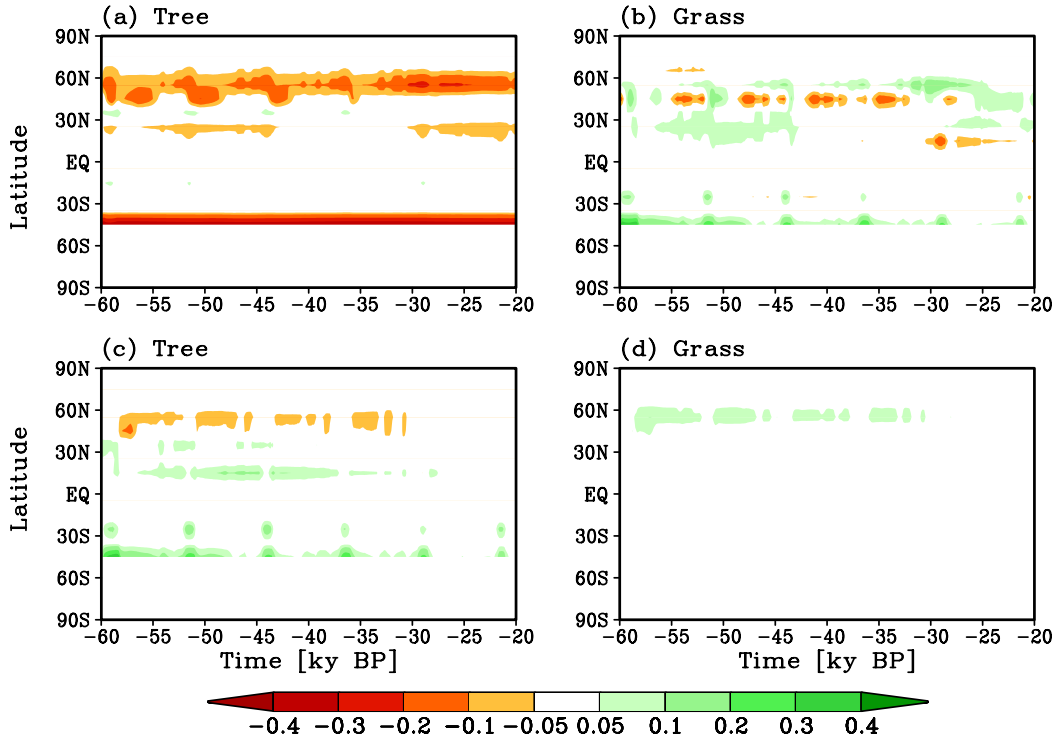

Figure 6.19: Zonally averaged change of tree fraction (a, c) and grass fraction (b, d) for $\hat{f}_{syn_{(00)}}$ (a, b) and $\hat{f}_{syn_{(20)}}$ (c, d) over time.

As already seen for $\hat{f}_{veg}$ and $\hat{f}_{syn_{(00)}}$, the change in grass fraction does not show a notable temperature effect, while the tree fraction increase causes a warming over the taiga-tundra effect and an increased evapotranspiration with increased greenhouse effect.

The increase in sea-ice in $\hat{f}_{syn_{(00)}}$ makes up about 13% of the overall $AOV_{00}-A_{00}$ increase while the decrease in sea-ice in $\hat{f}_{syn_{(20)}}$ causes 16% of the $AOV_{20}-A_{20}$ decrease. This change in sea-ice and, therefore, albedo of about 13–16% of the respective $AOV-A$ sea-ice change explains why $\hat{f}_{syn}$ has a stronger effect over the ocean than over land, in contrast to $\hat{f}_{veg}$. At the same time it also explains why the temperature changes caused by $\hat{f}_{oce}$ are still much larger as it causes 87–84% of the sea-ice decrease.

That the run AO_{00}, which is warmer than AOV and AO_{20}, has a much longer decay time of D/O events than AOV and especially AO_{20} (Figure 6.21) can be explained by a larger stability of the "warm" mode of the glacial ocean circulation in AO_{00} because of the warmer temperatures and a decreasing stability of the "warm" mode for colder temperatures (Ganopolski and Rahmstorf 2002; see chapter 1 for a short summary). AO_{20} is the coldest run of the three (AO_{00}, AO_{20} and AOV), and its "cold" mode is, therefore, more stable, while its "warm" mode is less stable as in the other two runs. This leads to some D/O events (e.g. at 57 ky BP and 48 ky BP) in AO_{20} with a shorter period compared to AOV because the "warm" mode in AO_{20} is very unstable and its

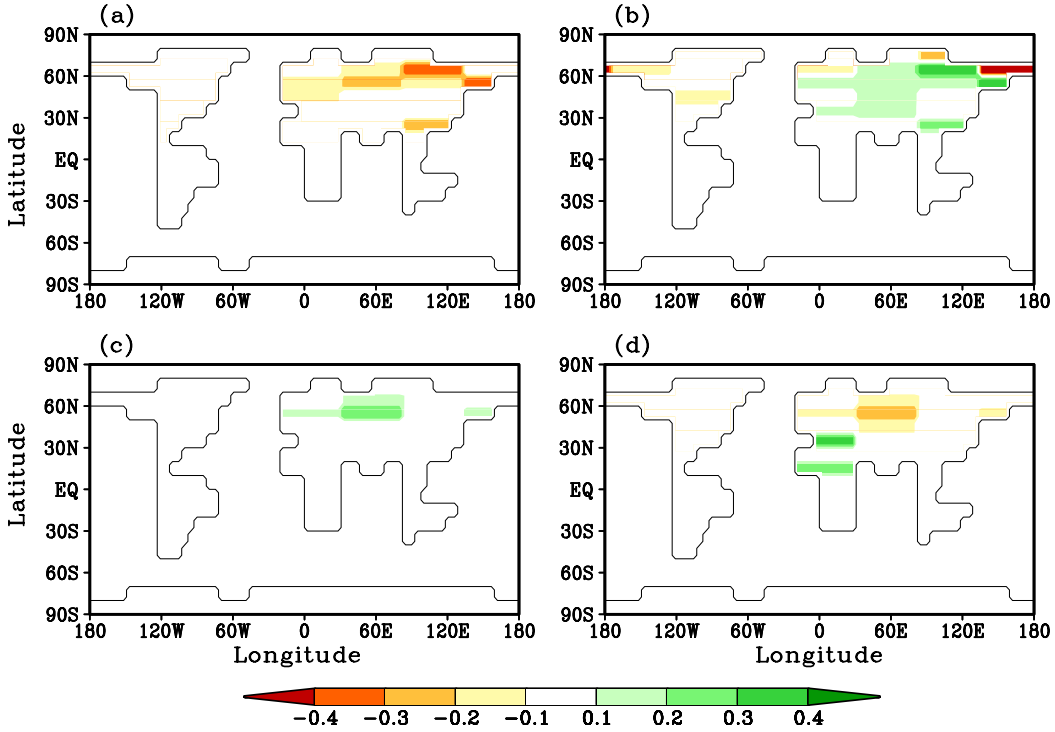

Figure 6.20: Vegetation change between $A0V$ and AV at around 45 ky BP. The area where changes occur stays the same during the period from 60–20 ky BP, only the magnitude of the vegetation change changes slightly. In (a) the tree fraction change and in (b) the grass change for $\hat{f}_{syn_{(00)}}$ is shown, while in (c) the tree fraction change and in (d) the grass fraction change for $\hat{f}_{syn_{(20)}}$ is shown.

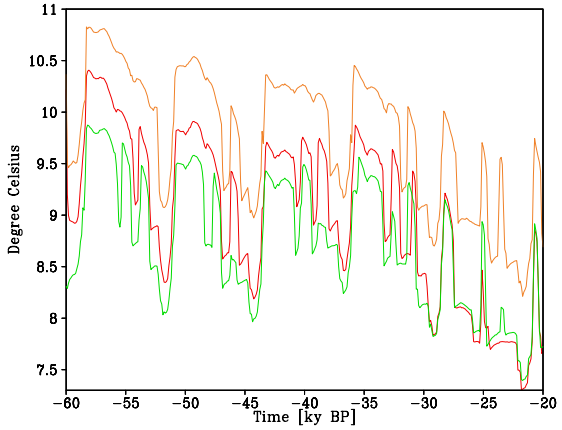

Figure 6.21: Annual averaged surface air temperature on the NH from AOV (in red)), AO_{20} (in green) and AO_{00} (in orange).

decay time is, therefore, short. This is true for as long as the difference between AOV and AO_{20} is large enough, which is the case for the first 25.000 years of the run, because afterwards the temperatures of AOV and AO_{20} are more and more converging so that the stability of their ocean circulation becomes also very similar, due to the prescribed vegetation from 20 ky BP in AO_{20}.
That AO_{00} is warmer than AOV and AO_{20} is colder than AOV is, thereby, caused by the different prescribed vegetation states and its effects on the temperature. However, that these small temperature changes are accompanied by changes in the stability of the ocean circulation that then lead to the described changes in timing and shape of D/O events is the result of the non-linearity of the circulation and not of the different vegetation states themselves! The difference in duration and timing of D/O events leads to the peaks in the feedback plots (Fig. 6.9 (e), (f) and 6.8) for $\hat{f}_{syn}$.

6.2.2 Precipitation

In Figure 6.22, the global factors are shown over the period from 60–20 ky BP. As already seen for the temperature factors, the ocean factor makes up the major part of the change, while the synergy factor is again larger than the pure vegetation factor.

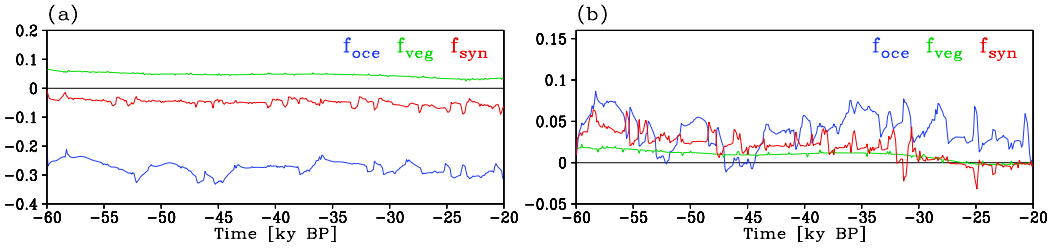

Figure 6.22: Annual and globally averaged precipitation factors [in mm/day], for "00" (a) and "20" (b). The ocean factor is the blue line, the vegetation factor green and the synergy factor red.

In difference to the temperature factor, the vegetation factor $\hat{f}_{veg_{(00)}}$ has the opposite sign than the synergy and ocean factor for "00". The interactive vegetation, therefore, leads to a moister climate in AV compared to A for both reference states. The interactive ocean, on the other hand, leads to a dryer climate compared to the use of the fixed "00" ocean in A_{00}, while it leads to a moister climate compared to the fixed "20" ocean in A_{20}. As for the temperature factor, the changes caused by the factors for "00" are larger than the changes by the "20" factors, for the same reasons as explained for the temperature.

Ocean Factor $\hat{f}_{oce}$

For $\hat{f}_{oce_{(00)}}$ the precipitation is decreased and for $\hat{f}_{oce_{(20)}}$ it is increased (Fig.6.22). Globally averaged over the period 60–20 ky BP the precipitation decrease caused by $\hat{f}_{oce_{(00)}}$

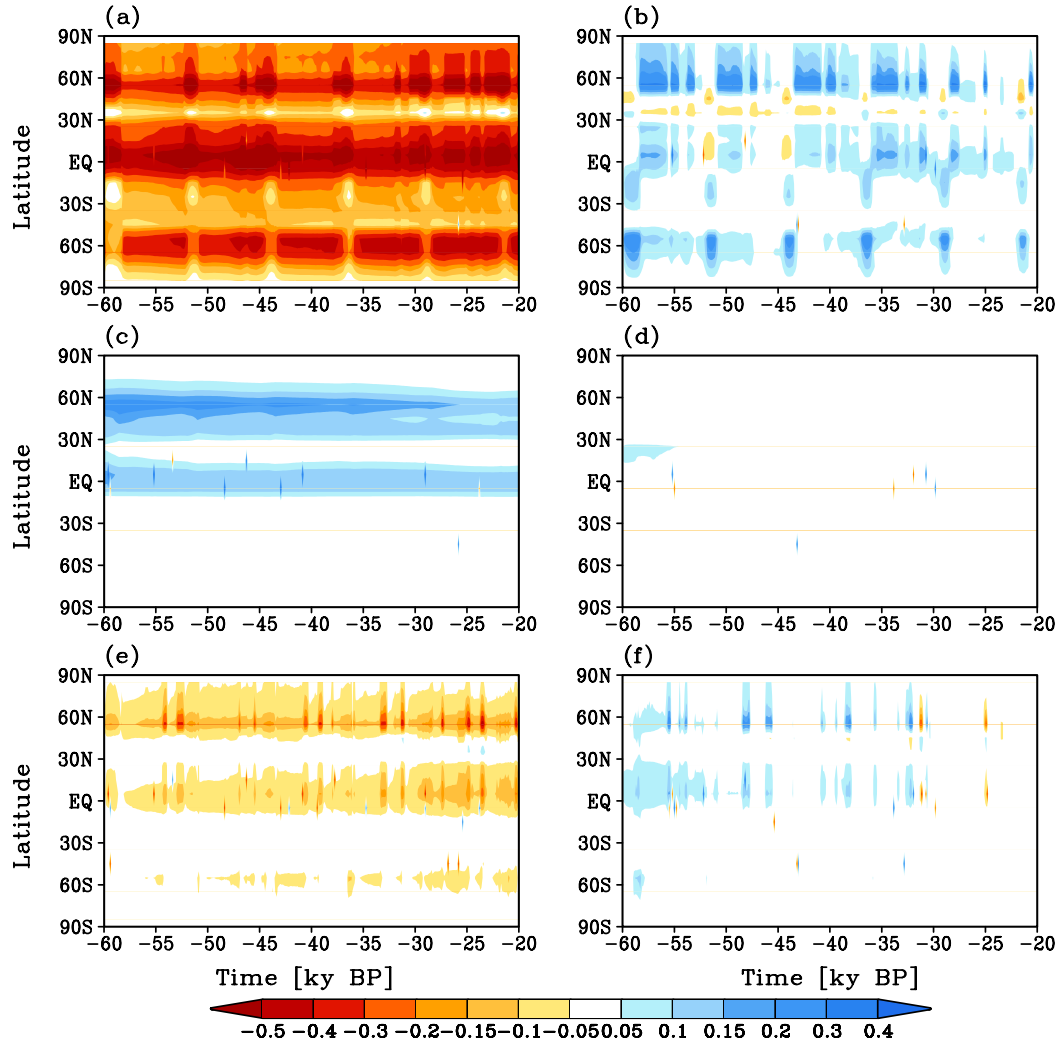

Figure 6.23: Zonally averaged annual precipitation factors $\hat{f}_{oce_{(00)}}$ (a), $\hat{f}_{oce_{(20)}}$ (b), $\hat{f}_{veg_{(00)}}$ (c), $\hat{f}_{veg_{(20)}}$ (d), $\hat{f}_{syn_{(00)}}$ (e) and $\hat{f}_{syn_{(20)}}$ (f) with precipitation changes in mm/day.

is −0.28 mm/day, which are 99.2% of the decrease between *AOV* and A. Averaged only over the ocean it is a bit larger (−0.33 mm/day), only over land a bit smaller (−0.27 mm/day). For $\hat{f}_{oce_{(20)}}$ the global increase is +0.04 mm/day (which are 57.7% of *AOV*−A). Over land it is about the same as globally (+0.04 mm/day) and over the ocean a bit stronger with 0.06 mm/day.

The changes in precipitation due to $\hat{f}_{oce_{(20)}}$ and $\hat{f}_{oce_{(00)}}$ are not only caused by the change in temperature and the resulting change in evaporation, but also over the change in sea-ice area that also influences evaporation. The change for both $\hat{f}_{oce}$ factors is most pronounced in the regions where large scale atmospheric rising motion dominates, i.e. the region around the equator and in 50–60° N and S (Fig. 6.23 (a), (b)). The

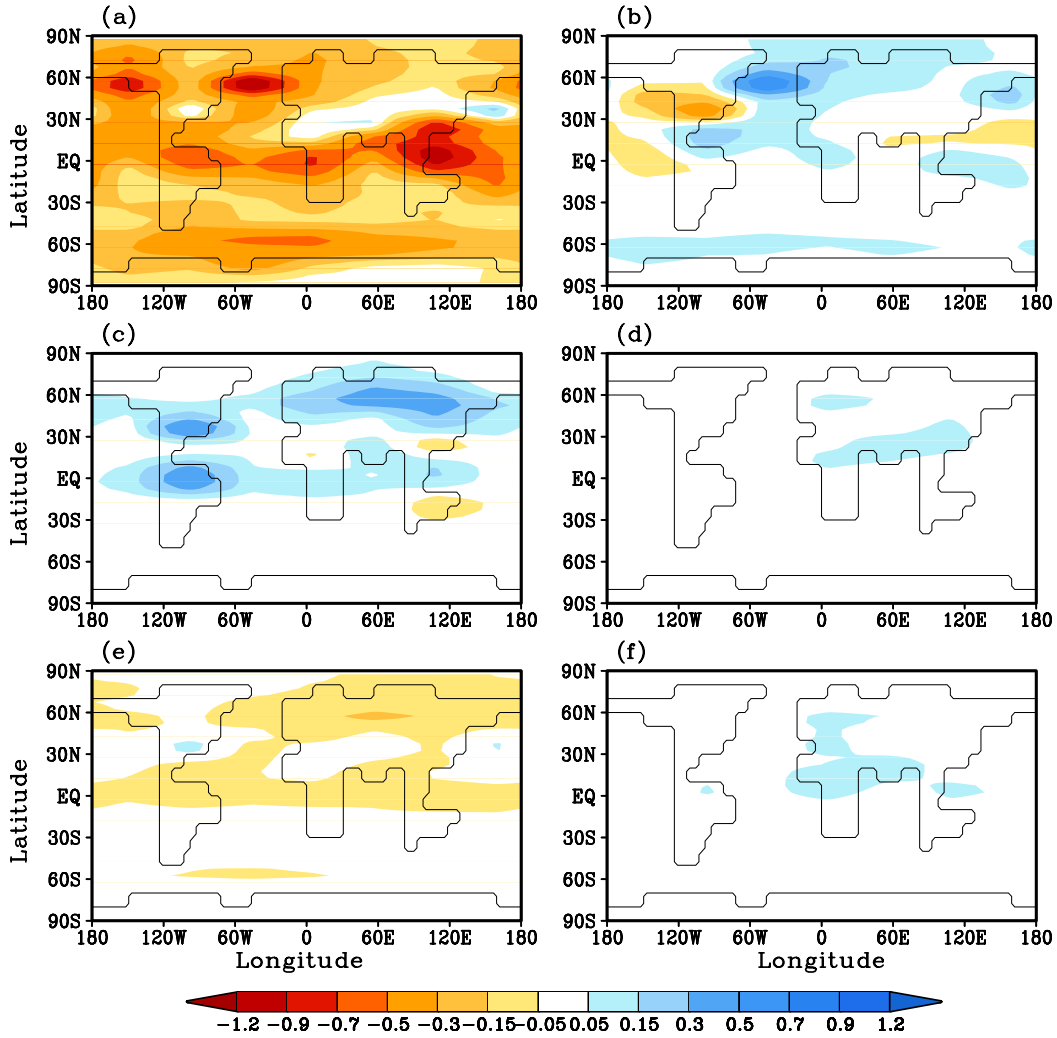

Figure 6.24: Between stadials and interstadials averaged precipitation factors from about 45 ky BP. The area where changes occur stays the same during the period from 60–20 ky BP. $\hat{f}_{oce_{(00)}}$ (a), $\hat{f}_{oce_{(20)}}$ (b), $\hat{f}_{veg_{(00)}}$ (c), $\hat{f}_{veg_{(20)}}$ (d), $\hat{f}_{syn_{(00)}}$ (e) and $\hat{f}_{syn_{(20)}}$ (f) with temperature changes in °C.

tropical region of maximum precipitation change, thereby, moves from mainly on the NH in summer to a position centered around the equator in winter, which can be explained with the shifted position of the Hadley cell in winter and summer. The reduced precipitation in $\hat{f}_{oce_{(00)}}$ in 50–60° N and 50–60° S as well as globally is strongest in the spring season on the respective hemisphere, as the sea-ice coverage is at its maximum then and the effect on evaporation is, therefore, largest. The warming in $\hat{f}_{oce_{(20)}}$, on the other hand, is strongest in fall on each hemisphere, as the sea-ice area is smallest in fall and the ocean is still warm and so evaporation from the ocean is largest (Fig. 6.25).

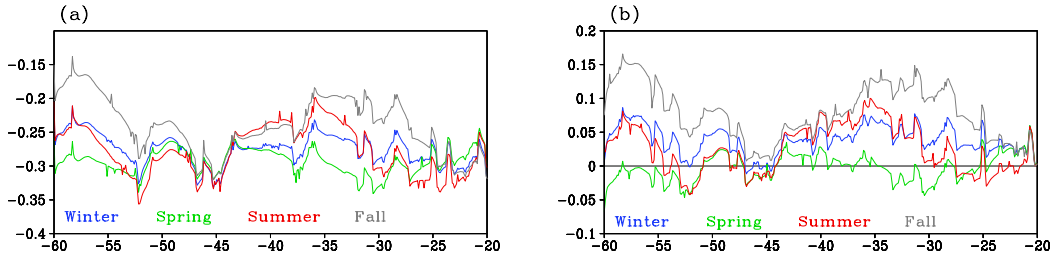

Figure 6.25: Globally averaged precipitation factor $\hat{f}_{oce}$ [in mm/day] for the four different seasons. In (a) $\hat{f}_{oce_{(00)}}$ is shown and in (b) $\hat{f}_{oce_{(20)}}$.

HE show up as (additional) decreases of precipitation on the NH and small increases (or reduced decreases) of precipitation on the SH in $\hat{f}_{oce_{(20)}}$ and $\hat{f}_{oce_{(00)}}$ (Fig. 6.23 (a), (b)).

Vegetation Factor $\hat{f}_{veg}$

The vegetation factor $\hat{f}_{veg_{(00)}}$ causes a change in the same direction as $\hat{f}_{veg_{(20)}}$ (Fig. 6.23 (c), (d), which is unexpected as the temperature change of $\hat{f}_{veg_{(00)}}$ was opposite to the effect of $\hat{f}_{veg_{(20)}}$. The discussion of the temperature factor of $\hat{f}_{veg_{(00)}}$, however, has already shown that for both $\hat{f}_{veg}$ factors an increase in evapotranspiration could be observed, even though this increase had opposite effects on temperature. For $\hat{f}_{veg_{(00)}}$ the cooling was due to more evapotranspiration and to more clouds (and, therefore, a higher planetary albedo) while for $\hat{f}_{veg_{(20)}}$ the evapotranspiration increase caused a warming due to the increased greenhouse effect.

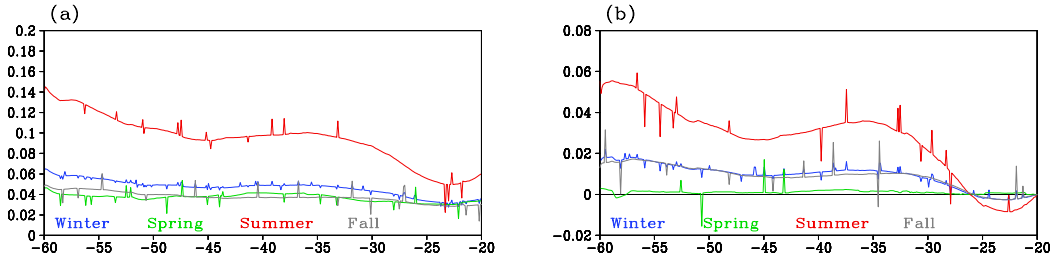

Figure 6.26: Globally averaged $\hat{f}_{veg}$ precipitation factors [in mm/day] for the four different seasons. In (a) $\hat{f}_{veg_{(00)}}$ is shown and in (b) $\hat{f}_{veg_{(20)}}$.

The increased evapotranspiration for both factors is the reason for the increased precipitation. The precipitation effect of both $\hat{f}_{veg}$ factors has its maximum in summer, when temperatures and evapotranspiration are highest, and is smaller in all other seasons (Fig. 6.26). Towards the LGM, the effect decreases for both factors, due to the decreasing tree fraction and, therefore, decreasing evapotranspiration in AV_{00} as well

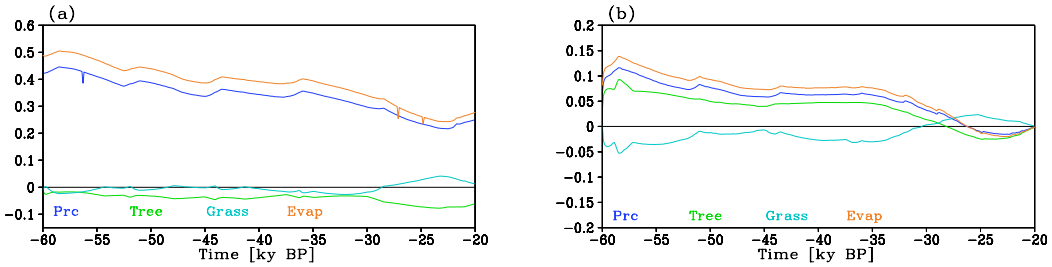

Figure 6.27: Summer precipitation-, tree-, grass- and evapotranspiration factors for $\hat{f}_{veg_{(00)}}$ (a) and $\hat{f}_{veg_{(20)}}$ (b), zonally averaged for 30–70° N.

as in AV_{20} toward the LGM as a reaction to the increasingly colder climate (Fig. 6.27).

Globally averaged over the period 60–20 ky BP, $\hat{f}_{veg_{(20)}}$ causes an increase in precipitation by 0.01 mm/day, with 0.02 mm/day over land and less than 0.01 mm/day over the ocean. For $\hat{f}_{veg_{(00)}}$ the global increase is 0.05 mm/day, with 0.09 mm/day over land and 0.01 mm/day over the ocean.

Synergy Factor $\hat{f}_{syn}$

The precipitation effects of $\hat{f}_{syn_{(00)}}$ and $\hat{f}_{syn_{(20)}}$ are again opposite, with $\hat{f}_{syn_{(00)}}$ causing a decrease and $\hat{f}_{syn_{(20)}}$ an increase in precipitation. The precipitation change is centered around 60° N and around the equator for both factors (Fig. 6.23 (e), (f)). The region around 60° N has its maximum in summer and is caused by increased evapotranspiration due to more trees and less sea-ice for $\hat{f}_{syn_{(20)}}$ and to decreased evapotranspiration in $\hat{f}_{syn_{(00)}}$ due to decreased tree fraction and increased sea-ice in $\hat{f}_{syn_{(00)}}$ (Fig. 6.28).

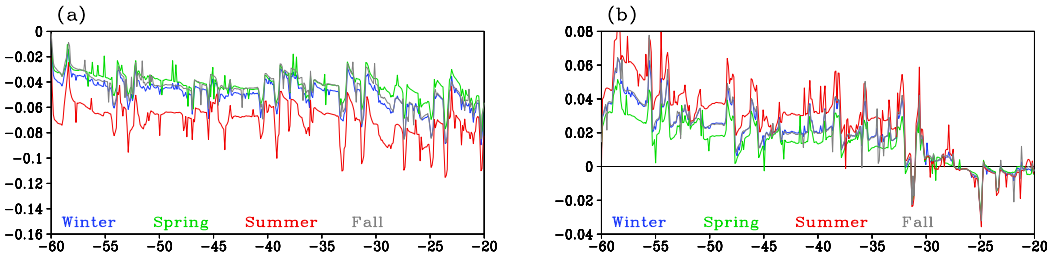

Figure 6.28: Globally averaged precipitation factors [in mm/day] for the four different seasons. In (a) $\hat{f}_{syn_{(00)}}$ is shown and in (b) $\hat{f}_{syn_{(20)}}$.

It is important to note that the effect of $\hat{f}_{syn_{(00)}}$ is a little bit larger than the effect of $\hat{f}_{veg_{(00)}}$ (by 0.002 mm/day if averaged over the period 60–20 ky BP) and occurs in the exact same place. This leads to an almost complete compensation of $\hat{f}_{veg_{(00)}}$ through $\hat{f}_{syn_{(00)}}$.

6.3 Evaluation of the Two Different Reference States

As already noted, the changes caused for the factors "00" are larger than the changes caused by the "20" factors and the "00" factors are negative while the "20" factors are positive (Table 6.2, 6.4). This is due to the different reference states that are used in their calculation. What is more important than the amplitude and direction of the factors, is the relative magnitude of the changes they cause and the place where these changes are found. It could be seen that the areas where the changes in temperature and precipitation occurred were very similar for the respective "00" and "20" factors. Also, the importance of the factors was similar for the temperature changes, with the ocean factor making up 83% of the $AOV - A$ difference in "00" and 77% in "20". The synergy factor caused 14% in "00" and 22% in "20" and the vegetation factor 3% in "00" and 1.3% in "20".
For precipitation a difference could be observed: The "00" vegetation factor was opposite to the ocean and synergy factor and about as large as the synergy factor while for "20" the vegetation factor was in the same direction as the ocean and vegetation factor and also much smaller than the synergy factor.

Overall, the comparison of the factors for the two different reference states shows that the order of the factors by their global importance is not dependent on the reference state chosen, but that variations in the percentage of the total $AOV - A$ change that each factor causes are dependent on how large the reason for the change is, i.e. how much the reference state differs from the fully coupled run. The sign of the factors mainly depends on the reference state chosen, with a colder reference state than the fully coupled run normally leading to positive factors and a warmer reference state than the full coupled run causing negative factors. For the precipitation change, however, the vegetation factor for "00" showed that this is not always true as the same response (here: increase in precipitation) can be caused by different effects ("00": increased evapotranspiration in spite of reduced tree fractions due to increased windspeed; "20": increased evapotranspiration due to increased vegetation). This highlights that factors always have to be considered as factors relative to a reference state and not as universal factors (as stated in section 2.2.) Hence, it cannot be concluded that a decrease in tree fraction during the glacial necessarily also leads to a decrease in precipitation.

The main feature of the factor separation for the period from 60–20 ky BP is thus seen in both "00" and "20": The ocean is by far the most important factor, followed by the synergy factor and then the vegetation factor.

As the changes caused by the vegetation and synergy factor for "20" were very small, it can be concluded that the use of a prescribed vegetation distribution from the LGM does not cause large changes in the simulation of the glacial period, while the use of a present day vegetation was able to cause regional changes of up to 2 °C in the northern latitudes, which might be problematic.

6.4 Comparison with Studies for the Mid-Holocene

Ganopolski et al. (1998a) investigated the role of vegetation during the Mid-Holocene for 6 ky BP. They also used the CLIMBER-2 model, though in an earlier version than the one I used. They performed four experiments (A, *AO*, *AV* and *AOV*) for the Mid-Holocene at 6000 years BP in addition to the control simulation which was performed for a preindustrial climate with CO_2 concentrations of 280 ppm and modern day insolation. The CO_2 concentration in the Mid-Holocene experiments was the same as for the control run and vegetation, SST and sea-ice were taken from the control run for experiments with fixed characteristics. The main result of the study by Ganopolski et al. (1998a) was that only in *AOV* a warming in winter could be seen that is also found in reconstructions for this time (Prentice et al. 1996; TEMPO Members 1996), while the runs *AO* and *AV* showed a colder climate in response to the reduced insolation. This warming was caused by the synergy of the taiga-tundra feedback and the sea-ice-albedo feedback.

In their paper, Ganopolski et al. (1998a) show a table with NH and SH temperature and precipitation changes for all four runs relative to present day, split up into summer, winter and annual averages. From this table Berger (2001) calculated the appropriate Stein and Alpert (1993) factors for NH and SH and I added the global values, shown in table 6.1 and table 6.3.

I want to compare the factors I calculated for the glacial period with the results from Ganopolski et al. (1998a) to investigate the importance of the atmosphere-vegetation feedback during glacial times compared to the Mid-Holocene. For the comparison I averaged my factors over the period 60–20 ky BP (shown in table 6.2 and 6.4). These averages are a good estimate for the values of the factors during the glacial as they interpolate between the stadials and interstadials. The factors for stadial periods and interstadial periods (see appendix B.3 for tables of the factors for a typical stadial and interstadial state) differ in the way that for the "00" factors the ocean factor causes larger changes during stadials than during interstadials, due to the "cold" circulation mode during stadials that causes colder temperatures and hence a larger difference to A_{00}. For "20" the ocean factor is larger in interstadials, also due to a change in circulation mode, here the change to the "warm" mode during interstadials in AO_{20} that causes warmer temperatures and, therefore, a larger difference to the colder A_{20} experiment. The vegetation factor for both "00" and "20" stays about the same during stadial and interstadial periods as the run *AV* is not perturbed by D/O events. The synergy factors $\hat{f}_{syn_{(20)}}$ and $\hat{f}_{syn_{(00)}}$ are slightly larger for interstadials, probably due to the more northward sea-ice margin during interstadial and the, therefore, larger interaction of the taiga-tundra feedback with the sea-ice-albedo feedback. As these variations do not change the percentages that each factor contributes to the total change by much, an average of the factors over the whole period gives the main information about the importance of the factors while it smoothes the peaks in the synergy and ocean factor that are only due to the slightly different timing of D/O events and that, therefore, do not contain valuable information.

		$\mathrm{A}\hat{O}$	$\mathrm{A}\hat{V}$	$\mathrm{A}\widehat{OV}$	AOV$-A$
Annual	Global	-0.1	$+0.2$	$+0.8$	$+0.8$
	NH	-0.1	$+0.2$	$+0.8$	$+0.9$
	SH	-0.1	$+0.1$	$+0.7$	$+0.7$
	NH_L	-0.1	$+0.3$	$+0.8$	$+1.0$
Summer	Global	-0.2	$+0.2$	$+0.6$	$+0.6$
	NH	-0.4	$+0.3$	$+0.7$	$+0.6$
	SH	0	$+0.1$	$+0.5$	$+0.6$
	NH_L	-0.5	$+0.5$	$+0.8$	$+0.8$
Winter	Global	$+0.2$	$+0.1$	$+0.8$	$+1.0$
	NH	$+0.2$	$+0.1$	$+0.8$	$+1.1$
	SH	$+0.1$	0	$+0.7$	$+0.8$
	NH_L	$+0.3$	$+0.1$	$+0.8$	$+1.2$

Table 6.1: Temperature factors [in $^\circ$ C], calculated from the temperature changes relative to the present day for the Mid-Holocene shown in Ganopolski et al. (1998a). To avoid confusion of the factors of Ganopolski et al. 1998a with my factors $\mathrm{A}\hat{O}$ is here the ocean factor, $\mathrm{A}\hat{V}$ the vegetation factor and $\mathrm{A}\widehat{OV}$ the synergy factor.

		$\hat{f}_{oce_{(00)}}$	$\hat{f}_{veg_{(00)}}$	$\hat{f}_{syn_{(00)}}$	$\hat{f}_{ref_{(00)}}$	$\hat{f}_{oce_{(20)}}$	$\hat{f}_{veg_{(20)}}$	$\hat{f}_{syn_{(20)}}$	$\hat{f}_{ref_{(20)}}$
Annual	Global	-2.7	-0.1	-0.4	-3.2	$+0.6$	0	$+0.2$	$+0.8$
	NH	-3.1	-0.2	-0.6	-3.8	$+0.7$	0	$+0.2$	$+0.9$
	SH	-2.4	0	-0.3	-2.7	$+0.5$	0	$+0.1$	$+0.6$
	NH_L	-2.8	-0.3	-0.6	-3.7	$+0.7$	0	$+0.2$	$+0.9$
Summer	Global	-2.6	-0.2	-0.4	-3.2	$+0.4$	0	$+0.2$	$+0.6$
	NH	-2.5	-0.4	-0.5	-3.4	$+0.3$	0	$+0.2$	$+0.5$
	SH	-2.7	0	-0.3	-3.0	$+0.4$	0	$+0.1$	$+0.5$
	NH_L	-2.3	-0.5	-0.6	-3.4	$+0.3$	0	$+0.2$	$+0.5$
Winter	Global	-2.8	0	-0.4	-3.2	$+0.7$	0	$+0.2$	$+0.9$
	NH	-3.6	-0.1	-0.6	-4.3	$+0.9$	0	$+0.2$	$+1.1$
	SH	-2.0	0	-0.3	-2.3	$+0.5$	0	$+0.1$	$+0.6$
	NH_L	-3.3	-0.1	-0.6	-4.0	$+0.9$	0	$+0.2$	$+1.1$

Table 6.2: Temperature change [in $^\circ$ C] caused by the factors averaged over 60–20 ky BP

For the comparison with the Mid-Holocene, I will only discuss the difference between the "00" factors and the factors of Ganopolski et al. (1998a) since these factors show the effect of present day ocean and vegetation characteristics on climate, which is the same approach Ganopolski et al. (1998a)took. Therefore, it makes sense to compare only the "00" factors and not the "20" factors, especially as it has been discussed in the previous section that the "20" vegetation and synergy factor are only small.

It can be seen that vegetation played an important role in the Mid-Holocene, as important and sometimes even more important than the ocean effect. Most striking, however, is that in the Mid-Holocene the synergy effect $\widehat{AOV}$ is much larger than both individual factors $A\hat{O}$ and $A\hat{V}$.

For the glacial period from 60–20 ky BP that I investigated, the picture is different: The dominant factor is by far the ocean factor $\hat{f}_{oce}$ while the synergy factor $\hat{f}_{syn}$ is always smaller than the ocean factor, but larger than the vegetation factor $\hat{f}_{veg}$. The fact that the ocean is less important than the synergy factor in the Mid-Holocene but more important than it is in the glacial period, shows the dominant influence of the ocean during glacial times.

		A$\hat{O}$	A$\hat{V}$	A$\widehat{OV}$	AOV$-A$
Annual	Global$_L$	-0.01	$+0.06$	$+0.09$	$+0.14$
	NH$_L$	-0.02	$+0.11$	$+0.09$	$+0.18$
	SH$_L$	0	0	$+0.09$	$+0.09$
Summer	Global	-0.05	$+0.13$	$+0.08$	$+0.16$
	NH$_L$	-0.06	$+0.24$	$+0.11$	$+0.29$
	SH$_L$	-0.03	$+0.02$	$+0.04$	$+0.03$
Winter	Global	$+0.02$	$+0.01$	$+0.09$	$+0.11$
	NH$_L$	0	$+0.01$	$+0.05$	$+0.06$
	SH$_L$	$+0.04$	0	$+0.12$	$+0.16$

Table 6.3: Precipitation factors in mm/day over land, calculated from the differences in precipitation shown in Ganopolski et al. (1998a)

A detailed comparison of the temperature changes caused by the factors shows that the temperature change caused by the ocean factor $\hat{f}_{oce_{(00)}}$ is about 10–30 times larger than $A\hat{O}$. The effect of the vegetation factor $\hat{f}_{veg_{(00)}}$ on the NH is as large as the effect caused by $A\hat{V}$. For the synergy factor $\hat{f}_{syn_{(00)}}$ the temperature change caused by it on the NH is only about 70% of the change $\widehat{AOV}$ caused while on the SH it is only about 40%. The combined change from all three factors is, due to the much larger ocean factor, about 3 to 4 times the temperature change that was caused in the study of Ganopolski et al. (1998a). For precipitation the ocean factor $\hat{f}_{oce_{(00)}}$ shows about the same relation to $A\hat{O}$ as seen for temperature: $\hat{f}_{oce_{(00)}}$ is about 10 times larger than $A\hat{O}$, except in summer where it is only 5–6 times larger. The precipitation effect of the vegetation factor is about the same in $\hat{f}_{veg_{(00)}}$ and $A\hat{V}$ in summer while it is about 80%

smaller in $\hat{AV}$ in winter. For the synergy factor $\hat{f}_{syn_{(00)}}$ and $\widehat{AOV}$ in summer the effect is again about the same, while in winter the effect of $\widehat{AOV}$ is about 2–3 times larger than the effect of $\hat{f}_{syn_{(00)}}$.

This means that the first, most obvious difference between the factors for the Mid-Holocene and the "00" factors for the glacial is that the temperature change has different signs: Compared to today, the "00" factors cool the climate in the glacial while they warm it in the Mid-Holocene. The second, most important difference is that for both the precipitation and the temperature effect the ocean factor is the dominant factor for the glacial while for the Mid-Holocene the synergy factor was the most important factor. This is not only the consequence of a smaller synergy factor but also a result of the much larger ocean factor in the glacial. It has also become apparent that the difference between Mid-Holocene and glacial temperature factors is even larger on the SH. The reason for the even larger difference for the SH is that in the study of the Mid-Holocene Ganopolski et al. (1998a) found that vegetation cover changes are also important in the subtropics, where feedbacks between vegetation and precipitation led to a greening of the Sahara. In the study of the glacial climate, vegetation changes in the subtropics occurred, but did not have a large effect on temperature or precipitation, so that the SH synergy factor is much smaller in the glacial.

Overall, this means that even though the vegetation factor seems to be very small in the glacial compared to the ocean factor, the temperature changes caused on the NH by $\hat{f}_{veg_{(00)}}$ are as large as during the Mid-Holocene, just opposite. What changes is mainly the magnitude of the ocean factor and of the synergy factor, with the ocean factor $\hat{f}_{oce_{(00)}}$ causing larger changes than in the Mid-Holocene study for both temperature and precipitation. The synergy factor is smaller than during the Mid-Holocene for both temperature and precipitation for the glacial factors, probably because of a larger sea-ice area in the glacial that extends further south than during the Mid-Holocene so that the synergy between the sea-ice-albedo feedback and the taiga-tundra feedback is reduced.

		$\hat{f}_{oce_{(00)}}$	$\hat{f}_{veg_{(00)}}$	$\hat{f}_{syn_{(00)}}$	$\hat{f}_{ref_{(00)}}$	$\hat{f}_{oce_{(20)}}$	$\hat{f}_{veg_{(20)}}$	$\hat{f}_{syn_{(20)}}$	$\hat{f}_{ref_{(20)}}$
Ann.	Glob_L	−0.27	+0.09	−0.05	−0.23	+0.04	+0.02	+0.03	+0.09
	NH_L	−0.29	+0.13	−0.08	−0.24	+0.04	+0.04	+0.04	+0.12
	SH_L	−0.26	+0.05	−0.03	−0.24	+0.04	0	+0.01	+0.05
Sum.	Glob_L	−0.29	+0.15	−0.09	−0.23	+0.02	+0.05	+0.04	+0.11
	NH_L	−0.39	+0.25	−0.15	−0.29	+0.04	+0.10	+0.07	+0.20
	SH_L	−0.17	+0.04	−0.01	−0.14	0	0	+0.01	+0.01
Win.	Glob_L	−0.28	+0.05	−0.04	−0.27	+0.06	0	+0.02	+0.08
	NH_L	−0.23	+0.05	−0.04	−0.22	+0.04	+0.01	+0.02	+0.07
	SH_L	−0.34	+0.04	−0.05	−0.35	+0.08	−0.01	+0.02	+0.09

Table 6.4: Precipitation changes caused by the factor averaged over 60–20 ky BP [in mm/day].

6.5 Comparison of the Transient and the Equilibrium Simulation of the LGM

The global LGM temperature simulated in the transient run *AOV* for the LGM is with 9.2 °C about 0.1 °C warmer than the simulated temperature in the equilibrium run LGM_{ACIFV} (9.1° C). The important difference between the equilibrium experiments and the transient experiments at the LGM is that the ocean circulation is in the "cold" glacial ocean mode for AO_{00}[3] but in the "warm" glacial mode for LGM_{ACIF}. This means that while in the equilibrium experiment the present day vegetation kept the ocean circulation in the "warm" glacial mode, it was in the "cold" glacial mode in the transient experiment (Fig. 6.29 (a), (b)) with the same prescribed present day vegetation.

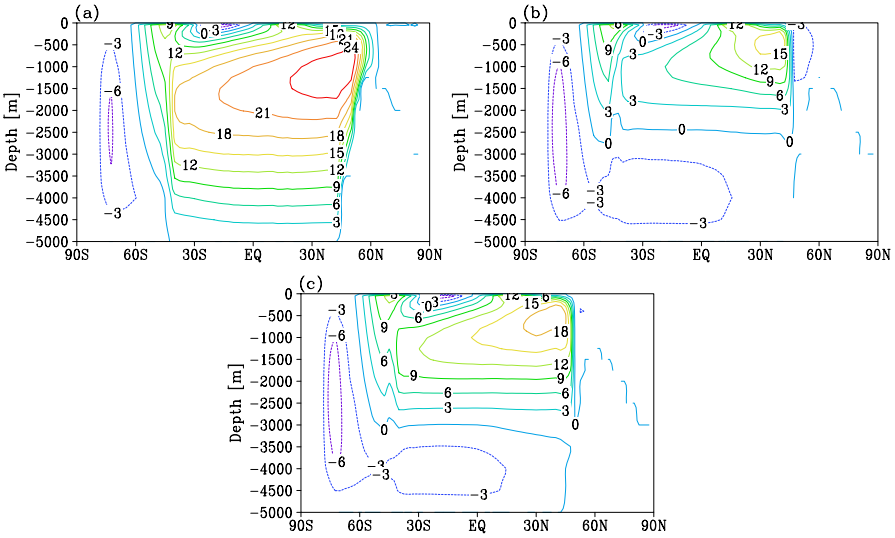

Figure 6.29: Atlantic overturning stream function [in Sv] for the LGM. In (a) it is from the simulation LGM_{ACIF}, in (b) from the simulation AO_{00} and in (c) from the new simulation $LGM_{ACIF_{(190)}}$.

A difference between the transient and equilibrium experiments is the atmospheric CO_2 concentration at the LGM: For the equilibrium experiments the CO_2 concentration was set to 200 ppm, in accordance with the CO_2 concentration of the PMIP (2001) experiments, while for the transient simulation the reconstructions from Petit el al. (1999) were used, which show a concentration of 190 ppm at 21 ky BP. Therefore, it can be suspected that the additional cooling caused by the 10 ppm lower concentration in the transient run AO_{00} was enough to make the system cross the threshold towards the "cold" mode. This would be in line with the conclusions from the equilibrium experiment, where it was stated that not the vegetation itself but the small additional cooling

[3]Only the "00" runs were considered for this comparison as all the "20" runs were already almost the same for the LGM (and the "20" factors, therefore, almost zero) because they converge at 20 ky BP.

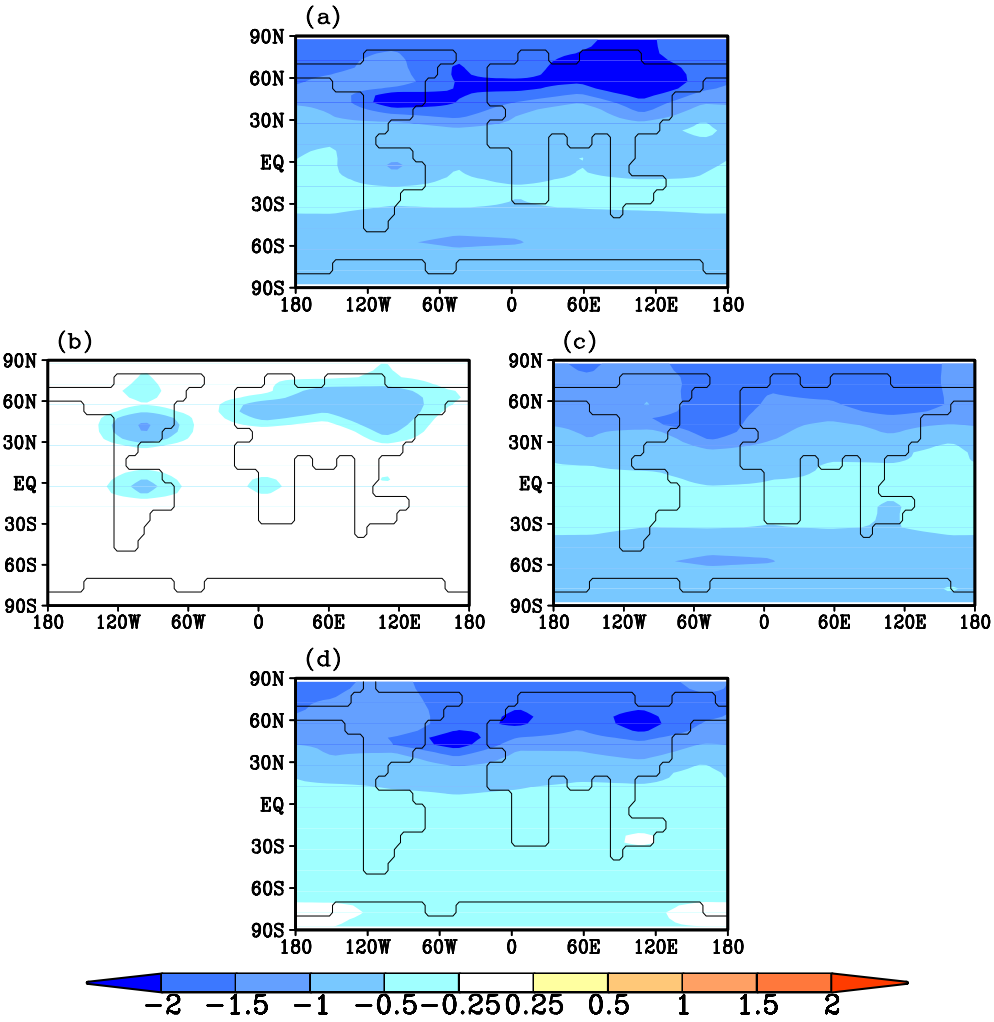

Figure 6.30: Annual averaged temperature change [in °C]. In (a) the combined change caused by $\hat{f}_{veg_{(00)}}$ and $\hat{f}_{syn_{(00)}}$ is shown, while (b) shows the individual effect of $\hat{f}_{veg_{(00)}}$ and (c) the effect of $\hat{f}_{syn_{(00)}}$. In (d) the temperature difference between $LGM_{ACIFV_{(190)}}$ and $LGM_{ACIF_{(190)}}$ is seen, which is the temperature change caused by the atmosphere-vegetation feedback and its synergies and, therefore, should be compared to (a).

that it caused was the reason for the switch in ocean circulation, as it is a threshold process. To test this hypothesis, an additional experiment has been performed: A simulation like LGM_{ACIF}, but with a CO_2 concentration of 190 ppm (called $LGM_{ACIF_{(190)}}$) instead of the before used 200 ppm. It turned out that the additional lowering of the CO_2 concentration by 10 ppm in $LGM_{ACIF_{(190)}}$ was indeed enough to cross the threshold of the ocean circulation and to trigger the switch to the "cold" mode (Fig. 6.29). It could also be shown in further additional experiments not presented here that the

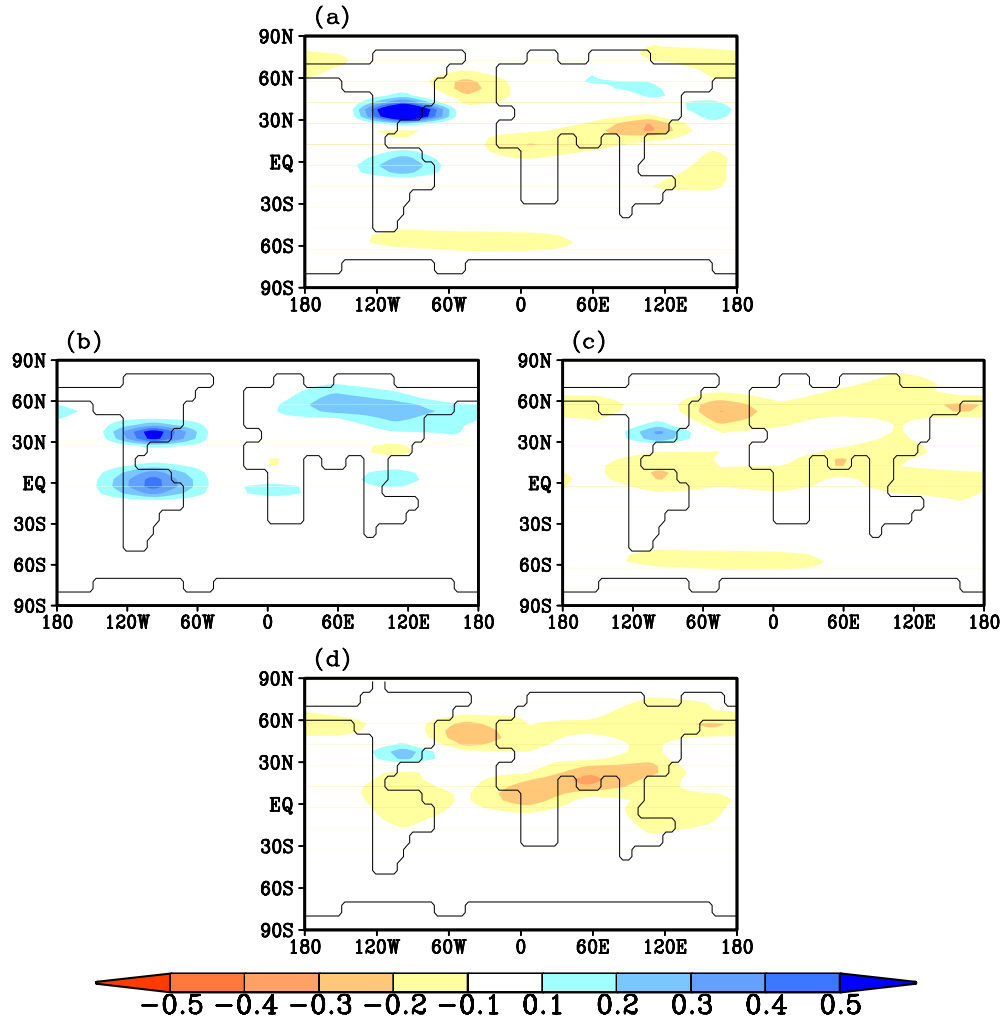

Figure 6.31: Annual averaged precipitation change [in mm/day]. In (a) the combined change caused by $\hat{f}_{veg_{(00)}}$ and $\hat{f}_{syn_{(00)}}$ is shown, while (b) shows the individual effect of $\hat{f}_{veg_{(00)}}$ and (c) the effect of $\hat{f}_{syn_{(00)}}$. In (d) the precipitation difference between $LGM_{ACIFV_{(190)}}$ and $LGM_{ACIF_{(190)}}$ is seen, which is the precipitation change caused by the atmosphere-vegetation feedback and its synergies and, therefore, should be compared to (a).

equilibrium state of the ocean circulation was always independent of the initial state of the ocean circulation at the beginning of the experiments. All this shows how close the ocean circulation is to the threshold already in LGM_{ACIF} and also proves that the vegetation is really not the reason for the change in the ocean circulation but just works as a trigger for it.

The temperature change caused by the combined effect of the vegetation factors in the equilibrium experiments is much larger than the cooling caused by $\hat{f}_{veg}$ in the transient

experiment (Fig. 6.31). The reason is that the cooling by the vegetation factor in the transient experiment is really only caused by the taiga tundra feedback or hydrological effects due the vegetation changes, while in the equilibrium experiment these effects could be amplified by synergy effects with the interactive ocean so that they were larger. To compare the temperature effect of the atmosphere-vegetation feedback for the LGM in the two studies, the temperature change caused by $\hat{f}_{veg_{(00)}}$ and $\hat{f}_{syn_{(00)}}$ for the LGM and the result from the equilibrium experiment are shown in Figure 6.30. For the equilibrium experiments the shown temperature change is the difference between $LGM_{ACIF_{(190)}}$ and an experiment named $LGM_{ACIFV_{(190)}}$ that has the same setup as LGM_{ACIFV}, only with a CO_2 level lowered to 190 ppm. This difference was chosen here for the comparison with the transient experiment as the difference between LGM_{ACIFV} and LGM_{ACIF} does not only show the effect of the vegetation but also the much larger effect of the change in ocean circulation. As the run $LGM_{ACIFV_{(190)}}$ is already in the "cold" ocean mode, the difference between $LGM_{ACIF_{(190)}}$ and $LGM_{ACIFV_{(190)}}$, therefore, only includes the effect of the vegetation. Globally, this difference is 0.6° C, which is only 0.1 °C less than the difference between LGM_{ACIF} and LGM_{ACIFV} (0.7 °C). This shows that globally the change in the ocean circulation does not change the temperature much, even so regionally it is of great importance.

It can be observed that the pattern of the total temperature change due to the atmosphere-vegetation feedback and its synergies is about 0.5–1 °C stronger in the result from the transient experiment, but that the pattern of cooling is about the same in both cases. Therefore, it can be suspected that the pattern of the pure atmosphere-vegetation feedback and the pattern of the synergy effect in the equilibrium experiments of the LGM is about the same as in the transient experiment, just a bit smaller. For the precipitation (Fig. 6.31) the pattern from the equilibrium experiment and the transient experiment is also about the same, even though more differences occur than for temperature. The most pronounced difference is seen over South America, where the overall sum of the atmosphere-vegetation feedback together with synergies with the ocean shows an increase of precipitation, while the difference between $LGM_{ACIF_{(190)}}$ and $LGM_{ACIFV_{(190)}}$ shows a small decrease of precipitation in about the same region. The other regions with the largest changes are about the same in both studies, with a decrease of precipitation over the North Atlantic and the tropics and an increase over southern North America. That there are differences between the transient and the equilibrium simulation is not the result of a different vegetation change (Fig. 6.32) but the consequence that the equilibrium runs yield the equilibrium response of the climate to these vegetation changes while the transient run shows the transient response that is not yet in full equilibrium with the forcings.

Overall, it can be concluded that the changes between the equilibrium simulation and the transient simulation of the LGM are not very large and that also the regions where the atmosphere-vegetation feedback and its synergy have an effect are about the same in both experiments. This is true as long as the non-linear response of the ocean circulation is not mixed up with the vegetation effect in the equilibrium study.

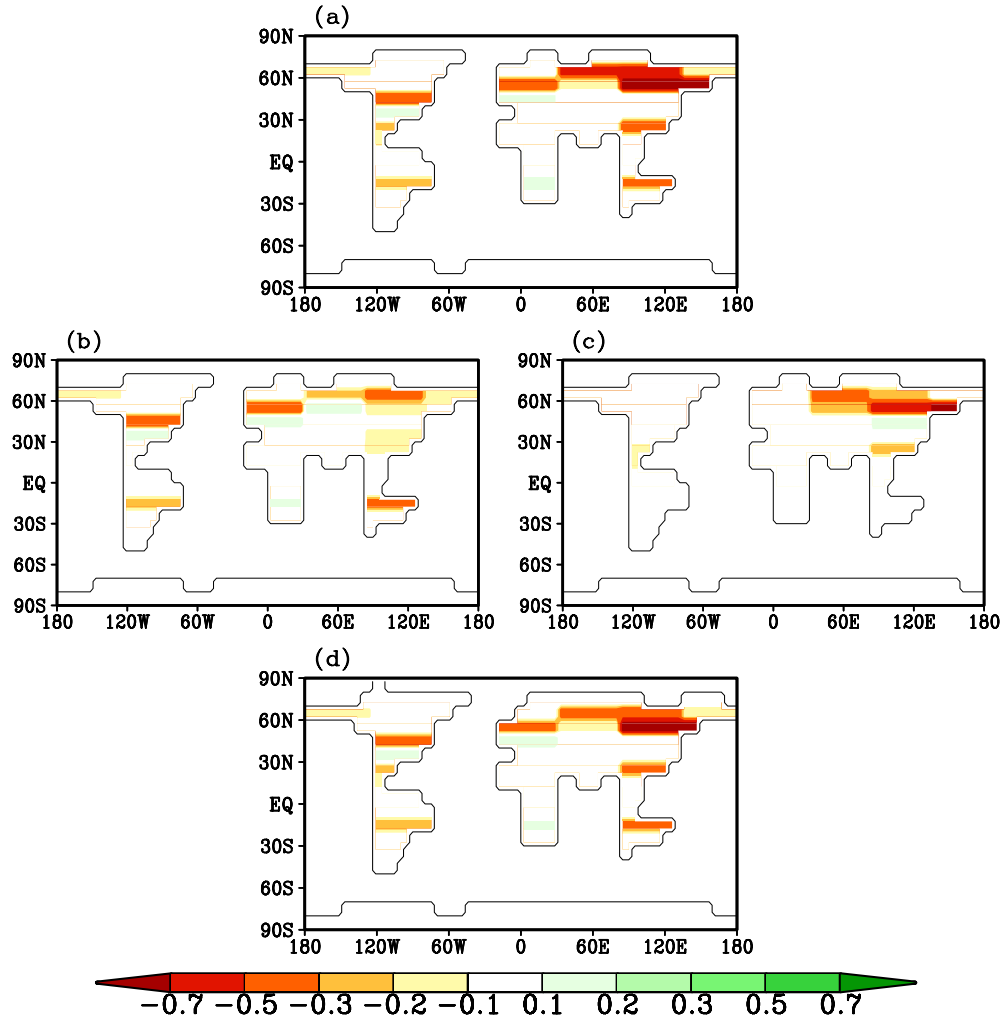

Figure 6.32: Change in tree fraction. In (a) the combined change caused by $\hat{f}_{veg_{(00)}}$ and $\hat{f}_{syn_{(00)}}$ is shown, while (b) shows the individual effect of $\hat{f}_{veg_{(00)}}$ and (c) the effect of $\hat{f}_{syn_{(00)}}$. In (d) the tree fraction difference between $LGM_{ACIFV_{(190)}}$ and $LGM_{ACIF_{(190)}}$ is seen.

Chapter 7

Conclusions and Summary

In this work the influence of the atmosphere-vegetation feedback during the last glacial period has been investigated.

Regarding the importance of the atmosphere-vegetation feedback and its synergies I was able to show in equilibrium experiments that at the LGM the effect of the taiga-tundra feedback in the high northern latitudes of Eurasia, amplified by the synergy with the sea-ice-albedo feedback, is almost as large as the effect of CO_2 in the same region. Thereby, the taiga-tundra feedback caused an additional LGM cooling of about 2–2.5 °C over Siberia. Over North America the cooling was smaller (only about 1.5° C), due to the more southward extent of the inland ice so that vegetation changes in the high northern latitudes, where the taiga-tundra feedback is strongest, were only small.

In the equilibrium experiments for the LGM I was able to show that CLIMBER-2.3 has two different equilibrium ocean circulation modes with associated temperature differences of up to 7 °C over the North Atlantic when either a fixed present day vegetation or an interactive vegetation is used. These two equilibrium states are independent of the initial state of the ocean circulation, the simulated ocean state only depends on whether the modeled climate crosses the threshold of the ocean circulation or not.
Without the interactive vegetation the ocean is in the "warm", interstadial glacial mode while with the interactive vegetation it is in the "cold", stadial glacial mode. This result stands in contrast to the previous findings by Ganopolski and Rahmstorf (1998b) who found a much colder LGM climate (colder by 1.4° C) with an ocean circulation in the "cold" mode when a prescribed present day vegetation was used. Their result was obtained with an earlier version of CLIMBER-2, thus the current version of CLIMBER-2 differs from their version by an improved ocean parametrization and a lower climate sensitivity. Hence, the changes in the simulated LGM climate between my study and the earlier study by Ganopolski and Rahmstorf (1998b) (caused by the improvement of the model) lead to a different equilibrium ocean circulation for the same experimental setup because the climate change simulated in my model version was too small to cross the threshold of the ocean circulation as long as the present day vegetation was used. Therefore, these at first glace contradictory results even strengthens the point made

by Ganopolski and Rahmstorf (1998b) that the thermohaline circulation is a highly non-linear system with thresholds. This is especially true as I could also show that not only the use of the interactive vegetation could trigger the change to the "cold" ocean mode, but that also an additional decrease of CO_2 concentration by only 10 ppm could trigger this change. These 10 ppm are exactly the difference between the CO_2 concentration used in the PMIP (2001) studies for the LGM (200 ppm) and the CO_2 concentration from reconstructions for this time (190 ppm) (Petit et al. 1999). This highlights that not only the use of a realistic vegetation versus the use of a present day vegetation but also the choice of the CO_2 concentration and probably also other small changes in the model-setup (e.g. the amount and extent of the inland ice cover) can act as a trigger for a change in the ocean circulation, due to its non-linear behavior.

I also studied the transient influence of the atmosphere-vegetation feedback and its effect on the glacial climate compared to the ocean-atmosphere feedback and their synergy effect over part of the last glacial period from 60–20 ky BP. What I found out is that over the period of the last glacial the magnitude of the atmosphere-vegetation feedback and its synergy with the ocean stayed about the same during stadials and interstadials while the atmosphere-ocean feedback showed some changes over these times, with a larger cooling relative to the present day reference state during stadials compared to interstadials. For the reference state from 20 ky BP, a smaller warming was seen during stadials than during interstadials. Thus the relative importance among the three factors did not change so that I averaged the changes caused by the factors over the glacial period to compare them with the results from a study of the Holocene by Ganopolski et al. (1998a).

I was able to find out that the use of an interactive ocean had a much larger effect on climate in the glacial period than in the study of the Mid-Holocene at 6 ky BP performed by Ganopolski et al. (1998a). The ocean, thereby, influenced the climate over changes in ocean circulation that in turn led to a change in SST and sea-ice coverage. The larger influence of the ocean on climate during the glacial than during the Holocene is due to large changes in the ocean circulation and, consequently, of sea-ice coverage and SST compared to the present day circulation, while the ocean circulation as well as sea-ice cover and SST in the Mid-Holocene were very similar to today.

The synergy term between the atmosphere-ocean feedback and the atmosphere-vegetation feedback turned out to be smaller in my study than during the Mid-Holocene in the study by Ganopolski et al. (1998), probably due to less amplification of the taiga-tundra feedback by the sea-ice-albedo effect than during the Holocene as the sea-ice extended far to the south in the glacial.

The temperature change on the NH caused by the atmosphere-vegetation feedback during the glacial (i.e. the difference between experiments with either interactive vegetation or prescribed present day vegetation while the ocean is fixed) had about the same absolute value as simulated for 6 ky BP (Mid-Holocene) by Ganopolski et al. (1998a). Instead of a warming, as seen in the study of the Mid-Holocene, the atmosphere-vegetation feedback caused a cooling during the glacial period. A second set of experiments, which

used the vegetation distribution from 20,000 years BP instead of the present day vegetation for comparison with the interactive vegetation, showed a globally much smaller temperature change due to the atmosphere-vegetation feedback than at 6 ky BP. The reason for this was that the vegetation difference between the fixed vegetation from 20 ky BP and the interactive vegetation was smaller than the difference between the fixed present day vegetation and the interactive vegetation. Compared to the use of a present day vegetation the atmosphere-vegetation feedback caused a cooling on the NH of 0.5° C, while compared to the use of a fixed 20 ky BP vegetation it was only a warming of 0.04° C on the NH. The synergy effect between the taiga-tundra feedback and the sea-ice albedo feedback caused an additional temperature change of 0.55 °C over land on the NH compared to the simulations with fixed present day vegetation and ocean characteristics. On the other hand, the synergy effect for the use of the 20 ky BP vegetation and ocean was also only small (maximum +0.24° C). Thus it can be concluded that the use of a modeled vegetation distribution from the LGM for the simulation for the last glacial period would not cause very large mistakes in the simulation whereas the use of a present day vegetation would cause problems, due to the locally important temperature changes on the order of 1–2 °C caused by the atmosphere-vegetation feedback and the synergism with the ocean-atmosphere feedback.

Furthermore, I was able to show that, due to the largest vegetation changes there, the atmosphere-vegetation feedback has been causing temperature and precipitation changes mainly in the high northern latitudes for the last glacial period. This is the same "hot-spot" as in the Holocene so that not only the magnitude but also the region where the atmosphere-vegetation feedback is important is the same as in the Holocene.

Overall, this study leads to the conclusion that the atmosphere-vegetation feedback is as important for the last glacial period as it was for the Holocene. The synergy factor between the atmosphere-vegetation feedback and the atmosphere-ocean feedback has been found to be smaller in the glacial than in the Holocene, due to the larger sea-ice extent that causes a sea-ice margin further south so that the interaction between the taiga-tundra feedback and the sea-ice albedo feedback is reduced. The results from the equilibrium experiments strengthen the point that the climate system, and especially the ocean circulation, shows a strong non-linear behavior. Therefore, small changes can have a large impact on climate. Thus, it is important to include as many components of the climate system, as realistic as possible, in climate models in order to arrive at a realistic simulation and the best possible understanding of climate dynamics.

Outlook:

While working on this thesis, additional questions and ideas have occurred that, due to the time limitation, could not be investigated, but that would be worth to be investigated in future studies to help complete the understanding of the atmosphere-vegetation feedback during the last glacial period.

Since the ocean factor is so dominant during the glacial period, it would be interesting to compare the effect of an interactive vegetation compared to a fixed vegetation to the effect of a factor that is of about the same magnitude. In the equilibrium study of the LGM, the CO_2 factor was found to be of about the same importance regionally as the vegetation influence. Therefore, it would be interesting to study the effect of a present day CO_2 concentration versus a glacial concentration on the climate in different seasons and also in different regions.

Calov et al. (2002) already used the inland ice module SICOPOLIS to model HE events interactively in an equilibrium study with CLIMBER-2, so it would be interesting to use their approach in a transient experiment to investigate feedbacks between the other components of the climate system and the inland ice. The ultimate goal would be to simulate the last glacial climate with all components included interactively, so that no part of the climate system would have to be prescribed.

In the equilibrium study it would be interesting to investigate the influence of a slab ocean versus the full interactive ocean, as this would make it possible to study the effect of the deep ocean in the equilibrium experiment and to separate the vegetation effect from the non-linear ocean effect while the synergy with the sea-ice-albedo effect would still be possible. For a study like this the FSB factor could be substituted with the ocean factor. Since it has been shown now that the effect of the astronomical forcing does not contribute significantly to the LGM climate, the number of factors investigated could be reduced to four (CO_2, inland ice and orography, ocean and vegetation), so that the total number of experiments necessary would be 16, with only eight additional experiments to the experiments that I have already performed.

Appendix A

Additional Material for the LGM

A.1 Factor Separation Equations for the LGM

$$\hat{f}_R = REF$$

$$\begin{aligned}
\hat{f}_A &= LGM_A - REF \\
\hat{f}_C &= LGM_C - REF \\
\hat{f}_I &= LGM_I - REF \\
\hat{f}_F &= LGM_F - REF \\
\hat{f}_V &= LGM_V - REF
\end{aligned}$$

$$\begin{aligned}
\hat{f}_{AC} &= LGM_{AC} - LGM_A - LGM_C + REF \\
\hat{f}_{AI} &= LGM_{AI} - LGM_A - LGM_I + REF \\
\hat{f}_{AF} &= LGM_{AF} - LGM_A - LGM_F + REF \\
\hat{f}_{AV} &= LGM_{AV} - LGM_A - LGM_V + REF \\
\hat{f}_{CI} &= LGM_{CI} - LGM_C - LGM_I + REF \\
\hat{f}_{CF} &= LGM_{CF} - LGM_C - LGM_F + REF \\
\hat{f}_{CV} &= LGM_{CV} - LGM_C - LGM_V + REF \\
\hat{f}_{IF} &= LGM_{IF} - LGM_I - LGM_F + REF \\
\hat{f}_{IV} &= LGM_{IV} - LGM_I - LGM_V + REF \\
\hat{f}_{FV} &= LGM_{FV} - LGM_F - LGM_V + REF
\end{aligned}$$

$$\begin{aligned}
\hat{f}_{ACI} &= LGM_{ACI} - LGM_{AC} - LGM_{AI} - LGM_{CI} + LGM_A + LGM_C + LGM_I - REF \\
\hat{f}_{ACF} &= LGM_{ACF} - LGM_{AC} - LGM_{AF} - LGM_{CF} + LGM_A + LGM_C + LGM_F - REF \\
\hat{f}_{ACV} &= LGM_{ACV} - LGM_{AC} - LGM_{AV} - LGM_{CV} + LGM_A + LGM_C + LGM_V - REF \\
\hat{f}_{AIF} &= LGM_{AIF} - LGM_{AI} - LGM_{AF} - LGM_{IF} + LGM_A + LGM_I + LGM_F - REF \\
\hat{f}_{AIV} &= LGM_{AIV} - LGM_{AI} - LGM_{AV} - LGM_{IV} + LGM_A + LGM_I + LGM_V - REF
\end{aligned}$$

$$
\begin{aligned}
\hat{f}_{AFV} &= LGM_{AFV} - LGM_{AF} - LGM_{AV} - LGM_{FV} + LGM_A + LGM_F + LGM_V - REF \\
\hat{f}_{CIF} &= LGM_{CIF} - LGM_{CI} - LGM_{CF} - LGM_{IF} + LGM_C + LGM_I + LGM_F - REF \\
\hat{f}_{CIV} &= LGM_{CIV} - LGM_{CI} - LGM_{CV} - LGM_{VI} + LGM_C + LGM_I + LGM_V - REF \\
\hat{f}_{CFV} &= LGM_{CFV} - LGM_{CF} - LGM_{CV} - LGM_{FV} + LGM_C + LGM_F + LGM_V - REF \\
\hat{f}_{IFV} &= LGM_{IFV} - LGM_{IF} - LGM_{IV} - LGM_{FV} + LGM_I + LGM_F + LGM_V - REF
\end{aligned}
$$

$$
\begin{aligned}
\hat{f}_{ACIF} &= LGM_{ACIF} - LGM_{ACI} - LGM_{ACF} - LGM_{AIF} - LGM_{CIF} \\
&\quad + LGM_{AC} + LGM_{AI} + LGM_{AF} + LGM_{CI} + LGM_{CF} + LGM_{IF} \\
&\quad - LGM_A - LGM_C - LGM_I - LGM_F + REF \\
\hat{f}_{ACIV} &= LGM_{ACIV} - LGM_{ACI} - LGM_{ACV} - LGM_{AIV} - LGM_{CIV} \\
&\quad + LGM_{AC} + LGM_{AI} + LGM_{AV} + LGM_{CI} + LGM_{CV} + LGM_{IV} \\
&\quad - LGM_A - LGM_C - LGM_I - LGM_V + REF \\
\hat{f}_{ACFV} &= LGM_{ACFV} - LGM_{ACF} - LGM_{ACV} - LGM_{AFV} - LGM_{CFV} \\
&\quad + LGM_{AC} + LGM_{AF} + LGM_{AV} + LGM_{CF} + LGM_{CV} + LGM_{FV} \\
&\quad - LGM_A - LGM_C - LGM_F - LGM_V + REF \\
\hat{f}_{AIFV} &= LGM_{AIFV} - LGM_{AIF} - LGM_{AIV} - LGM_{AFV} - LGM_{IFV} \\
&\quad + LGM_{AI} + LGM_{AF} + LGM_{AV} + LGM_{IF} + LGM_{IV} + LGM_{FV} \\
&\quad - LGM_A - LGM_I - LGM_F - LGM_V + REF \\
\hat{f}_{CIFV} &= LGM_{CIFV} - LGM_{CIF} - LGM_{CIV} - LGM_{CFV} - LGM_{IFV} \\
&\quad + LGM_{CI} + LGM_{CF} + LGM_{CV} + LGM_{IF} + LGM_{IV} + LGM_{FV} \\
&\quad - LGM_C - LGM_I - LGM_F - LGM_V + REF \\
\hat{f}_{ACIFV} &= LGM_{ACIFV} - LGM_{ACIF} - LGM_{ACIV} - LGM_{ACFV} - LGM_{AIFV} - LGM_{CIFV} \\
&\quad + LGM_{ACI} + LGM_{ACF} + LGM_{ACV} + LGM_{AIF} + LGM_{AIV} \\
&\quad + LGM_{AFV} + LGM_{CIF} + LGM_{CIV} + LGM_{CFV} + LGM_{IFV} \\
&\quad - LGM_{AC} - LGM_{AI} - LGM_{AF} - LGM_{AV} - LGM_{CI} \\
&\quad - LGM_{CF} - LGM_{CV} - LGM_{IF} - LGM_{IV} - LGM_{FV} \\
&\quad + LGM_A + LGM_C + LGM_I + LGM_F + LGM_V - REF
\end{aligned}
$$

That makes the fully coupled LGM experiment (called LGM_{ACIFV}) the sum of all these factors:

$$
\begin{aligned}
LGM_{ACIFV} = {} & \hat{f}_R + \hat{f}_A + \hat{f}_C + \hat{f}_I + \hat{f}_F + \hat{f}_V + \hat{f}_{AC} + \hat{f}_{AI} + \hat{f}_{AF} + \hat{f}_{AV} + \hat{f}_{CI} \\
& + \hat{f}_{CF} + \hat{f}_{CV} + \hat{f}_{IF} + \hat{f}_{IV} + \hat{f}_{FV} \\
& + \hat{f}_{ACI} + \hat{f}_{ACF} + \hat{f}_{ACV} + \hat{f}_{AIF} + \hat{f}_{AIV} + \hat{f}_{AFV} + \hat{f}_{CIF} + \hat{f}_{CIV} + \hat{f}_{CFV} + \hat{f}_{IFV} \\
& + \hat{f}_{ACIF} + \hat{f}_{ACIV} + \hat{f}_{ACFV} + \hat{f}_{AIFV} + \hat{f}_{CIFV} + \hat{f}_{ACIFV}
\end{aligned}
$$

A.2 Table with Results for the LGM Experiment

Here the calculated Stein and Alpert factors for global annual temperatures and precipitation for all 32 factors are shown for reference, as only seven of them were discussed in detail in chapter 5. Zeros in the table show hereby that the global effect caused was smaller than 0.01 °C or 0.001 mm/day.

Factor	Temp °C	Temp %	Prc mm/day	Prc %
$\hat{f}_R$	13.99	–	2.683	–
$\hat{f}_A$	−0.01	0.2	0.003	−0.8
$\hat{f}_C$	−1.32	27.5	−0.125	31.9
$\hat{f}_I$	−2.96	61.7	−0.200	51.0
$\hat{f}_F$	0	0	0	0
$\hat{f}_V$	0	0	0	0
$\hat{f}_{AC}$	0.01	−0.2	0.001	−0.2
$\hat{f}_{AI}$	0.03	−0.5	0.003	−0.8
$\hat{f}_{AF}$	0	0	0	0
$\hat{f}_{AV}$	−0.05	1.0	−0.006	1.5
$\hat{f}_{CI}$	0.03	−0.5	0.007	−1.8
$\hat{f}_{CF}$	0.03	−0.5	0.001	−0.3
$\hat{f}_{CV}$	−0.07	1.5	−0.013	3.3
$\hat{f}_{IF}$	0	0	0.001	−0.1
$\hat{f}_{IV}$	−0.48	9.9	−0.064	16.4
$\hat{f}_{FV}$	0	0	0	0
$\hat{f}_{ACI}$	0.02	0.4	0.001	−0.2
$\hat{f}_{ACF}$	−0.01	0.3	−0.001	0.2
$\hat{f}_{ACV}$	0.01	−0.2	0.001	−0.2
$\hat{f}_{AIF}$	0.02	−0.5	0.002	−0.4
$\hat{f}_{AFV}$	0	0	0	0
$\hat{f}_{CIF}$	−0.03	0.6	−0.001	0.2
$\hat{f}_{CIV}$	−0.14	2.9	−0.002	0.4
$\hat{f}_{IFV}$	0	0	0	0
$\hat{f}_{ACIF}$	−0.01	0.2	0.002	−0.4
$\hat{f}_{ACIV}$	0.01	−0.1	−0.001	0.2
$\hat{f}_{ACFV}$	−0.05	1.0	0.004	−1.0
$\hat{f}_{AIFV}$	−0.03	0.5	−0.002	0.5
$\hat{f}_{CIFV}$	0.02	−0.3	0.002	−0.4
$\hat{f}_{ACIFV}$	0.04	−0.9	0	0

Appendix B

Additional Material for 60–20 ky BP

B.1 Factor Separation Equations for 60-20 ky BP

Here the equations (2.2)–(2.5) from page 20 are applied to the runs performed for the full glacial period:

$$\begin{aligned}
\hat{f}_{ref} &= A \\
\hat{f}_{oce} &= AO - A \\
\hat{f}_{veg} &= AV - A \\
\hat{f}_{syn} &= AOV - AV - AO + A
\end{aligned}$$

With makes the simulations a sum of the factors as follows:

$$\begin{aligned}
A &= \hat{f}_{ref} \\
AO &= \hat{f}_{ref} + \hat{f}_{oce} \\
AV &= \hat{f}_{ref} + \hat{f}_{veg} \\
AOV &= \hat{f}_{ref} + \hat{f}_{oce} + \hat{f}_{veg} + \hat{f}_{syn}
\end{aligned}$$

These equations were used for both sets of experiments.

B.2 Prescribed Vegetation and Ocean States for 60–20 ky BP

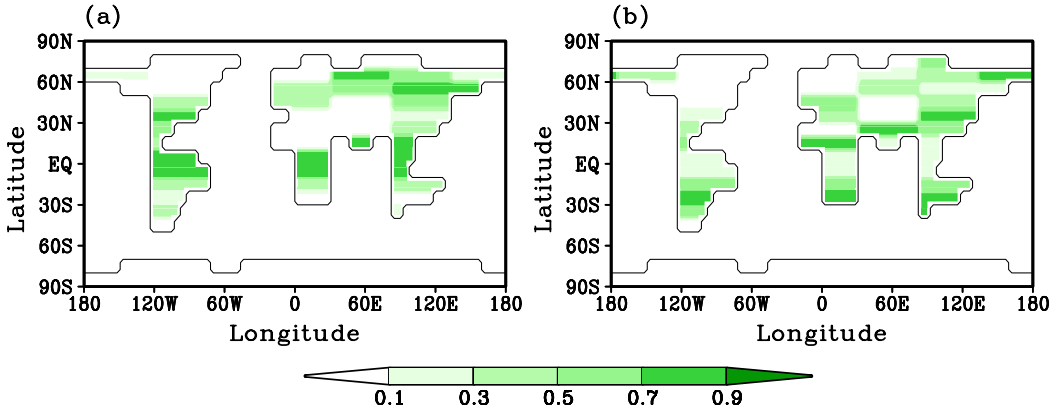

Figure B.1: Prescribed "00" tree- (a) and grass fraction (b) distribution, the inland ice area is already taken into account.

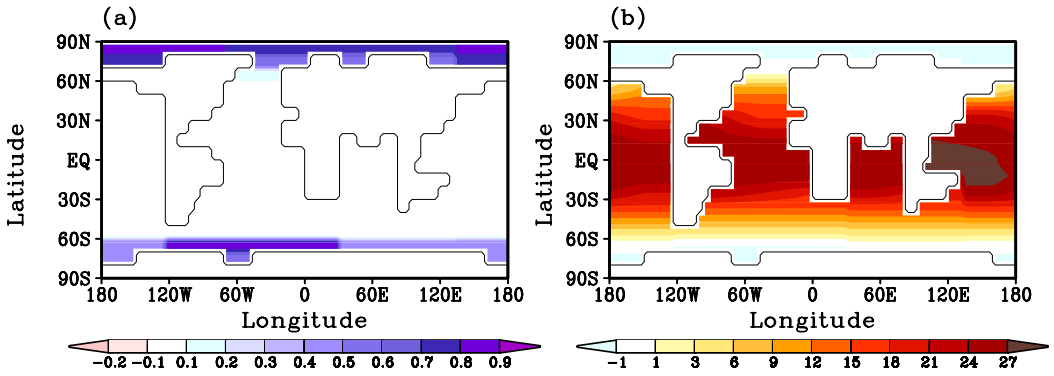

Figure B.2: Prescribed "00" sea-ice fraction (a) and prescribed "00" SST [in °C] (b). The ocean in "00" is in the "warm" interglacial mode.

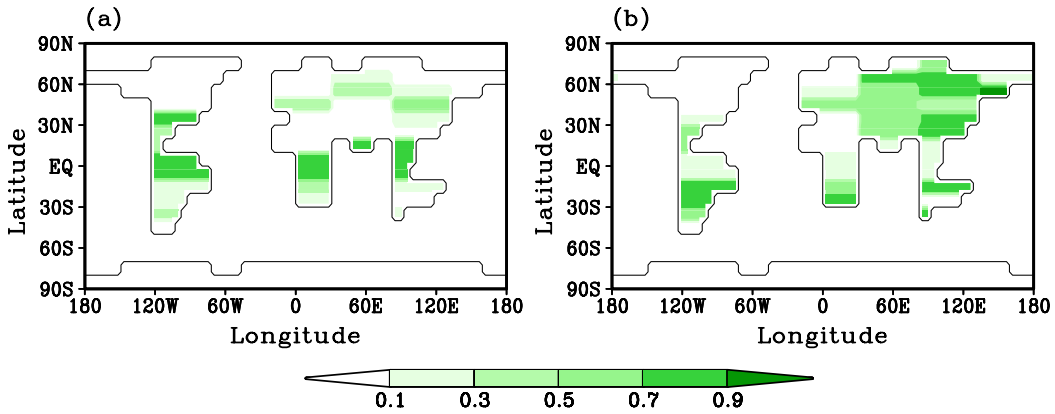

Figure B.3: Prescribed "20" tree- (a) and grass fraction (b) distribution, the inland ice area is already taken into account.

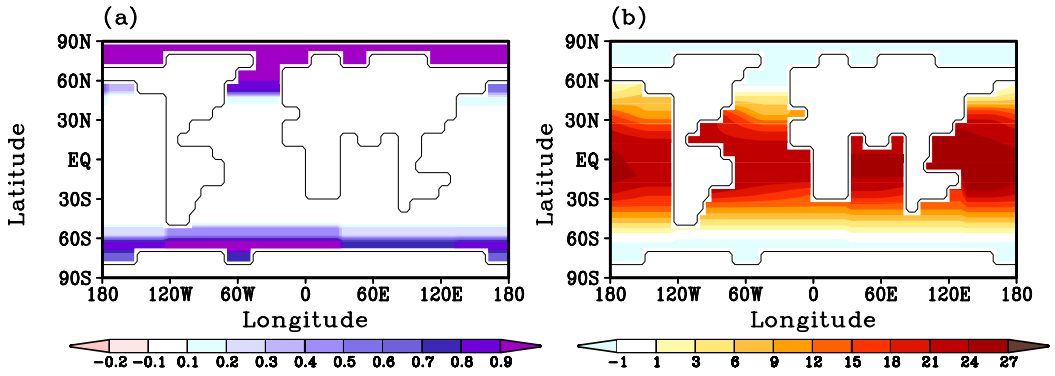

Figure B.4: Prescribed "20" sea-ice fraction (a) and prescribed "20" SST [in °C] (b). The ocean in "20" is in the "cold" glacial mode.

B.3 Factors for Stadials and Interstadials

		$\hat{f}_{oce_{(00)}}$	$\hat{f}_{veg_{(00)}}$	$\hat{f}_{syn_{(00)}}$	$\hat{f}_{ref_{(00)}}$	$\hat{f}_{oce_{(20)}}$	$\hat{f}_{veg_{(20)}}$	$\hat{f}_{syn_{(20)}}$	$\hat{f}_{ref_{(20)}}$
Annual	Global	−2.5	−0.1	−0.4	−3.0	+0.8	0	+0.2	+1.0
	NH	−2.6	−0.2	−0.5	−3.3	+1.2	0	+0.3	+1.5
	SH	−2.3	0	−0.3	−2.6	+0.5	0	+0.2	+0.7
	NH_L	−2.4	−0.3	−0.5	−3.2	+1.1	0	+0.3	+1.4
Summer	Global	−2.5	−0.2	−0.4	−3.1	+0.5	0	+0.2	+0.6
	NH	−2.3	−0.4	−0.5	−3.2	+0.6	+0.1	+0.3	+1.0
	SH	−2.7	0	−0.4	−3.1	+0.3	0	+0.2	+0.5
	NH_L	−2.1	−0.5	−0.5	−3.1	+0.6	+0.1	+0.3	+1.0
Winter	Global	−2.4	0	−0.4	−2.8	+1.1	0	+0.2	+1.3
	NH	−3.0	−0.1	−0.5	−3.6	+1.6	0	+0.3	+1.9
	SH	−1.9	0	−0.3	−2.2	+0.6	0	+0.1	+0.7
	NH_L	−2.7	−0.1	−0.5	−3.3	+1.5	0	+0.3	+1.8

Table B.1: Temperature change [in ° C] caused by the factors for a typical interstadial period from the transient runs.

		$\hat{f}_{oce_{(00)}}$	$\hat{f}_{veg_{(00)}}$	$\hat{f}_{syn_{(00)}}$	$\hat{f}_{ref_{(00)}}$	$\hat{f}_{oce_{(20)}}$	$\hat{f}_{veg_{(20)}}$	$\hat{f}_{syn_{(20)}}$	$\hat{f}_{ref_{(20)}}$
Annual	Global	−3.2	−0.1	−0.4	−3.7	+0.2	0	+0.2	+0.4
	NH	−3.6	−0.2	−0.5	−4.3	+0.2	0	+0.2	+0.4
	SH	−2.7	0	−0.3	−3.0	+0.1	0	+0.1	+0.4
	NH_L	−3.4	−0.3	−0.5	−4.2	+0.2	0	+0.2	+0.4
Summer	Global	−3.1	−0.2	−0.4	−3.7	0	0	+0.2	+0.2
	NH	−3.0	−0.4	−0.5	−3.9	−0.1	+0.1	+0.2	+0.2
	SH	−3.1	0	−0.3	−3.4	0	0	+0.1	+0.1
	NH_L	−2.8	−0.5	−0.5	−3.8	−0.1	+0.1	+0.2	+0.2
Winter	Global	−3.3	0	−0.4	−3.7	+0.4	0	+0.2	+0.6
	NH	−4.2	−0.1	−0.5	−4.8	+0.4	0	+0.2	+0.6
	SH	−2.3	0	−0.2	−2.5	+0.3	0	+0.1	+0.4
	NH_L	−3.9	−0.1	−0.4	−4.5	+0.4	0	+0.2	+0.6

Table B.2: Temperature change [in ° C] caused by the factors for a typical stadial period from the transient runs.

References

Adams J.M. and Faure H., Palaeovegetation maps of the Earth during the Last Glacial Maximum, and the early and mid Holocene: an aid to archaeological research, *Journal of Archaeological Science*, Vol: 24: 623–647, **1997**.

Alley, R.B., Anandakrishnan, S., Jung, P., Stochastic resonance in the North Atlantic, *Paleoceanography*, Vol: 16: 190–198, **2001**.

Berger, A., Long-Term variations of daily insolation and quaternary climatic changes, *Journal of the Atmospheric Sciences*, Vol: 35: 2362-2367, **1978** .

Berger, A., The role of CO_2, sea-level and vegetation during the Milankovitch-forced glacial-interglacial cycles. In: Bengtsson, L.O. and Hammer, C.U. (eds.), *Geosphere-Biosphere Interactions and Climate*, Proceedings of the workshop held at Pontifical Academy of Science, 119–146, Cambridge University Press, **2001**.

Berger A. and Loutre M.F., Insolation values for the climate of the last 10 million years, *Quaternary Sciences Review*, Vol: 10, No. 4: 297–317, **1991**.

Berger, A., Dutrieux, A., Loutre, M.F., Tricot, Ch., Paleoclimate sensitivity to CO_2 and insolation, *Scientific Report, Institut d'Astronomie et de Geophysique Georges Lemaitre*, **1996**.

Birchfield, G.E., Wang, H., Rich, J.J., Century/millennium internal climate variability: an ocean-atmosphere-continental icesheet model, *Journal of Geophysical Research*, Vol: 99: 12459–12470, **1994**.

Blunier, T., Chappellaz, J., Schwander, J., Dallenbach, A., Stauffer, B., Stocker, T.F., Raynaud, D., Jouzel, J., Claussen, H.B., Hammer, C.U., Johnsen, S.J., Asynchrony of Antarctic and Greenland climate change during the last glacial period, *Nature*, Vol: 394: 739–743, **1998**.

Bond, G., Heinrich, H., Broecker, W., Labeyrie, L., McMagnus, J., Andrews, J., Huon, S., Jantschik, R., Clasen, S., Simet, C., Tedesco, K., Klas, M., Bonani, G., Ivy, S., Evidence for massive discharge of icebergs into the North Atlantic ocean during the last glacial, *Nature*, Vol: 360: 245–249, **1992**.

Bond, G., Kromer, B., Beer, J., Muscheler, R., Evans, M.N., Showers, W., Hoffmann, S., Lotti-Bond, R., Hajdas, I., Bonani, G., Persistent solar influence on North Atlantic climate during the holocene, *Science*, Vol: 294: 2130–2136, **2001**.

Braun, H., Christl, M., Ganopolski, A., Rahmstorf, S., Mangini, A., Kromer, B., Roth, K., Kubatzki, C., Claussen, M., Solar forcing of Dansgaard-Oeschger events in the coupled climate system model CLIMBER-2, *submitted*, **2004**.

Broccoli, A. J., and S. Manabe, The influence of continental ice, atmospheric CO2, and land albedo on the climate of the last glacial maximum, *Climate Dynamics*, Vol: 1: 87–99, **1987**.

Broecker, W.S. and Van Donk, J., Insolation changes, ice volumes, and the 0_18 in deep-sea cores. *Rev. Geophys. Space Phys.*, Vol: 8: 169–198, **1970**.

Broecker, W.S., Peteet, D.M., Rind, D., Does the ocean-atmosphere system have more than one stable mode of operation? *Nature*, Vol: 315: 21-26, **1985**

Broecker W.S., Bond, G., Klas, M., Bonani, G., Wolfi, W., A salt oscillator in the glacial North Atlantic? The concept. *Paleoceonography*, Vol: 5: 469–477, **1990**.

Broecker, W., Bond, G., Mieczyslawa, K., Clark, McManus, J., Origin of the northern Atlantic's Heinrich events, *Climate Dynamics*, Vol: 6: 265–273, **1992**.

Brovkin, V., Ganopolski, A., Svirezhev, Y., A continuous climate-vegetation classification for use in climate-biosphere studies. *Ecological Modelling* Vol: 101: 251–261, **1997**.

Brovkin, V., Ganopolski, A., Claussen, M., Kubatzki, C., Petoukhov, V., Modelling climate response to historical land cover change, *Global Ecology and Biogeography*, Vol: 8: 509–517, **1999**.

Brovkin, V., Claussen, M., Ganopolski, A., Bendtsen, J., Kubatzki, C, Petoukhov, V. and Andreev, A., Carbon Cycle, vegetation and climate dynamics in the Holocene: Experiments with the CLIMBER-2 model,*Globalgeochemical Cycles*, Vol: 16, No. 4, 1139, **2002a**.

Brovkin, V., Ganopolski, A, Svirezhev, Yu., von Bloh, W., Bondeau, A., Claussen, M., Cramer, W, Petoukhov, V., Rahmstorf, S., VEgetation COntinuous DEscription Model (VECODE), *PIK Technical Report, Draft*, **2002b**.

Brovkin, V., Lewis, S., Loutre, M.-F., Claussen, M., Crucifx, M., Ganopolski, A., Kubatzki, C and Petoukhov, V., Stability analysis of the climate-vegetation system in the northern high latitudes, *Climatic Change*, Vol: 57: 119–138, **2003**.

Calov, R.,Petoukhov, V., Claussen, M., Greve, R., Large-scale instabilities of the Laurentide ice sheet simulated in a fully coupled climate-system model, *Geophysical Review Letters*, Vol: 29(24): 2216, doi: 10.1029/2002GL016078, **2002**.

Cane, M.A. and A.C. Clement, A role for the tropical Pacific coupled ocean-atmosphere system on Milankovitch and millennial time scales. Part II: global impacts, In: *AGU Monograph: Mechansimus of millenial scale global climate change*, **1999**.

Chappell, J., Sea level changes forced ice breakouts in the last glacial cycle: new results from coral terraces, *Quaternary Science Review*, Vol: 21: 1129–1240, **2002**.

Claussen, M., Biogeophysical Feedbacks and the Dynamics of Climate, *Global Geophysical Cycles in the climate system*, 61–71, Academic Press, San Diego, **2001**.

Claussen, M., Feedbacks, synergismy, multiple equilibria and teleconections, in: Kabat, P., Claussen, M., Dirmeyer, P.A., Gash, J.H.C., Guenni, L., Meybeck, M., Pielke, R.A., Vrsmarty, C.J., Ltkemeier, S., (eds.), *Vegtation, Water, Humans and the Climate: A New Perspective on an Interactive System*, Springer-Verlag, Heidelberg, **2004**.

Claussen, M., Kubatzki, C., Brovkin, V., Ganopolski, A., Hoelzmann, P., Pachur, H.J., Simulation of an Abrupt Change in Saharan Vegetation at the end of the Mid-Holocene, *Geophysical Research Letters*, Vol: 24, No: 14: 2037–2040, **1999**.

Claussen, M., Ganopolski, A., Schellnhuber, J., Cramer, W., Earth System Models of Intermediate Complexity, *Global Change Newsletter*, Vol: 41: 4–6, **2000**.

Clausen, M., Brovkin, V., Ganopolski, A., Biogeophysical versus biogeochemical feedbacks of large-scale land cover change, *Geophysical Research Letters*, Vol. 28, No. 6, 1011–1014, **2001**.

Claussen, M., Mysak, L.A., Weaver, A.J., Crucifix, M., Fichefet, T., Loutre, M.-F., Weber, S.L., Alcamo, J., Alexeev, V.A., Berger, A., Calov, R., Ganopol ski, A., Goosse, H., Lohmann, G., Lunkeit, F., Mokhow, I.I., Petoukhov, V, Stone , P, Wang, Z., Earth system models of intermediate complexity: closing the gap in the spectrum of climate system models, *Climate Dynamics* Vol. 18: 579–586, **2002**.

Claussen, M., Ganopolski, A., Brovkin, V., Gerstengarbe, F.-W., Werner, P., Simulated global-scale response of the climate system to Dansgaard/Oeschger and Heinrich events, *Climate Dynamics* Vol. 21: 361–370, **2003a**.

Claussen, M., Brovkin, V., Ganopolski, A., Kubatzki, C., Petoukhov, V., Climate change in northern Africa: The past is not the future, *Climatic Change*, Vol: 57: 99–118, **2003b**.

Clement, A.C. and Cane, M.A., A role for the tropical Pacific coupled ocean-atmosphere system on Milankovitch and millennial time scales. Part I: a modelling study of tropical Pacific variability. In:*AGU Monograph: Mechansimus of millenial scale global climate change*, **1999**.

CLIMAP, Seasonal reconstructions of the Earth's surface at the last glacial maximum. *Map Series, Technical Report MC-36, Geological Society of America, Boulder, Colorado*, **1981**.

Crowley, T.J. and G.R. North, Paleoclimatology. *Oxford Monographs on Geology and Geophysics*, No. 18, Oxfort University Press, New York, **1990**

Crowley, T.J., North Atlantic deep water cools the Southern Hemisphere, *Paleoceanography*, Vol: 7: 489–497, **1992**.

Crowley, T.J., Ice age terrestrial carbon changes revisited, *Global Biochemical Cycles*, Vol: 9: 377–389, **1995**.

Crowley, T.J. and S. Baum, Effect of vegetation on an ice-age climate model simulation, *Journal of Geophysical Research*, Vol. 102, No. D14, 16,463–16,480, **1997**.

Dansgaard, W., Claussen, H.B., Gundestrup, N., Hammer, C.U., Johnsen,S.F., Kristinsdottir, P.M., and N. Reeh, A new Greenland deep ice core, *Science*, Vol: 218: 1273–1277, **1982**.

Dansgaard, W., Johnsen, S.J., Clausen, H.B., Dahl-Jensen, D., Gundestrup, N.S., Hammer, C.U., Hvidberg, C.S., Steffensen, J.P., Sveinbjornsdottir, A.E., Jouzel, J., Bond, G., Evidence for general instability of past climate from a 250-kyr ice-core record, *Nature*, Vol: 364: 218–220, **1993**.

Dawson, A.G., Ice Age Earth. Late Quaternary Geology and Climate. *A volume in the Routledge physical environment series*, edited by Keith Richards, London and New York, **1992**.

Dickinson, RE., Henderson-Sellers, A., Kennedy, PJ., Wilson, MF., Biosphere-Atmosphere Tranfer Scheme (BATS) for the NCAR, CCM, NCAR/TN-275-STR, *National Center for Atmospheric Research, Boulder, Coloado, USA*, 69 pp, **1986**.

Dong, B., and P.J. Valdes, Simulations of the last glacial maximum climate using a general circulation model: prescribed versus computed sea surface temperatures, *Climate Dynamics*, Vol: 14: 571–591, **1998**.

Duplessy, J.C., N.J. Shackleton, R.G. Fairbancks, L. Labeyrie, D. Oppo and N. Kallel, Deepwater source variations during the last climatic cycle and their impact on the global deepwater circulation, *Paleoceanography*, Vol: 3, 343–360, **1988**.

Dutrieux, A. and A. Berger, Classical feedback method and seperation factor method: comparison and application to O-D energy balance model, *Scientific Report 1997/ 13, Institut d'Astronomie et de Geophysique Georges Lemaitre, University Catholique des Louvain (UCL), Louvain-La-Neuve, Belgium*, **1997**.

EPICA community members, Eight glacial cycles from an Antarctic ice core, *Nature*, Vol: 429: 623–628, **2004**.

Fast, I. Modelltheoretische Analyse der Wechselwirkungsprozesse im Klimasystem des Holozäns, *Diplomarbeit im Fach Meteorologie an der FU Berlin*, **2002**.

Ganopolski, A. Glacial integrative modelling, *Phil. Trans. Royal. Soc. Lond.*, Vol. 361: 1871–1884, **2003**.

Ganopolski, A., Kubatzki, C., Claussen, M., Brovkin, V., Petoukhov, V., The influence of Vegetation-Atmosphere-Ocean Interaction on Climate during the Mid-Holocene, *Science*, Vol: 280: 1916–1919, **1998a**.

Ganoploski, A., Rahmsdort, S, Petoukhov, V., Claussen,M. Simulation of modern and glacial climates with a coupled global model of intermediate complexity , *Nature*, Vol. 391: 351–356, **1998b**.

Ganopolski, A., Petoukhov, V., Rahmstorf, S., Brovkin, V., Claussen, M., Eliseev, A., Kubatzki, C., CLIMBER-2: a climate system model of intermediate comple xity. Part II: model sensitivity, *Climate Dynamics* Vol: 17: 735–751, **2001**.

Ganopolski, A. and Rahmstorf, S., Rapid changes of glacial climate simulated in a coupled climate model, *Nature* Vol: 409: 153–158, **2001**.

Ganopolski and Rahmstorf, Abrupt glacial climate changes due to stochastic resonance, *Physical Review Letters*, Vol: 88(3): 038501-1-038501-4, **2002**.

Greve, R., On the Response of the Greenland Ice Sheet to Greenhouse Climatic Change, *Climatic Change*, Vol:46: 289-303, **2000**.

Grootes, P.M., M. Stuiver, J.W.C. White, S.J. Johnsen, and J. Jouzel, Comparison of oxygen isotope records from the GISP2 and GRIP Greenland ice cores *Nature*, Vol: 366: 552–554, **1993**.

Grootes, P.M., and M. Stuiver. Oxygen 18/16 variability in Greenland snow and ice with 10-3- to 105-year time resolution, *Journal of Geophysical Research 102*, 26455-26470, **1997**.

Hansen, J., G. Russell, D. Rind, P. Stone, A. Lacis, S. Lebedeff, R. Ruedy, and L. Travis, Efficient three-dimensional global models for climate studies: Models I and II, *Monthly Weather Review*, Vol: 111: 609–662, **1983**.

Hays, J.D., Imbrie, J. and N.J. Shackleton, Variations in the earth's orbit: Pacemaker of the ice ages, *Science*, Vol: 194: 1121–1132, **1976**.

Heinrich, H., Origin and consequences of cyclic ice rafting in the northeast Atlantic Ocean during the past 130,000 years, *Quaternary Research*, Vol: 29(2): 142–152, **1988**.

Henderson-Sellers, A. and McGuffie, K., A climate modelling primer. *1st edition J. Wiley New York*, **1987**.

Henderson-Sellers, A. and McGuffie, K., Concpts of good science in climate change modelling. Comments on S. Shackley et al. *Climatic Change* Vol: 42: 597–610, **1998**.

Hewitt, C.D., and J.F.B. Mitchell, Radiative forcing and response of a GCM to ice age boundary conditions: cloud feedback and climate sensitivity, *Climate Dynamics*, Vol: 13: 821–834, **1997**.

Hewitt, C.D., Broccoli, A.C., Mitchell, J.F., Stouffer, R.J., A coupled model study of the last glacial maximum: was part of the North Atlantic relatively warm?, *Geophysical Research Letters*, Vol: 28: 1571–1574, **2001**.

Hewitt, C. D., R. J. Stouffer, A. J. Broccoli, J. F. B. Mitchell, and P. J. Valdes, The effect of ocean dynamics in a coupled GCM simulation of the Last Glacial Maximum, *Climate Dynamics*, Vol: 20(2/3): 203–218, **2003**.

IPCC,*Climate Change 2001: The scientific Basis, Contribution of working group I to the Third Assessment Report of the Intergovernmental Panel on Climate Change* Houhton, J.T., Y. Ding, D.J. Griggs, M. Noguer, P.J. van der Linden, X. Dai, K. Maskell, C.A. Johnson (eds.), Cambridge University Press, Cambridge, United Kingdom and New York, NY, USA, 881pp, **2001**.

Kim, S.-J., G.M. Flato, G.J. Boer and N.A. McFarlane, A coupled climate model simulation of the Last Glacial Maximum, Part 1: transient multi-decadal response, *Climate Dynamics*, Vol: 19: 515–537, **2002**.

Kim, S.-J., G. M. Flato, and G. J. Boer, A coupled climate model simulation of the Last Glacial Maximum, Part 2: approach to equilibrium, *Climate Dynamics*, Vol: 20(6): 635–661, **2003**.

Kim, S. J., The effect of atmospheric CO2 and ice sheet topography on LGM climate, *Climate Dynamics*, Vol: 22(6/7): 639–652, **2004**.

Kitoh, A., Murakami, S., Koide, H., A simulation of the Last Glacial Maximum with a coupled atmosphere-ocean GCM, *Geophysical Research Letters*, Vol: 28: 2221–2224, **2001**.

Knorr, W., Schnitzler, K.-G., and Govaerts, Y., The role of bright desert regions in shaping North African Climate, *Geophysical Research Letters*, Vol:28(18), 3489–3492, **2001**.

Kubatzki, C., Wechselwirkungen zwischen Klima und Landoberfläche im Holozän, *Dissertation im Fachbereich Geowissenschaften, FU Berlin*, 182 Pages, **2000**.

Kubatzki, C., Claussen, M. Simulation of the global bio-geophysical interactions during the Last Glacial Maximum, *Climate Dynamics* Vol: 14: 461–471, **1998**.

Kubatzki, C., Montoya, M., Rahmstorf, S., Ganopolski, A., Claussen, M., Comparision of the last interglacial climate simulated by a coupled global model of intermediate complexity and an AOGCM, *Climate Dynamics*, Vol: 2, No: 2: 131-137, **2000**.

Kudrass, H.R., Hofmann, A., Doose, H., Emeis, K., Erlenkeuser, H., Modulation and amplification of climatic change in the Northern Hemisphere by the Indian summer monsoon during the past 80 ky, *Geology*, Vol:29(1): 63–66, **2001**.

Lewis, S., Foley, J.A., Pollard, D. CO_2, climate, and vegetation feedbacks at the Last Glacial Maximum, *Journal of Geophysical Research*, Vol. 104, No. D24, 31,191–31,198, **1999**.

Leuschner D.C. and F. Sirocco, The low-latitude monsoon climate during Dansgaard-Oeschger cycles and Heinrich events, *Quaternary Science Review*, Vol: 19: 243–254, **2000**.

Lieth, H., Modeling the Primary Productivity of the World, *Primary Productivity of the Biosphere*, Springer Verlag (Berlin), 237–263, **1975**.

Lynch-Stieglitz, J., W.B. Curry, N. Slowey and G.A. Schmidt, The overturning circulation of the glacial Atlantic: A view from the top, Reconstructing Ocean History: A Window into the Future, edited by F. Abrantes and A. Mix, *Kluwer Academic/Plenum, New York*, pp: 7-31, **1999**.

Mailhot, J. and Chouinard, C., Numerical forecasts of explosive winter storms: Sensitivity experiments with a meso-α scale model, *Mon. Weather Review*, Vol: 117: 1311–1343, **1988**.

Milankovitch, M., Mathematische Klimalehre und astronomische Theorie der Klimaschwankungen, in: *Handbuch der Klimatologie* (Kppen and Geiger eds.), Band 1, Teil A. Springer-Verlag, 176 pp., **1930**.

Mix, A.C., Bard, E., Schneider, R., Environmental processes of the ice age: oceans, glaciers (EPILOG), *Quaternary Science Review*, Vol: 20: 627–657, **2001**.

Muller, R.A. and G.J. MacDonald, *Ice Ages and Astronomical Causes*, 318 pages, Springer-Verlag, Berlin, Heidelberg, New York, **2000**.

Peixoto, J.P. and Oort, A.H., *Physics of Climate*, Springer-Verglag New York, Inc., 520 pages, **1992**.

Peltier, W. R., Ice Age Paleotopography, *Science*, Vol: 256: 195–201, **1994**.

Petoukhov, V., Ganopolski, A., Brovkin, V, Claussen, M., Eliseev, A., Kubatzki, C, Rahmstorf, S. CLIMBER-2: a climate system model of intermediate complexity. Part I: model description and performance for present climate, *Climate Dynamics* Vol: 16: 1–17, **2000**.

Petit, J.R., Jouzel, J., Raynaud, D., Barkov, N.I., Barnola, J.-M., Basile, I., Bender, M., Chappellaz, J., Davis,M, Delaygue, G., Delmotte, M., Kotlyakov, V.M., Legrand, M., Lipenkov, V.Y., Lorius, C., Pepin, L., Ritz, C., Saltzman, E., Stievenard, M., Climate and atmospheric history of the past 420,000 years from the Vostok ice core, Antarctica, *Nature*, Vol: 399: 429–436, **1999**.

PMIP, Paleoclimate Modeling Intercomparison Project (PMIP), *Proceedings of the third PMIP workshop, Canada, 4-8 October 1999, P. Braconnot (Ed)*, WCRP-111, WMO/TD-1007, 271 pp, **2000**.

Prentice, I.C., Cramer, W., Harrison, S.P., Leemans, R., Monserud, R.A. and Solomon, A.M., A global biome model based on plant physiology and dominance, soil properties and climate. *Journal of Biogeography*, Vol: 19: 117–134, **1992**.

Prentice, I.C., Guiot, J., Huntley, B., Jolly, D., Cheddadi, R., Reconstruction biomes from palaeoecological data: A general method and its application to European pollen data at 0 and 6ka, *Climate Dynamics*, Vol: 12: 185–194, **1996**.

Rahmstorf, S., Rapid climate transitions in a coupled ocean-atmosphere model, *Nature*, Vol: 372: 82–85, **1994**.

Rahmstorf, S., Bifurcations of the Atlantic thermohaline circulation in response to changes in the hydrological cycle, *Nature*, Vol: 378: 145–149, **1995**.

Rahmstorf, S., The Thermohaline Ocean Circulation: A System with dangerous thresholds, Editorial Comment, *Climate Change*, Vol: 46: 247–256, **2000**.

Rahmstorf, S., and R.B. Alley, Stochastic resonance in glacial climate, *EOS*, Vol: 83: 129–135, **2002**.

Rahmstorf, S. and A. Ganopolski, Long-term global warming scenarios computed with an efficient coupled climate model, *Climatic Change*, Vol: 43: 353–367, **1999**.

Salzman, B., A survey of statistical-dynamical models of the terrestrial climate, *Adv. Geophysics*, Vol: 20: 183–304, **1978**.

Semtner, AJ., A model for the thermodynamic growth of sea-ice in numerical investigations of climate, *Journal of Physical Oceanography*, Vol: 6: 379–389, **1976**.

Stein, U. and Alpert, P., Factor Separation in numerical simulations, *Journal of Atmospheric Sciences*, Vol: 50, No: 14: 2107-2115, **1993**.

Stocker, T.F., The seesaw effect, *Science*, Vol: 282: 61–62, **1998**.

Stuiver, M., P.M. Grootes, and T.F. Braziunas. The GISP2 d18O climate record of the past 16,500 years and the role of the sun, ocean and volcanoes, *Quaternary Research*, Vol: 44: 341–354, **1995**.

TEMPO Members (J.E. Kutzbach, P.J. Bartlein, J.A. Foley, S.P. Harrison, S.W. Hostetler, Z. Liu, I.C. Prentice, T. Webb III), Potential role of vegetation feedbacks in the climate sensitivity of high-latitude regions: a case study at 6000 years before present, *Global Biogeochemical Cycles*, Vol: 10:727–736, **1996**.

Tushingham, A.M. and W.R. Peltier, Ice-3G: A new global model of late pleistocene deglaciation based upon geophysical predictions of post-glacial relative sea level change, , *Journal of Geophysical Research*, Vol: 96(B3): 4497–4523, **1991**.

Van Geel, B., Raspopov, O.M., Rensen, H., van der Pflicht, J., Dergachev, V.A., Meijer, H.A.J., The role of solar forcing upon climate change, *Quaternary Science Reviews*, Vol: 18: 331–338, **1999**.

Voelker AHL and workshop participants Global distribution of centennial-scale records for marine isotope states (MIS) 3: a database, *Quaternary Science Review*, Vol: 21: 1185–1214, **2002**.

Weaver, A. J., and E. S. Sarachik, Evidence for decadal variability in an ocean general circulation model: An advective mechanism, *Atmosphere-Ocean*, Vol: 29: 197–231, **1991**.

Weaver, A. J., M. Eby, A. F. Fanning and E. C. Wiebe, Simulated influence of carbon dioxide, orbital forcing and ice sheets on the climate of the last glacial maximum, *Nature*, Vol: 394: 847–853, **1998**.

Webb III, T., Ruddiman, W.F., Street-Perrott, F.A., Markgraf, V., Kutzbach, J.E., Bartlein, P.J., Wright, H.E.Jr., Prell, W.L., Climatic Changes during the past 18,000 years: Regional syntheses, mechanisms and causes. In: Wright, Jr.H.E., Kutzbach, J.E., Webb III, T., Ruddiman, W.F., Street-Perrott, F.A. and Bartlein, P.J. (Eds): *Global Climates since the Last Glacial Maximum*, chapter 19, **1993**.

Winton, M. and Sarachik, E.S., Thermohaline oscillations induced by strong steady salinity forcing of ocean general circulation models, *Journal of Physical Oceanography*, Vol: 23: 1389–1410, **1993**.

Wright, D.G. and Stocker, T.F., A zonally averaged ocean model for the thermohaline circulation. Part I: Model development and flow dynamics, *Journal of Physical Oceanography*, Vol: 21(12): 1713–1724, **1992**.

Wyputta, U., McAveney, B.J. Influence of vegetation changes during the Last Glacial Maxximum using the BMRC atmospheric general circulation model, *Climate Dynamics*, Vol: 17: 923–932, **2001**.

Acknowledgements

I want to thank Prof. Dr. Cubasch and Prof. Dr. Claussen for the supervision of my thesis. Furthermore, I want to thank Prof. Dr. Claussen for offering me the chance to write my Diploma thesis at the PIK and for the helpful guidance I received from him during the work on my thesis.

In addition I especially want to thank Dr. Claudia Kubatzki, who proof-read my thesis and helped me with valuable comments to further improve it, and Dr. Andrey Ganopolski, who always had time to answer my questions and to discus my results. Dr. Victor Brovkin I want to thank for helping me in solving problems with VECODE and for the discussion of my results.

For taking the time to carefully proofread the manuscript for grammar and spelling mistakes I want to thank Antje Kroschewski. Stephan Berndts I want to thank for the last minute help with LaTeX.

I also want to thank the whole CLIMBER group because they provided help, advice and a friendly and productive atmosphere during the two years I spend at the PIK.

I'm grateful for the numerous reference letters that Prof. Dr. Malberg, Prof. Dr. Claussen and Prof. Dr. Wehry wrote me during the past years because their friendly support helped me to realize my plan to study abroad.

My family has helped me not only during the work on my thesis but during the past 25 years by providing support and encouragement in whatever I choose to do.

The "Studienstiftung des deutschen Volkes" I want to thank for their support and for the possibilities their support offered me during the last three years.

To come to an end I want to thank everybody who made my life as a student during the past 6 years so successful and fun at the same time, and especially Kerstin Prömmel for her friendship.